Molecule-assisted atomic chain formation : mechanisms and properties of new one-dimensional conductors

Thijssen, W.H.A.

Molecule-assisted atomic chain formation:

mechanisms and properties of new one-dimensional conductors.

W.H.A. (Robert) Thijssen

2007

Cover: *Artistic impression of a methodological investigation of a suspended atomic wire of gold and oxygen atoms.* **Design:** *Rashevskaya and Bremmer 2007.*

ISBN: 978-90-8559-336-2
Casimir PhD Series, Delft-Leiden: 2007-15

The work described in this thesis is part of the scientific program of the "Stichting voor Fundamenteel Onderzoek der Materie" (FOM).

Printed by Optima Grafische Communicatie, Rotterdam: www.ogc.nl

Molecule-assisted atomic chain formation:

mechanisms and properties of new one-dimensional conductors.

Proefschrift

ter verkrijging van
de graad van Doctor aan de Universiteit Leiden,
op gezag van Rector Magnificus prof.mr. P.F. van der Heijden,
volgens besluit van het College voor Promoties
te verdedigen op dinsdag 11 december 2007
klokke 11:15 uur

door

Wilhelmus Hendrikus Alphonsus Thijssen

geboren te Groesbeek in 1977

Promotiecommissie

Promotor:	Prof. Dr. J.M. van Ruitenbeek
Referent:	Prof. Dr. H. van Kempen (Radboud Universiteit Nijmegen)
Overige leden:	Prof. Dr. J.W.M. Frenken
	Prof. Dr. G. Nienhuis
	Prof. Dr. M. Orrit
	Dr. K.S. Thygesen (Technical University of Denmark)
	Prof. Dr. Ir. H.J.W. Zandvliet (Universiteit Twente)

Nature does nothing uselessly

Aristotle

Contents

1

Introduction

We humans have since ancient times been interested in electrical phenomena. Thales of Miletos, a Greek philosopher and scientist, discovered in the 6th century BC that after he had rubbed a piece of amber, with some fur it would attract another piece. This phenomenon is now understood as static electricity. In fact the word "electron" originates from the Greek word for "amber". During the eighteenth century many experiments to control static electricity were conducted, resulting e.g. in the invention of the Leyden jar, the first capacitor, by Pieter van Musschenbroek. By that time it was also realized that the occurrence of electrical discharge when two static pieces are brought together, is due to the transport of electrical charge. Today most people are familiar with the concept of electricity and electric current. The understanding of electricity has made many technological advances possible, which have not only broadened our understanding of nature but has improved the quality of our lives as well: think of not only the ubiquitous light bulbs but also of all kinds of consumer electronics, computers, medical equipment etcetera.

When switching on a lamp you close an electrical circuit. Because the resistance of the tungsten wire in the light bulb and electrical cables in this circuit is small, a current starts to flow through the wire, causing it to heat up to around 2000 ^oC, making it glow. The current (I) due to a voltage difference (V) over a resistance (R) is linearly proportional to the voltage and inversely proportional to the resistance (I = V/R). This relationship between electric current and voltage is commonly known as Ohm's law, after German physicist Georg Ohm. An electric current is the transport of electric charge, which is carried by electrically charged particles. Electric transport in metals is performed by electrons, which carry the quantum of electric charge, namely $1.6{\cdot}10^{-19}$ Coulomb. Electrons in a metal are in principle free to move through the material, but when a voltage difference is applied over the metal the resulting current is finite due to a finite resistance. What determines the resistance of a piece of material? How do the geometrical dimensions of the piece of material influence the resistance? What happens to the resistance when the current has to pass through a constriction consisting of only a few or just a single atom?

In a macroscopic metallic rod the number of electrons is extremely large. A voltage difference applied over the material causes the electrons to experience a net electric field, which forces them to accelerate in the direction opposite to the electric field. The actual time an electron accelerates is limited because electrons scatter with lattice vibrations and impurities in the metal and each other. These scattering events result in the loss of kinetic energy and cause the metal to be resistive. The longer the average acceleration time between scattering events, the smaller the resistance.

Changing the dimensions of a rod will result in a different resistance. When the diameter becomes smaller, fewer electrons can pass per second through the rod and a longer rod results in a smaller effective electric field felt by the electrons inside the rod. The resistance of a conducting rod can be expressed in a simple formula,

$$R = \frac{l}{\sigma \cdot A} \tag{1.1}$$

where the resistance R is linearly proportional to the length l of the rod and inversely proportional to the conductivity σ and the cross-sectional area A of the rod. The conductivity is a material and temperature dependent constant. Material properties and temperature determine the average acceleration time of the electrons between scattering events. According to formula 1.1 the resistance of the thinnest possible metallic wire, only one atom thick and a few atoms long, would have a resistance around 300 Ω at room temperature[1]. In reality the resistance is around 13000 Ω. The reason for this discrepancy lies in the fact that we have entered the realm of atomic size conductors. There the "classical" many-particle macroscopic laws of physics do not hold anymore and are replaced by quantum physics. In the quantum world electrons cannot be considered as localized particles anymore, but as delocalized traveling waves, having similar properties as e.g. electro-magnetic waves. When an electro-magnetic wave has to pass through a wave-guide, the diameter of the guide has to be such that the wavelength fits inside. This principe also holds when an electron-wave is traveling through an atomic size contact. Chapter 2 will provide a theoretical groundwork for the conduction properties of atomic scale constrictions.

Technological advances during the past 25 years have made it possible for the first time to enter into the world of individual atoms and their properties. With the development of the Scanning Tunneling Microscope (STM) [1] in the early 1980's it became possible not only to "see" individual atoms, but later also to manipulate atoms [2], resulting in fascinating new physical phenomena. Towards the end of the decade the transport properties of nanoscopic constrictions were being measured. In a famous experiment by Van Wees *et al.* [3] the predicted quantization of conduction was measured in a two-dimensional electron gas. Also around that time a technique called the mechanically-controlled break-junction (MCBJ) was developed and somewhat later introduced and further developed at the Kamerlingh Onnes Laboratory at Leiden University. With

[1] For gold $\sigma = 45{\cdot}10^{6}\ \Omega^{-1}\ \mathrm{m}^{-1}$, $l = 10^{-9}$ m, $A = 7{\cdot}10^{-20}\mathrm{m}^{2}$

the MCBJ technique one can create constrictions of only a few or just a single atom in diameter by controllably breaking a metallic wire, as will be described in chapter 2. It was found that metallic contacts of only a single atom in diameter always display a resistance around 10 kΩ, depending on the chemical valence of the atom under study [4].

Gold is a noble metal and a single-atom contact of gold has a resistance close to 13 kΩ, the inverse of the conductance quantum G_0. But gold was also found to have the surprising property that a one-gold-atom thick freely suspended wire can be formed [5, 6]. In the following years these thinnest wires were studied in detail both experimentally and theoretically. Interesting suggestions have been made that the structural as well as the electronic properties of these ultimate one-dimensional conductors can be modified by introducing molecules. Chapter 3 will introduce the atomic wires and demonstrate the effect that introducing oxygen has on the formation, transport and structural properties of atomic wires of the noble metals gold, silver and copper, most notably the reinforcing effect on the linear bonds in the wires.

Different single molecules captured in different metal junctions, resulted in different electrical and structural properties of these contacts. Especially useful in determining the configuration of a molecule in the junction is examining the vibrational properties of the single-molecule junction as was done for C_{60} between Au leads [7] and more recently for a single hydrogen molecule captured in a platinum junction [8]. Measuring the energy of these molecular vibration-modes is not easy. It requires not only a very sensitive measurement of the differential conductance of the junction but also some degree of repeatability in order to determine the energy of the modes. A small correction to the current due to backscattered electrons signals the energy of a molecular vibration-mode [8]. For most single-molecule junctions that have been investigated in the research of this thesis differential conductance spectra have been obtained that display anomalous peak-like features around the energies of the vibration-modes of the molecule in the junction. Chapter 4 demonstrates that these anomalies can also be attributed to vibration-modes and be used as a tool to identify the energy of vibration-modes.

After it was shown that a single hydrogen molecule can be contacted by platinum electrodes, the system became a sort of benchmark since hydrogen is the simplest molecule in existence and it was studied in combination with other metals. The properties of gold atomic wires in a hydrogen environment have been studied in the past both experimentally and theoretically. One important issue that has not yet sufficiently been resolved is the question whether hydrogen remains in molecular form once it reacts with the gold wires, or that it dissociates into hydrogen atoms. Chapter 5 addresses this question and provides by a series of experimental results giving additional evidence that hydrogen remains molecular.

Magnetism in atomic size constrictions has drawn a lot of attention in the past years since it is believed to hold the prospect of using the magnetic properties in tuning the transport properties of the constriction. Many experimental reports claim that the resistance of e.g. nickel atomic contacts changes hugely

upon applying an external magnetic field, even though calculations are not consistent with these claims. Some calculations actually suggest that strong magnetic polarization dependent transport properties in ferromagnetic atomic contacts can occur when a molecule is captured in the junction by modifying the local electronic properties. Oxygen stood out as an interesting candidate and chapter 6 describes the experiments done on nickel-oxygen atomic junctions, showing the formation of magnetic atomically thin wires as well as features associated with magnetism on the atomic scale.

Finally, chapter 7 shows results for STM experiments that actually come back to the original outset of the research that was intended to be done for this thesis. With the help of an STM it should be possible to actually control the formation of atomically thin suspended wires by simply pulling a prepositioned wire from a surface. Due to technical malfunctions of the UHV-LT-STM in Leiden these experiments were performed at the University of Twente, where it was recently discovered that atomic platinum wires can be created on a germanium surface. The atomic manipulation of self-organized atomic wires on a surface at room temperature demonstrates the robustness of these one-dimensional structures. However it has not (yet) been possible to perform these experiments at cryogenic temperatures, which could answer fundamental questions about the physics of these remarkable structures.

2

Theoretical and experimental concepts

This chapter provides an introduction to the basic theoretical concepts concerning the physical properties like conductance and electron-phonon interactions from contacts of mesoscopic size to junctions consisting of only a single atom or molecule. Also the experimental tools used to create atomic contacts and atomic wires under cryogenic conditions are introduced. It is explained how specific physical properties of these atomic structures are measured. The chapter aims to lay a foundation necessary to understand the experimental observations and their physical interpretation that are presented in the following chapters of this thesis.

2.1 Transport properties of nanoscale contacts

An electric current is generated by the transport of electrons that flow through a conductive material when an electric field is being applied over the material. Strictly speaking a current can be carried by any kind of particle that has a non-zero electric charge, like e.g. ions in a solution or holes in a semiconductor. Since the work presented in this thesis deals solely with electric transport by electrons the discussion will be limited to them. The solid-phase of matter is the physical state in which the energy minimization by sharing electrons of a system consisting of a very large ensemble of atoms or molecules, is larger than the increase in energy due to electrostatic repulsion and thermal energy present in the system. In the case of metallic condensed matter all atoms give up at least one electron, which form a sea of electrons, also called the Fermi sea. These electrons can freely move through the material. In the simplest approximation for describing the transport properties of the electrons in the electron sea, they are described in terms of non-interacting free particles in the so-called Fermi-gas. This model takes into account the quantum nature of the electrons and, since they are fermions, the Pauli exclusion principle. Macroscopic properties of metals like heat capacity, thermal conductivity and electric conductivity have been described very well with this model (see e.g. Ref. [9] and references therein). Georg Ohm realized at the beginning of the 19th century that for a conducting material at constant temperature the current density (j) increases linearly with increasing electric field ($\mathbf{E}$) applied over the material, resulting in the famous Ohm's law: $\mathbf{j} = \sigma\mathbf{E}$. Paul Drude formulated in 1900 an expression for the electric conductivity σ:

$$\sigma = \frac{ne^2\tau}{m} \tag{2.1}$$

Here n is the charge density, e the electron charge, m is the electron mass and τ the average time the electric field accelerates the electrons. n and τ are the most important in determining the conductivity since the electron charge is a universal constant and the effective electron mass is given for a certain material. Typically n and τ are temperature dependent quantities, but for metals n is not temperature dependent. Electrons scatter with defects, lattice vibrations (i.e. phonons) and each other when travelling through a metal. When the average time between scattering events is larger, then the conductivity will be larger as well, since the electrons are accelerated by the electric field for a longer time. When the temperature is lowered the number of thermally excited phonons in the metal decreases and thus the probability of scattering events between electrons and phonons decreases as well. Pure metals have therefore a much better conductivity at cryogenic temperatures then at room temperature.

When the electric transport takes place in the above described manner by constant scattering of electrons the conductor is called "diffusive". Now suppose that the dimensions of a metallic piece of material are shrunk such that the average distance between two scattering events becomes larger than the

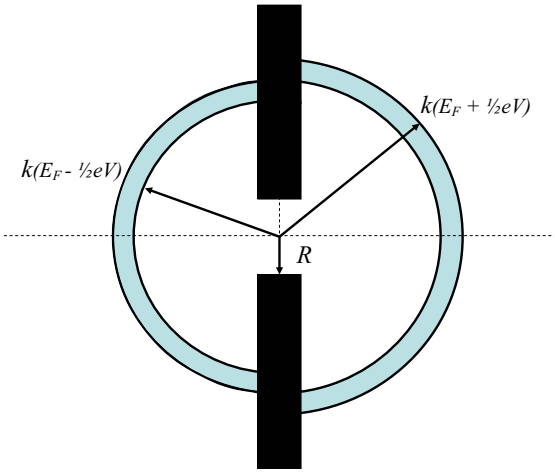

Figure 2.1: *Schematic view in reciprocal space of the electron distribution for an orifice that connects two electron reservoirs. The shaded area represents the net current caused by a voltage difference between the two reservoirs.*

length of the material. In that case the material would become a perfect conductor, since the electrons are not hampered anymore by scatterers. Such a conductor is called "ballistic". Even though the electrons behave ballistically, the conductance of these scaled-down conductors is finite. This is because a ballistic contact is coupled to macroscopic electrodes. When an electric current starts to flow and electrons arrive at the interface with the ballistic contact, they travel without losing energy through the contact. The electrons arrive with an energy above the local chemical potential at the other electrode. In order to equilibrate with the Fermi-sea these electrons will scatter with phonons, which causes resistance to occur. But how large is the resistance of a ballistic contact coupled to electrodes?

Sharvin considered this problem in 1965 and he worked out a semi-classical model in which he considered the conduction electrons as a dilute gas that has to flow through a circular orifice [10]. He considered in a simplified picture two electron reservoirs on the left and the right hand side that are separated by a thin wall in which a circular orifice is present (see figure 2.1). By applying a higher voltage V to the right electron reservoir, the electron distribution near the orifice is locally redistributed such that electron states are emptied at the left hand side and occupied at the right hand side. This results effectively in a potential on the left hand side of E_F-$\frac{1}{2}V$ and E_F+$\frac{1}{2}V$ on the right hand side. The higher voltage causes a larger amount of both empty states on the left and occupied states on the right. The current density j flowing through the orifice is proportional to the total amount of displaced electron states as is schematically depicted in figure 2.1 and can be obtained by integrating over the empty states

on the left and the occupied states on the right.

$$j = 2\left(\frac{1}{2\pi}\right)^3 \int ev\cos(\theta)d^3\mathbf{k} \tag{2.2}$$

The factor 2 enters the equation because of spin degeneracy. By writing the electron velocity $v = \hbar k/m$, switching to spherical coordinates and performing the angular parts of the integral the current density is expressed as:

$$j = \frac{e\hbar}{4\pi^2 m}\int k^3 dk = \frac{e\hbar}{4\pi^2 m}\int \frac{k^2}{2}dk^2 \tag{2.3}$$

Now it is possible to convert the integration over wave vectors into an integration over energy. Since $k^2 = 2mE/\hbar^2$ and $dk^2 = (2m/\hbar^2)dE$, the current density can be written as:

$$j = \frac{e}{4\pi^2}\frac{\hbar}{2m}\left(\frac{2m}{\hbar^2}\right)^2 \int_{E_F}^{E_F+eV} EdE \approx \frac{e}{4\pi^2}\frac{2m}{\hbar^3}E_F eV = \frac{2e^2}{h}\frac{k_F^2}{4\pi}V \tag{2.4}$$

Here the Fermi energy E_F is written in terms of the Fermi wave vector k_F as $\hbar^2 k_F^2/2m$. In order to obtain the current I the current density has to be integrated over the area of the orifice:

$$I = \int jdA = \pi R^2 j = \frac{2e^2}{h}\left(\frac{k_F R}{2}\right)^2 V \tag{2.5}$$

This results in the conductance of the orifice:

$$G = \frac{I}{V} = \frac{2e^2}{h}\left(\frac{k_F R}{2}\right)^2 \tag{2.6}$$

Equation 2.6, better know as the Sharvin conductance is a very important result. It tells us that the conductance in the ballistic regime is proportional to the area of the orifice, as in the "classical" diffusive regime in which Ohm's law holds. It differs in that the Sharvin conductance is only determined by the radius of the orifice and does not dependent on the length of the conductance channel, as is the case for the "diffusive" Ohm's law. The Sharvin conductance is obtained by assuming the electrons in the left and right reservoir to be free non-interacting particles. In reality electrons in a confined geometry such as an atomic-scale contact behave quantum mechanically. The Sharvin conductance describes the conductance of mesoscopic contacts very well, even when they are only a few nanometers in diameter. In the next section the quantum mechanical wave nature of electrons will be taken into account, since Sharvin's conductance does break down for the narrowest contacts, consisting of only a few or a single atom.

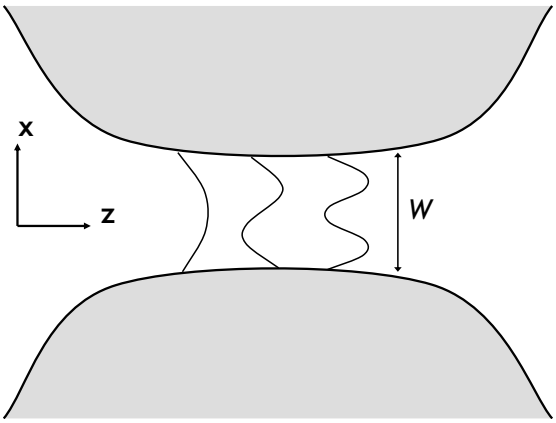

Figure 2.2: *Schematic view of a ballistic two-dimensional constriction. Due to the hard wall potential, the wave functions are quantized in the x-direction.*

2.2 Conductance quantization

One of the most well known problems in an undergraduate quantum mechanics course is to find the solutions to the Schrödinger equation for the so-called ”particle-in-a-box”. When a particle is confined in an infinite square potential well, the solutions for the Schrödinger equation become quantized. The energy difference between the quantized states in the well is inversely proportional to the square of width of the well. For an completely isolated system at T = 0 the energy levels are delta functions. In reality however there is always a finite temperature and the system is coupled to the outside world, which cause the energy levels to be broadened. To be able to observe this quantization in a real system the energy spacing between the quantized levels should be large enough to compensate for the broadening of the levels. Conductance quantization is a result of the quantization of conduction electron wave functions due to the confinement inside the constriction or channel through which they propagate. By decreasing the width of the channel the wavelength of the electron waves should decrease in order to fit in the channel. The minimal channel-width allowing for electron transmission is determined by the Fermi wavelength (λ_F), which is the shortest electron-wavelength in a metal. Since λ_F is about 0.5 nm for metals the quantization will be best observed when the channel is only a few atoms wide. This of course only holds when the temperature of the electron gas is sufficiently low, such that the thermal smearing does not cause the energy-levels of different wave functions to overlap.

This thesis is concerned with the conductance of contacts of only one atom in diameter. Let us therefore consider a two-dimensional constriction, with a width W and a length much larger than the width as depicted in figure 2.2. For simplicity the temperature will be kept at zero and the electrons are considered non-interacting. The Schrödinger equation in cartesian coordinates for

this one-dimensional system with a hard wall boundary is:

$$-\frac{\hbar^2}{2m}\left(\frac{\partial^2}{\partial x^2}+\frac{\partial^2}{\partial z^2}+V(x,z)\right)\Psi(x,z)=E\Psi(x,z), \tag{2.7}$$

in which the potential $V(x,z)$ represents in this simplified model a hard wall boundary between the material and the vacuum around it. Electrons that pass through the constriction can propagate freely in the z-direction, but are quantized in the x-direction. For a slowly varying boundary potential $V(x,z)$, the solutions $\Psi(x,z)$ of the Schrödinger equation and the eigenvalues $E(x,z)$ are:

$$\Psi(x,z)=A\sin\left(\frac{n_x\pi}{W(z)}x\right)\mathrm{e}^{\pm ik_z z}\quad\text{and}\quad E(x,z)=\frac{\hbar^2}{2m}\left[\left(\frac{n_x\pi}{W(z)}\right)^2+k_z^2\right] \tag{2.8}$$

This result indicates that as the width W of the constriction becomes very large the energy spectrum for the possible electron states that fit in the constriction approaches a continuum as expected. But as the width narrows only the states with the highest energy, will have a wavelength short enough to fit in the channel, as long as this wavelength is longer or equal to λ_F Because electrons are fermions every eigenfunction having a wavelength that fits in the channel can be filled with two electrons, one for each spin direction.

For this simplified model an eigenfunction of the atomic constriction, which can be occupied by conduction electrons is called an eigenchannel or conduction channel. Strictly speaking the channels are eigenfunctions of the product of the transmittance matrix with its complex conjugate ($t^\dagger t$). In order to determine the conductance of a channel, it is necessary to look at the freely propagating electron wave in the z-direction. The one-dimensional continuum equation gives the current density in terms of the propagating wave functions:

$$j(z)=\frac{i\hbar}{2m}\left(\Psi(z)\frac{\partial\Psi^*(z)}{\partial z}-\Psi^*(z)\frac{\partial\Psi(z)}{\partial z}\right) \tag{2.9}$$

Landauer first considered this problem in 1957 [11] and introduced the notion that an electron-wave propagating through a constriction has a certain probability to be transmitted. The transmitted wave is the only one contributing to the conductance and can be written as:

$$\Psi_t(z)=\frac{1}{\sqrt{L}}t_n\mathrm{e}^{ik_z z} \tag{2.10}$$

Here the length of the channel is L and t_n is the transmission probability amplitude for the n^{th} channel. This wave function can be used to evaluate $j(z)$ of equation 2.9, yielding

$$j_n(k)=\frac{\hbar k_n}{mLW}T_n \tag{2.11}$$

Here T_n = $(t^\dagger t)_{nn}$ is the total transmittance of the n^{th} eigenchannel of the constriction. To obtain the total current through the constriction all contributions

from all eigenchannels have to be added up and integrated over the width of the channel. Furthermore the two-fold spin degeneracy of the electrons has to be taken into account:

$$I = \sum_n I_n = 2eW \sum_{n,k} j_n(k) = \frac{2e\hbar}{mL} \sum_n T_n \sum_k k \tag{2.12}$$

By converting the sum into an integral by using $\sum k = \int k \frac{dk}{\Delta k} = \frac{L}{2\pi} \int k dk$ and by converting the integral over k to E the total current for the n^{th} channel is evaluated by integrating over all electron states:

$$I_n = \frac{2e}{h} T_n \left(\int_{E_F}^{0} dE + \int_{0}^{E_F} dE \right) \tag{2.13}$$

This equation yields zero, of course, because there is no voltage difference applied over the constriction. By applying a potential difference of eV the current of the channel can be evaluated:

$$I_n = \frac{2e}{h} T_n \int_{E_F - \frac{eV}{2}}^{E_F + \frac{eV}{2}} dE = \frac{2e^2}{h} V T_n \tag{2.14}$$

The total conductance of the constriction is then given by:

$$G = \frac{I}{V} = \frac{2e^2}{h} \sum_n T_n \tag{2.15}$$

The result of equation 2.15 is known as Landauer's formula and it tells us that the total conductance of a ballistic constriction in two dimensions is equal to the elementary conductance quantum $2e^2/h$ = G_0 times the sum over all transmittances of all channels that fit in the constriction. Experimentally Landauer's formula was first demonstrated by van Wees *et al.* [3] in 1988. They used a two-dimensional electron gas (2DEG) and by applying different gate voltages they were able to open or close conductance channels, resulting in conductance steps of $2e^2/h$.

2.3 Conductance of a single-molecule junction

2.3.1 Conductance of a single metal atom contact

The effect of conductance quantization can also be observed when the diameter of a metallic wire is reduced to only a few atoms or even a single atom. But what determines the conductance of a single atom or molecule contacted between metal electrodes? Landauer's formula tells that the conductance of a ballistic contact is the sum of all transmittances of all eigenchannels that fit

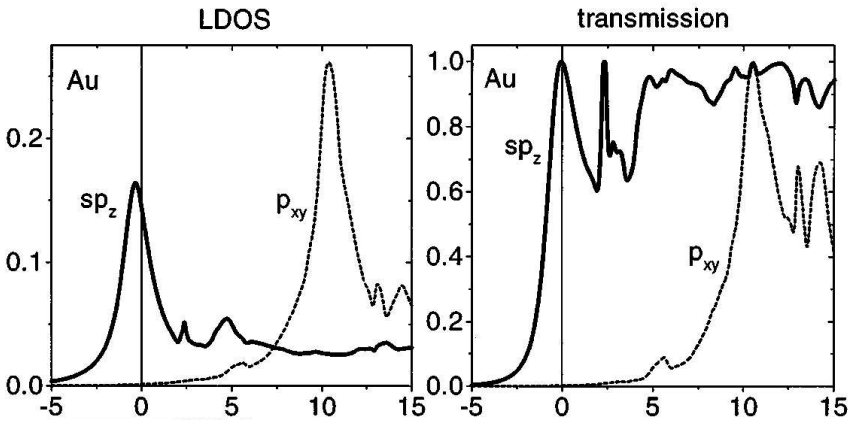

Figure 2.3: *LDOS and transmission for a single gold atom contact in an ideal configuration as a function of energy in eV, as obtained from a self-consistent tight binding model. The vertical line indicates the position of the Fermi energy. Graph taken from Ref. [13].*

in the constriction times $2e^2/h$. But how many channels does a single atom have and what is their transmittance? Electrons have to be transported via an atomic orbital of the single atom in the contact otherwise the transport will be purely due to tunneling. This means that the Local Density of States (LDOS) of the atom or molecule in the contact at the Fermi energy of the bulk metal electrodes needs to be finite. A microscopic model of a single-atom contact using an atomic orbitals basis set is used to determine the eigenchannels of single-atom junctions [12, 13]. It turns out that the number of channels is determined by the chemical valence of the atom in the junction. This result is perhaps not too surprising since the chemical valence indicates how many electrons are present in partially occupied atomic orbitals, for which it is energetically favorable to interact with electrons from neighboring atoms. The transmittance of the individual channels depends on the coupling of the atom to the electrodes (broadening of the atom's energy levels), the hybridization of the atomic orbitals with each other and the bulk-like states in the apexes of the electrodes. It can be determined from a self-consistent tight-binding model by imposing charge neutrality. Experimentally Scheer *et al.* [4, 14] have demonstrated that this model is correct. The conductance of a single noble metal (gold, silver, copper) atom contact originates from the single s-orbital and has a nearly 100% transmittance around the Fermi-level of bulk gold, resulting in a conductance near $2e^2/h$, in accordance with density functional calculations [15] and numerous experimental data [16–20]. In figure 2.3 the LDOS and transmission of a single gold atom contact is shown. Clearly a single sp_z-hybrid orbital is relevant at the Fermi energy yielding a transmission of nearly one. The other noble metals silver and copper have a very similar LDOS and transmission.

2.3.2 Conductance of a single molecule

When a single molecule is contacted by metal electrodes the conductance of the molecular junction will also depend on the overlap of the LDOS of the molecule with the Fermi level of the metal. Since the Lowest Unoccupied Molecular Orbital (LUMO) or the Highest Occupied Molecular Orbital (HOMO) are typically situated at a different energy then the Fermi energy of e.g. gold, it would seem unlikely that electron transport is possible at all. This is indeed true for large molecules that weakly couple to the metal electrodes. For those systems the coupling Γ is very small compared to the charging energy U and the molecule is said to be in the so-called Coulomb blockade regime. For molecules that strongly couple to the metal atoms, however, the molecule cannot be regarded as an isolated system anymore. In such case $\Gamma \sim U$ and the system is said to be in the self-consistent field regime, where charge transfer is fractional.

The chemical bond between the molecule and the apex atoms of the electrodes is formed by hydridizated orbitals, which results in an effective charge redistribution between the molecule and electrodes. The stronger the coupling of the molecular and metal orbitals, the more the hybridized orbitals are broadened. The charge redistribution also causes the hybridized orbitals of the molecule to be shifted in energy relative to the Fermi energy of the metal. In this way the LDOS of the molecule, formed by energy-shifted and broadened hybridized molecular orbitals, can have a large overlap with the orbitals of the electrodes.

A simple picture of molecular conduction through a single level is consid-

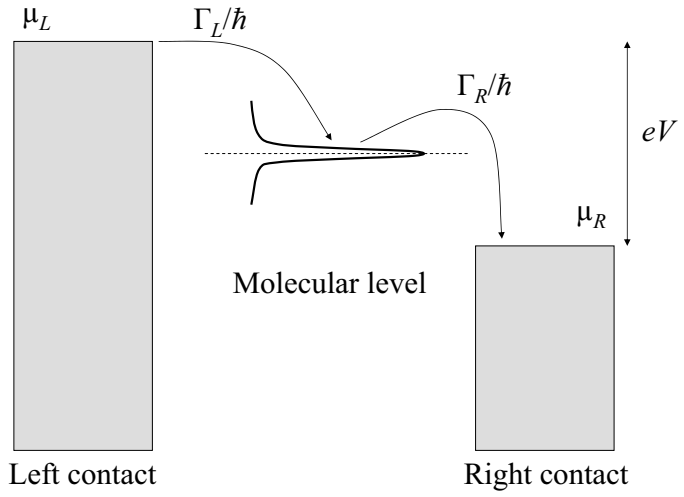

Figure 2.4: *Schematic drawing of a broadened molecular level coupled to electrodes. $\Gamma_L/\hbar$ and $\Gamma_R/\hbar$ represent the rates from the left electrode to the molecular level and from the molecular level to the right electrode, respectively.*

ered by Paulsson *et al.* [21]. The broadening Γ of the level plays a dominant role and can be related via the Heisenberg uncertainty principle to the time a conduction-electron spends on the molecule by $\Gamma = \hbar/\tau$. In practice the coupling to the left and right electrodes can be different. The total broadening is the sum of the two broadenings: $\Gamma = \Gamma_L + \Gamma_R$. The broadened molecular level is represented by a Lorentzian-shaped DOS

$$D(E) = \frac{1}{2\pi} \frac{\Gamma}{(E-\epsilon)^2 + (\Gamma/2)^2} \tag{2.16}$$

where ϵ is the energy of the discrete molecular level and Γ is assumed to be energy independent. Suppose now that the molecule is coupled to electrodes on the left and right and a positive bias voltage V is applied to the right, resulting in a lowering of the chemical potential μ_R with eV as displayed in figure 2.4. The number of electrons flowing per second from the left electrode to the broadened molecular level is $\Gamma_L/\hbar$ and $\Gamma_R/\hbar$ from the molecular level to the right electrode. When the molecular level ϵ is aligned with μ_L, the number of electrons occupying the level is

$$N_L = 2\int_{-\infty}^{\infty} D(E)dEf(E,\mu_L), \tag{2.17}$$

where $f(E,\mu_L)$ is the Fermi-Dirac distribution function and the factor 2 is due to spin degeneracy. Equally by aligning with μ_R the number would be

$$N_R = 2\int_{-\infty}^{\infty} D(E)dEf(E,\mu_R). \tag{2.18}$$

In the case when the molecular level is situated somewhere in between μ_L and μ_R (as in figure 2.4) the number of electrons occupying the molecular level N will be somewhere in between N_L and N_R. When a current flows in a steady state from the left electrode through the molecule to the right, the current from the left electrode to the molecule

$$I_L = \frac{e\Gamma_L}{\hbar}(N_L - N), \tag{2.19}$$

is equal to the current from the molecule to the right electrode

$$I_R = \frac{e\Gamma_R}{\hbar}(N_R - N), \tag{2.20}$$

from which

$$N = 2\int_{-\infty}^{\infty} D(E)\frac{\Gamma_L f(E,\mu_L) + \Gamma_R f(E,\mu_R)}{\Gamma_L + \Gamma_R}dE. \tag{2.21}$$

From this the current through the molecule becomes:

$$I = \frac{2e}{\hbar}\int_{-\infty}^{\infty} D(E)\frac{\Gamma_L\Gamma_R}{\Gamma_L + \Gamma_R}\left(f(E,\mu_L) - f(E,\mu_R)\right)dE \tag{2.22}$$

From equation 2.22 follows that a finite current will only flow when the molecular level lies in between μ_L and μ_R. Furthermore equation 2.22 also demonstrates that the maximum conductance through a single molecular level, by setting $f(E, \mu_L)$ to 1 and $f(E, \mu_R)$ to 0 and $\Gamma_L = \Gamma_R$, is equal to $2e^2/h$. This is the same result as was derived from the particle-in-a-box approach in section (2.2) and leads to a generalization that an isolated orbital coupled to electron reservoirs on both sides has a maximal conductance of $2e^2/h$. Experimentally a single hydrogen molecule contacted by platinum electrodes has for example been shown to have a conductance near $2e^2/h$ resulting from a single orbital, which forms a nearly 100% transparent conduction channel [8, 22, 23]. For this system the hybridization is very strong and the proper description is in the self-consistent field regime.

2.4 Experimental techniques

2.4.1 The mechanically controlled break-junction

For the study of single atom or molecule junctions the so-called mechanically controlled break-junction (MCBJ) technique is used. It was first introduced by Moreland and Ekin in 1985 [24] and has been further developed by Muller *et al.* [25]. The working principle of the technique is depicted in figure 2.5. First a surgical knife is used to make a notch in the middle of a metal wire under study. The diameter of the metal wire is reduced by at least 50 $\%$. Then the wire is fixed with two droplets of epoxy adhesive (Stycast 2850 FT with curing agent 24LV) on a phosphor-bronze bendable substrate, which is electrically insulated by a thin kapton foil. The epoxy droplets are depicted as black droplets in figure 2.5 and they should be placed very close to the notch, leaving a gap of only about 0.1-0.2 mm between them. This is important in order to make sure that the displacement ratio of the MCBJ is very small, which is necessary for highly stable junctions. After curing the epoxy for 24 hours the substrate is mounted in a three-point bending configuration between a piezo-element and

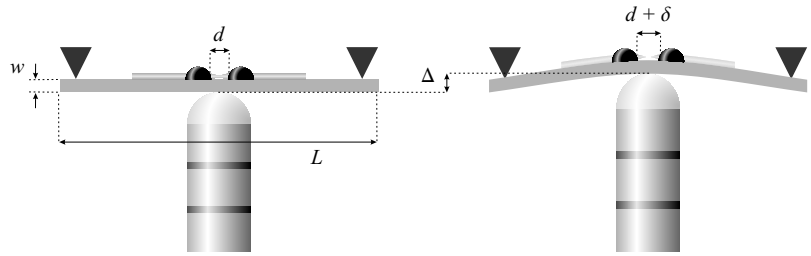

Figure 2.5: *Working principle of the mechanically controlled break-junction technique. A notched metal wire is carefully stretched in a three-point bending configuration by means of a piezo electric element. In this way subatomic displacements of the electrodes can be achieved.*

two counter supports, as shown in figure 2.5. The piezo-element is glued onto the bottom of a mechanical axle, which is used for the coarse displacement of the MCBJ. The piezo-element is controlled with a high-voltage supply, which supplies up to 1000 V, resulting in an extension of the element of about 10 μm at T=4.2K. The principle of the MCBJ is that the movement of the phosphor-bronze substrate is transferred into a reduced displacement of the two epoxy droplets (d in figure 2.5), causing the displacement of the electrodes. In the ideal case where the extension of the phosphor-bronze substrate occurs homogenously over the entire length between the two counter supports, the ratio between the displacement of the two electrodes (δ) and the elongation of the piezo-element (Δ) is given by [26]:

$$\frac{\delta}{\Delta} = \frac{6wd}{L^2} \tag{2.23}$$

Given a substrate thickness w = 1 mm, a distance d = 0.2 mm between the epoxy droplets and a substrate length L = 20 mm, the ratio $\frac{\delta}{\Delta}$ becomes about $3{\cdot}10^{-3}$.

2.4.2 Calibration of the displacement ratio

The displacement factor(k) is defined as the ratio between the displacement of the electrodes (δ) and the applied piezo voltage (V_p) in order to achieve it. The ratio cannot a priori be determined very accurately for a given MCBJ sample. It is therefore necessary to calibrate every sample prior to performing experiments. The calibration can be done by using the dependence of the tunneling current on the distance between two electrodes [27]:

$$I_t(\delta) = C \exp\left(-\frac{2\sqrt{2m\Phi}}{\hbar}\delta\right) \tag{2.24}$$

Here m is the electron mass and Φ is the work function of the metal under study and C is a constant. Assuming a linear dependence of the distance d on the piezo voltage V_p the logarithm of the current can be expressed as:

$$\ln(I_t(V_p)) = C^{'} - \frac{2}{\hbar}\sqrt{2m\Phi}kV_p \tag{2.25}$$

In figure 2.6 an example of a calibration measurement is shown. The slope of the curve is equal to the derivative $\frac{\mathrm{d}\ln(I_t)}{\mathrm{d}V_p}$, from which the value of k can be determined. The slope can differ by as much as 20% between different calibration measurements, due to different atomic configurations at the apexes of the electrodes. It is known that different crystallographic orientations result in small differences of the value of the work function. Therefore the calibration is repeated many times in order to obtain a good average value for the slope. This variation limits the accuracy of the calibration to about 10 %.

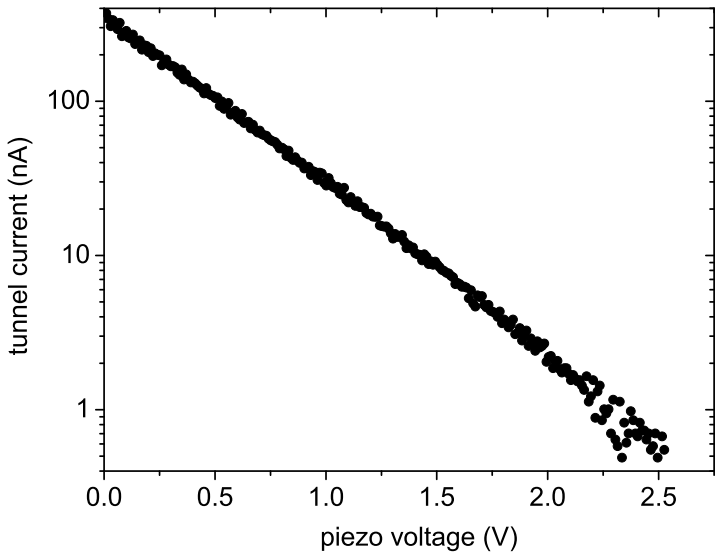

Figure 2.6: *Example of a displacement ratio calibration measurement for gold at T = 5 K. By increasing the piezo voltage the electrodes move apart, resulting in a decrease of the tunneling current.*

2.4.3 The insert

The bottom part of the insert used in the experiments is schematically drawn in figure 2.7. The insert basically consists of a long hollow metal tube of about 1.5 meters in length and a diameter of about 5 cm. Inside the tube pumping lines are mounted as well as tubes through which electrical wires, contacting the sample, piezo-element, local heater and thermometer are running. The mechanical axle used for the coarse movement of the piezo-element is running through the center of the tube. The axle is connected via a vacuum sealing O-ring to a rotatable screw, which can be rotated manually or with the help of an electro-motor. At the bottom of the metal tube the MCBJ sample can be mounted in a three-point bending configuration and a vacuum pot can be attached to the bottom of the insert in order to create a vacuum chamber for the sample. The design of the insert is such that it provides for three important experimental conditions:

Firstly, a good vacuum in the sample chamber at the bottom of the insert. This is achieved by connecting the vacuum chamber via the pumping lines to a turbo-molecular pump. After pumping and baking the insert mildly to about 90 ^{o}C overnight a pressure of about $1{\cdot}10^{-5}$ mbar is reached at the top of the insert. Due to the high pumping resistance of the narrow pumping lines the pressure in the sample chamber will inevitably be higher. When the insert is immersed in liquid helium the pressure at the top of the insert, which remains at room temperature, drops below $1{\cdot}10^{-6}$ mbar and in the sample chamber a

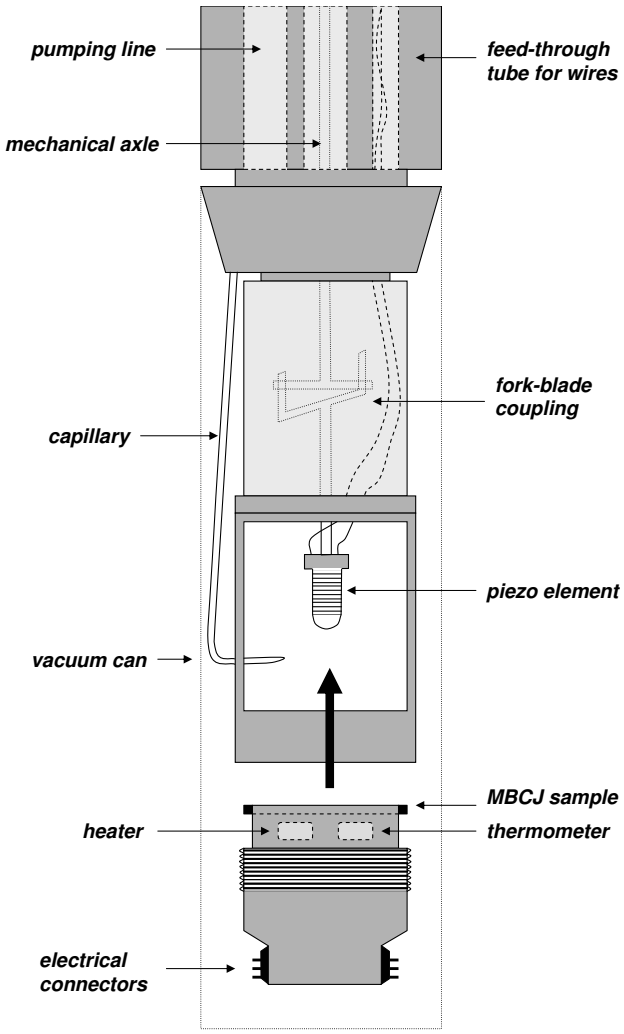

Figure 2.7: *Schematic view of the bottom part of the insert used for MCBJ experiments. The MBCJ sample holder at the bottom of the drawing is placed by screwing it inside the insert such that the piezo element presses onto the bending beam. Electrical wires (not shown) can be connected to the electrical connectors.*

much lower pressure (around 10^{-10} mbar) can be expected due to cryogenic pumping.

Secondly, the vacuum can and the sample have to be cooled efficiently to cryogenic temperatures. The cooling of the vacuum can is straightforward by immersing the insert in a cryostat filled with liquid helium. In order for the sample to reach a temperature very close to 4.2 K it needs to have a good thermal connection to the vacuum can and at the same time a bad connection to the

top of the insert, which remains at room temperature. The schematic drawing in figure 2.7 shows that the sample has a direct metal connection to the vacuum can. This ensures the effective cooling of the phosphor-bronze substrate. But the sample is thermally insulated from the substrate by the thin kapton foil and furthermore electrical connections run up from the sample to the top of the insert. To prevent a heat connection as much as possible, very thin copper or manganine wires (d = 25 μm) are used to connect the sample. The wires are also thermally anchored to the vacuum can very close to the sample. The cryogenic environment of the sample is important to ensure a high vacuum in the sample chamber. A major advantage in using the MCBJ is that when the sample is broken for the first time in a cryogenic vacuum environment, the fracture surfaces are extremely clean ensuring excellent experimental conditions.

Thirdly, the insert should provide mechanical stability for the sample, since the measurements are very sensitive for the smallest of mechanical vibrations that can couple into the atomic junction. Because of the displacement ratio, vibrations from outside are reduced by a factor of about 300. Furthermore the mechanical axle can be decoupled from the MCBJ by means of a fork-blade construction. Additionally, the insert is placed in a cryostat that is vibration-isolated from the floor by means of air dampers, which rest on separately founded concrete blocks.

The insert is furthermore equipped with a local heater very close to the sample. With the heater it is possible to heat the sample to approximately 60 K, while the vacuum can remains at the base temperature of about 5 K preventing the desorption of molecules from the walls. The local temperature is monitored with a platinum thermometer mounted close to the junction.

Finally, the insert is equipped with a capillary, which is used for introducing molecules to the junction. The capillary is made from stainless steel and has an inner diameter of 1 mm. The exit of the capillary points directly to the junction area of the MCBJ-sample, ensuring that the ballistic molecules travel straight to the junction without hitting the walls of the vacuum can. A heating wire runs all along the interior of the capillary and serves a twofold purpose. It is used to bake-out the capillary, by heating the inner wall up to 200^{o}C prior to measurements. Secondly, the heating wire prevents the premature condensation of introduced molecules. With this capillary hydrogen, deuterium, oxygen and carbon-monoxide have been introduced successfully to the MCBJ-sample in a cryogenic environment.

2.4.4 The electronics

Two electronic circuits are used for experiments on atomic contacts. One circuit is needed to control the displacement of the electrodes of the junction. This is done with a high-voltage supply, which powers the piezo-element. The high-voltage supply can be operated manually as well as computer controlled. The other circuit is used for two-point conductance measurements. A Digital-to-Analog Converter connected to the computer generates a bias voltage, which is divided and subsequently supplied to the junction. The current

flowing through the junction is converted into a voltage by an I-V converter. The voltage is supplied to the data acquisition card (DAC) and processed by a LabVIEW program.

2.5 Experiments on atomic-size contacts

2.5.1 Conductance histograms

The mechanically controlled break-junction technique is used to pull a macroscopic metal wire apart in order to create a contact of a single atom in diameter. During the pulling and subsequent thinning of the contact the atoms reconfigure continuously causing jumps in the conductance. Because of large the number of involved atoms, even in the last stages of the thinning process, it is impossible to predict beforehand what the evolution of the thinning of the contact and thus the conductance will be. In order to investigate conductance properties of atomic contacts, statistics are used. By repeatedly breaking and remaking the contact and recording the conductance-values that are encountered in the breaking processes a histogram is obtained that provides statistical conductance properties of the atomic contact. Figure 2.8 illustrates how a histogram is constructed. The conductance scale is divided into narrow conductance bins, which are filled with the number of times a measured conductance, for each of the breaking traces, fits in the bin's width. The resulting histogram taken for a copper MCBJ sample at T = 5 K is constructed from about 1000 breaking traces. Peaks in conductance histograms indicate conductances that are preferentially encountered in the final stages of breaking a nanowire. For the noble metals the conductance histograms are always dominated by a large peak at 1 G_0, which is interpreted as the conductance of a junction formed by a single metal-metal bond between two single atoms at the apexes of the electrodes [28]. This configuration occurs nearly always when pulling a wire apart.

2.5.2 Length histograms

Gold is a noble metal, resulting in a conductance of around 1 G_0 for a single gold atom contact. One would expect that since this is the smallest possible contact that can be made, additional pulling on this contact will result in the rupture of the contact. As will be discussed in more detail in chapter 3 this is not always the case for gold. Very often a wire of single gold atoms can be created, which retains a conductance of around 1 G_0 since it remains a ballistic conductor. The length of these one-dimensional structures can be measured with the MCBJ technique. In the previous section it was explained how the displacement of the two electrodes can be calibrated. The configuration in which both electrodes end in a single gold atom and the gap is bridged by a single gold-gold bond, has a conductance close to 1 G_0 [28]. This well defined relationship between conductance and geometrical configuration of the contact is the ideal starting point for the length measurement. A LabVIEW program is

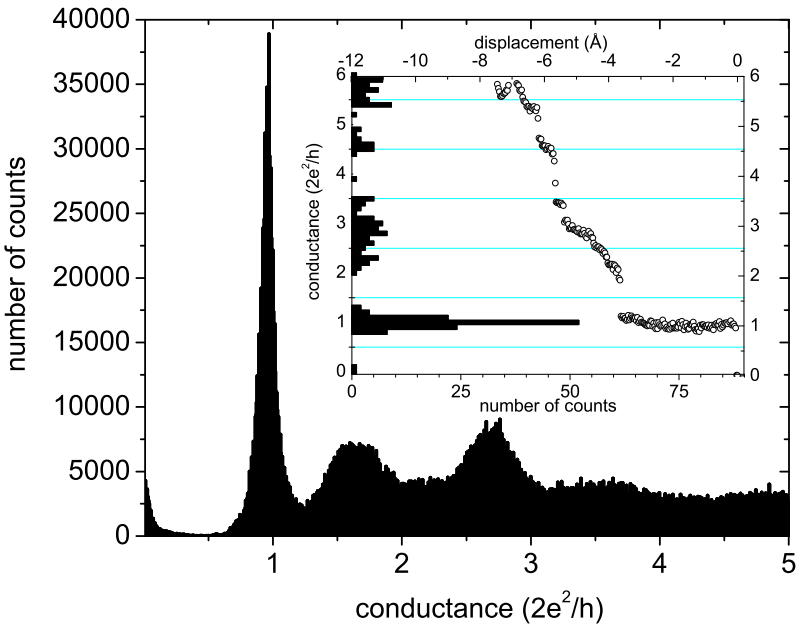

Figure 2.8: *Construction of a conductance histogram for copper at T = 5 K. The histogram was constructed from about 1000 breaking traces and a bias voltage of 50 mV was used. The inset shows for a single trace how the conductance bins are filled with the number of encountered conductance values.*

used that measures the difference in voltage over the piezo between the moment that the conductance of the circuit drops below 1.1 G_0 and the moment when the gold wire breaks, resulting in a abrupt decrease of the conductance deep into the tunneling regime. After the rupture the piezo voltage is reduced, which moves the two electrodes back towards each other. After reestablishing a sufficiently large mechanical contact (G>15 G_0) a new breaking run is commenced. As in the case of obtaining statistical knowledge about the conductance properties of atomic contacts, also the length measurements are done statistically. By repeating the length measurement many times, one can construct a so-called length histogram, as shown in figure 2.9. It is clear that well defined peaks emerge in the chain-length measurement. Those peaks indicate chain lengths, which have a larger probability for breaking. In chapter 3 the interpretation of the peaks and the properties of atomic chains will be explained in detail.

2.5.3 Differential conductance measurements

With the MCBJ technique in a vibration-isolated system at cryogenic temperatures it is not only study statistical properties of atomic contacts and wires, but

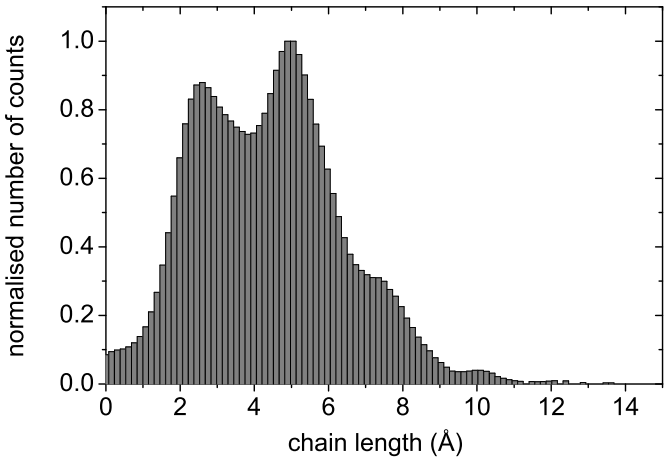

Figure 2.9: *Length histogram for gold at 5K. The peaks indicate chain lengths that have a larger breaking probability. The histogram is built up from about 3000 breaking events and the bias voltage was 50 mV.*

it is also possible to keep a freely suspended atomic wire stable for hours. This allows us to measure conductance properties of individual contacts by means of Point Contact Spectroscopy (PCS) or differential conductance (dI/dV) spectroscopy. Measuring the conductance of a contact differentially is much more sensitive than measuring I-V characteristics directly. It is possible to measure differences in conductance of less than one percent with sufficient accuracy. PCS is similar to Inelastic Electron Tunneling Spectroscopy (IETS), a technique that recently became popular in STM experiments . A main difference is that the previous one is performed when there is physical contact between two materials (resulting in a much lower resistance), as is the case for atomic contacts. A large advantage of PCS over IETS is that since PCS is performed on contacts with a much higher conductivity the RC-time of the circuit is much smaller, making a higher modulation frequency and thus a faster current sweep possible. A typical current sweep from +100 mV to -100 mV for a single gold atom contact can be done with a high resolution in 10 seconds.

A Lock-in amplifier is used to measure dI/dV. An AC signal with an RMS amplitude of 1 mV and a frequency of about 7 kHz is added to the DC input signal for the sample. The DC signal can be swept from positive to negative voltages and vice versa. The response signal originating from the sample is connected to the input of the Lock-in amplifier, which generates a voltage proportional to the first harmonic of the input signal. The first harmonic is proportional to the the first derivative of current to voltage, provided that the modulation amplitude is small compared to the energy scale of the non-linearities in dI/dV.

2.5.4 Using PCS to identify vibration-mode energies

By studying the PCS signal originating from inelastic electron scattering events it is possible to identify vibration-mode energies of the atoms or molecules present in the contact under study. The pioneering work in the early 1970's by Yanson *et al.* [30] on the non-linear I-V characteristics for thin metallic layers separated by a dielectric, led to the development of the theory of PCS in larger metallic contacts (i.e. with a resistance up to 10 Ω) for which Sharvin's formula holds [31]. It describes the spectroscopy in terms of a non-equilibrium electron distribution close to the contact as a result of the applied bias voltage.

Suppose that electrons arrive in the left electrode and have an energy eV higher than those in the right electrode as is schematically drawn in figure 2.10 (a). Since a point contact is ballistic, electrons travel through the contact and arrive at the left electrode retaining an energy eV larger than the Fermi energy. In order for those electrons to equilibrate with the Fermi sea they have to loose energy by scattering inelastically with e.g. phonons. The electrons can scatter in all directions. Figure 2.10(b) represents how a part of the scattered electrons can travel back through the contact and thus reduce the net current flowing from left to right. The cone with an angle corresponding to the solid angle determined by the orifice represents the part of the total electron population that can contribute to the backscattering when the scattering occurs at the position pictured in the figure. It is easy to understand that as the energy difference between the left and the right becomes larger, the relative contribution to the backscattering becomes larger as well. Furthermore, it

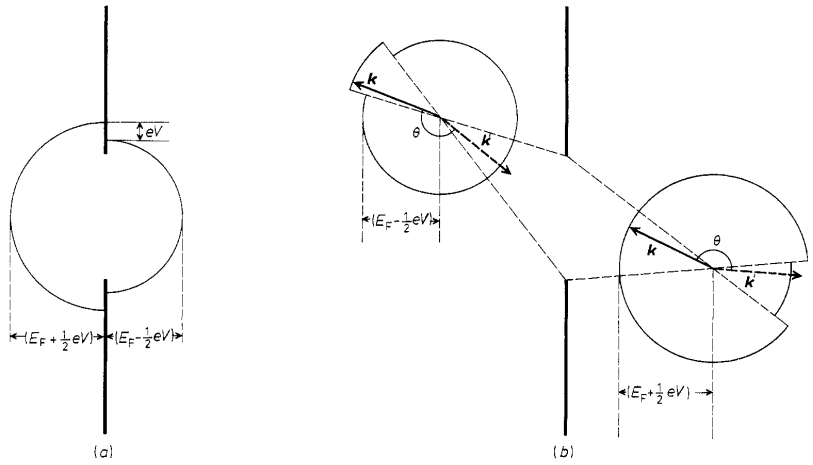

Figure 2.10: *Schematic drawing of the electron distributions in the Sharvin regime at the contact (a) and at positions near the contact (b). Electrons that scatter inelastically and change their wave vector from k to k' within the solid angle contribute to a correction to the current through the orifice. Taken from Ref. [29].*

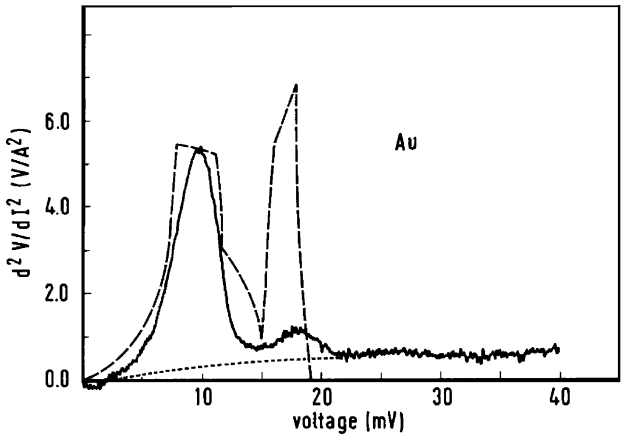

Figure 2.11: *Comparison between gold phonon density of states obtained by PCS and by neutron diffraction. Continuous line: d^2I/dV^2 spectrum obtained for a gold point contact with R = 3.3 Ω at T = 1.2 K. The dashed line represents the phonon density of states as was measured using neutron diffraction. Data taken from Ref. [29].*

is also clear that the probability for an electron to scatter back within the solid angle decreases with the square of the ratio (a/d) of the orifice radius (a) over the distance of the scatter center to the orifice (d). Therefore the backscattered current is almost entirely generated in a small spherical volume with radius $\sim a$. From early work on electron transport through metallic point contacts was concluded that PCS can be used as a tool to determine the phonon density of states of the metal [29–35]. It can be shown that d^2I/dV^2 is proportional to the electron-phonon interaction, which reflects the phonon density of states [29,32]. Figure 2.11 shows an example for a d^2I/dV^2 spectrum taken for a gold point contact. Clearly the resulting phonon spectrum, as obtained from PCS spectroscopy (continuous line) overlaps with the phonon density of states obtained from neutron diffraction (dashed curve). When the contact diameter is reduced to only a single atom the probability for electrons to backscatter is reduced, because of the ratio $(a/d)^2$. This ratio also limits the region from which electrons can inelastically scatter back to only about one lattice distance away from the contact or in the contact itself. An important consequence is that the d^2I/dV^2 spectrum no longer represents the bulk phonon density of states, but rather indicates the energy of local vibration-modes of, ultimately, the single atom or molecule in the contact.

Since the current reduction due to electron backscattering is very small for single atom contacts (typically about 1%), it can easily be hidden in conductance fluctuations that arise from interfering electron waves, which have scattered close to the contact [36, 37]. But when the current is carried by a single nearly fully transparent conduction channel, these fluctuations are severely suppressed [36, 38], creating the possibility for experimentally observing local

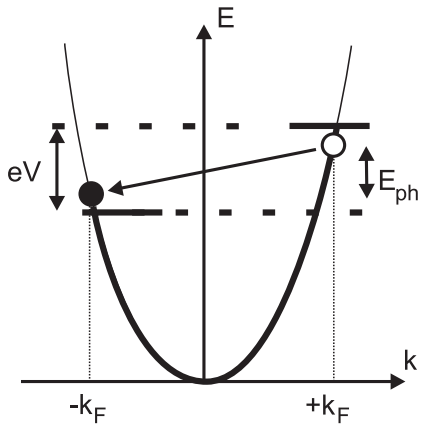

Figure 2.12: *Schematic view of the electronic states in a monovalent atomic chain. Since the chain is a ballistic conductor the chemical potentials of the forward (positive k) and backward (negative k) traveling states differ by an amount eV. In case of a fully transparent conduction channel the momentum change of the scattered electrons will always be close to* $2\hbar k_F$.

vibration-modes of a single-atom or molecule contact. A simplified picture of the backscattering process in this case is shown in figure 2.12. In this figure the electron band is represented by a single free-electron parabolic band. The right-moving electron states are filled up to an energy $E_F + eV$. When an inelastic scattering event occurs with a phonon, the electron with wave vector k_F loses an energy equal to E_{ph} and since all right-moving states are occupied below $E_F + eV$ the electron has to scatter to a left-moving state with a negative wave vector $-k_F$, causing a net reduction of the electron current. The backscattering will only occur when the transmission of the channel is close to one, since when the transmission is very low (as is e.g. the case for a tunnel junction) the picture reverses such that the left-moving states are filled up to $E_F + eV$ and the right-moving states empty, because almost all conduction electrons are reflected by the contact. This results in forward scattering after an electron has scattered inelastically and a net increase of the electron current. It has to be mentioned that this simplified picture of the PCS process does not correspond to the accepted framework based on Green's functions formalism [39–42], but the effect of the inelastic contribution to the current is similar. Differential conductance spectroscopy will be used in this thesis to determine the presence of small foreign atoms or molecules in atomic contacts and chains. Since the incorporated atoms or molecules have a much smaller mass than the metal atoms that contact them, the vibrational energy should be distinctly higher.

3

Formation and properties of metal-oxygen atomic chains

The formation and electrical and mechanical properties of atomic chains of noble metal atoms with incorporated oxygen have been studied. While monatomic chains of single gold atoms usually do not become longer than seven atoms, the incorporation of oxygen significantly enhances the linear bond strength between the individual atoms in the chain and therefore longer chains can be formed. Even more dramatically it is found that oxygen induces atomic chain formation in the noble metals silver and copper that in pure form do not form chains. The energies of local vibration-modes of these new atomic chains have been measured and they correspond very well with a simple model and preliminary DFT calculations. A comparison with several theoretical studies on oxygen incorporation in atomic chains is made, which clarifies the physics behind these remarkable atomic structures.[1]

[1]Parts of this chapter have been published in: W.H.A. Thijssen, D. Marjenburgh, R.H. Bremmer and J.M. van Ruitenbeek, Phys. Rev. Lett. **96**, 026806 (2006) and W.H.A. Thijssen, M. Strange, J.M.J. aan de Brugh and J.M. van Ruitenbeek, submitted to New Journal of Physics.

3.1 Introduction

In recent years physicists have managed to scale down the dimensions of metallic nanocontacts to the point that a contact can be made of only a single atom. Scientists are able to measure the physical properties of these contacts like the conductance, which is determined by the chemical valence of the metal under investigation [4]. Single atom contacts of monovalent metals like gold, silver and copper have a single conductance channel that is nearly fully transmitting, resulting in a conductance very close to $2e^2/h$ (= 1 G_0), as was discussed in chapter 2. Vibration-modes of the atom or molecule in the contact [43] have been measured as well as the linear bond strengths between the atoms [44–46]. Most intriguingly some metals, namely gold, platinum and iridium have been shown to have the tendency to form atomic chains of single atoms [6, 47]. This is the ultimate one-dimensional conductor and has a diameter of a single atom. The formation of these atomic wires has been supported by theoretical calculations [48–51]. Theory and experiment have indicated that the linear bond strength in a monatomic gold atomic chain is about twice as large as a single bulk bond [44, 51]. This opens the possibility for competition between linear bonds in the chain and atoms at the electrode apexes, which are bonded by only a few bulk bonds. By pulling on these weakly bound atoms, they can be pulled away from the electrodes into the atomic chain. The physical mechanism responsible for the increase in linear bond strength has been attributed to a relativistic contraction of the low energy s-electrons that move with a substantial fraction of the speed of light around the highly charged nucleus of e.g. a gold atom [47]. Due to the contraction of these electron orbitals their energy becomes slightly reduced. Since all s-orbitals are orthogonal, they will all be lowered in energy, which leads to a small lowering of the Fermi energy E_F. Because the d-electrons do not come close to the highly charged nucleus, their energies will remain unaffected. This results in a small depopulation of the d-band, since E_F is lowered. Since the states at the top of the d-band are of anti-bonding character, the depopulation will increase the bonding by the d-electrons. Later in this chapter a closer look at the bonding mechanism in atomic chains will be taken. At the time of the discovery of the formation of atomic chains two groups independently published the observation of atomic chains coincidentally in the same issue of *Nature* in 1998. Yanson *et al.* used a Mechanically Controlled Break-Junction (MCBJ) technique at cryogenic temperatures, as has been described in the previous chapter of this thesis [6]. Ohnishi *et al.* on the other hand used a very different technique by employing an Ultra High Vacuum-High Resolution Transmission Electron Microscope (UHV-HRTEM) to image the chains [5]. They prepared a freely suspended Au foil in which holes were burnt by using a high intensity electron beam from the TEM. The diameters of the two holes were delicately enlarged until only a single row of atoms separated them. By reducing the electron beam intensity they were able to image a chain of single gold atoms as can be seen in figure 3.1. The atomic chains such as the one that is shown in figure 3.1 are stable for about a second. It was very surprising that atomic gold chains seemed to

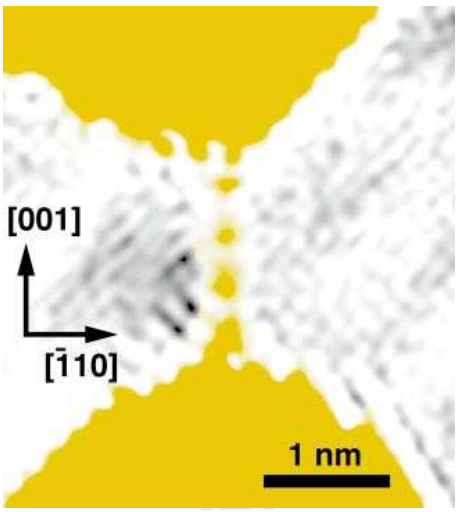

Figure 3.1: *HRTEM image of a suspended atomic gold chain taken by Ohnishi et al. [5]. The electrodes are situated at the top and bottom of the image. From the image it can be clearly seen that the interatomic distance between the gold atoms can be as large as 4 Å. The irregular structure left and right of the chain is due to interference of diffracted electron waves.*

be stable, albeit for a very short time, at room temperature. A very striking result from this observation was that the interatomic distance in the atomic chain was close to 4 Å, being much larger than the interatomic distance of 2.6 Å that is experimentally reported for atomic chains at 4.2 K [52] and calculated by molecular dynamics simulations [51]. It has since been suggested that the explanation for the large interatomic distances involves the incorporation of small foreign molecules. Many simulations have indeed been done on atomic wires with incorporation of foreign impurities: Hydrogen [53–55], nitrogen [53], carbon [53, 55, 56] and oxygen [53, 57, 58]. From these simulations oxygen stood apart since it was not only a likely candidate to be present in a room temperature UHV experiment. Furthermore it was predicted that incorporated oxygen would cause the linear gold-oxygen bond to be stronger than a gold-gold bond [57] or that the overall strength of the linear bonds in an atomic gold chain would be enlarged [58]. Therefore oxygen is an interesting candidate to investigate what its influence on atomic gold wires is.

3.2 The formation of atomic chains

Atomic wires of a single atom in diameter can be created with the MCBJ technique as was demonstrated by Yanson *et al.* [6] and discussed in chapter 2. A macroscopic gold wire is gently broken and in the breaking process the conductance is measured. What is typically observed in the final stages of the thinning process is a step-like decrease of the conductance, because of atomic

reconfigurations of the contact upon elongation, up to the point when the contact diameter is only the size of a single gold atom (see figure 3.2). A single gold-gold bond bridging two contacts has a nearly fully transmitting single channel conductance close to G_0. Upon further stretching the single gold atom contact there is a relatively high probability that the contact does not break but that more atoms are pulled from the electrodes to form a chain of single gold atoms. The formation of such an atomic chain is indicated by the long plateau at 1 G_0 in figure 3.2. Since the interatomic distance is about 2.5 Å the atomic chain that was formed in the figure was about 5 bond lengths long. An atomic chain is suspended between two electrodes and is kept under tension. Once the tension becomes too large the chain breaks at its weakest point, which is usually at the point where the chain is contacted to the banks. The chain breaks once the force needed to pull an additional atom out from the electrodes is larger than the force needed to break a linear gold-gold bond. Immediately after rupture of the chain the atoms that comprised the chain, will collapse back to the electrodes and the conductance will drop deep into the tunneling regime ($<$ 1 nS). Mechanical contact between the electrodes is remade by moving the electrodes towards each other again until the closest apex atoms from each of the two electrodes bind to each other and the conductance jumps to a value

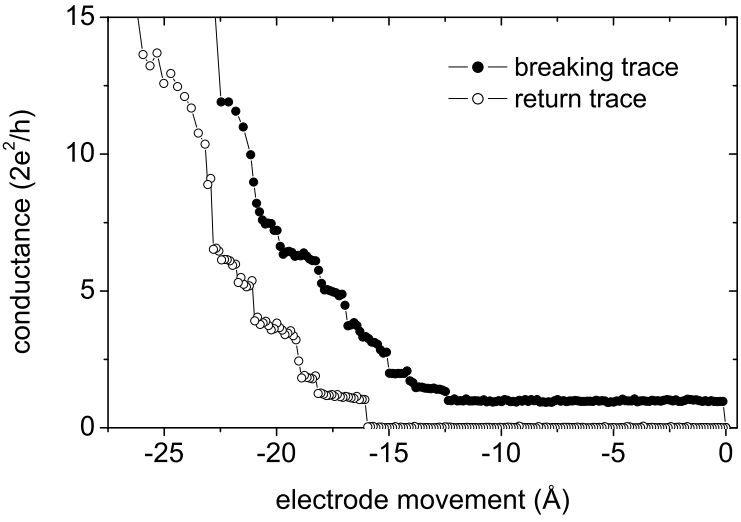

Figure 3.2: *A breaking trace of a Au contact as function of electrode movement. It can be clearly seen that the plateau at $2e^2/h$ is 12.5 Å long, which is much longer than the dimensions of a single gold atom. The return trace shows the evolution of the conductance when the electrodes moved towards each other after the chain had been broken. This trace was taken at T = 5 K with a bias voltage of 50 mV.*

of order $2e^2/h$. In figure 3.2 the so-called return trace is also shown. The displacement of the electrodes towards each other is typically about the length of the previously formed atomic chain. This is easily understood since the atoms have collapsed back to the electrodes leaving a vacuum gap of order of the length of the chain between the two electrodes. In figure 3.3 the average return length as a function of atomic chain length for the case of gold is displayed. From the graph it can be seen that the average return length has a finite value of about 4 Å when the chain length is close to zero. This can be explained by the relaxation of stress that was built up in the electrodes during the elongation process. Once mechanical contact has disappeared the atoms in the electrodes move back to their equilibrium position and the electrode apex moves slightly back. At the point that the atomic chains become longer than 4 Å the average return length increases linearly with increasing chain length, providing very strong support for the idea that atomic chains are indeed being formed.

To convince even the most sceptic readers, Yanson *et al.* [6] were able to conduct yet another experiment that confirmed the existence of atomic chains. By making use of a Scanning Tunneling Microscope (STM) they were able to move one of the two electrodes in lateral directions. In figure 3.4 the lateral displacements of a short and a long atomic chain are compared to each other. When atomic chains are indeed being formed it is expected that lateral displacement increases proportionately with the length of the chain. This is exactly what was demonstrated by Yanson *et al.*

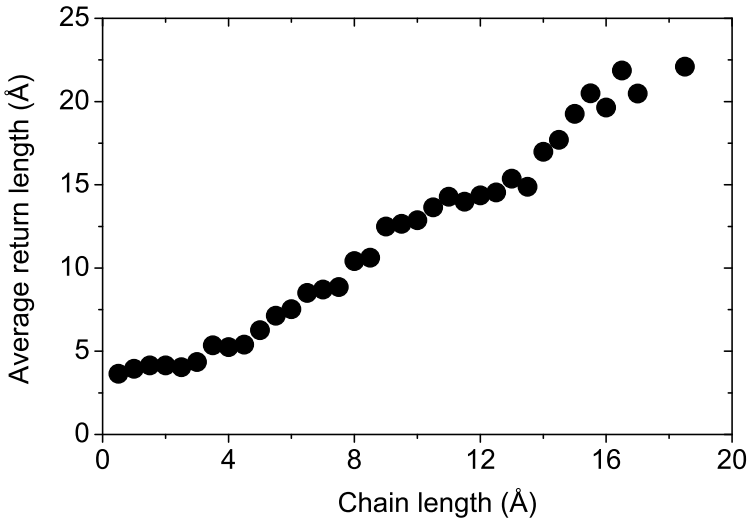

Figure 3.3: *Average return length of the electrodes for reestablishing physical contact between each other after an atomic gold chain is broken. The measurement is the average of about 3000 traces and was taken at T = 5 K and V_{bias} = 50 mV.*

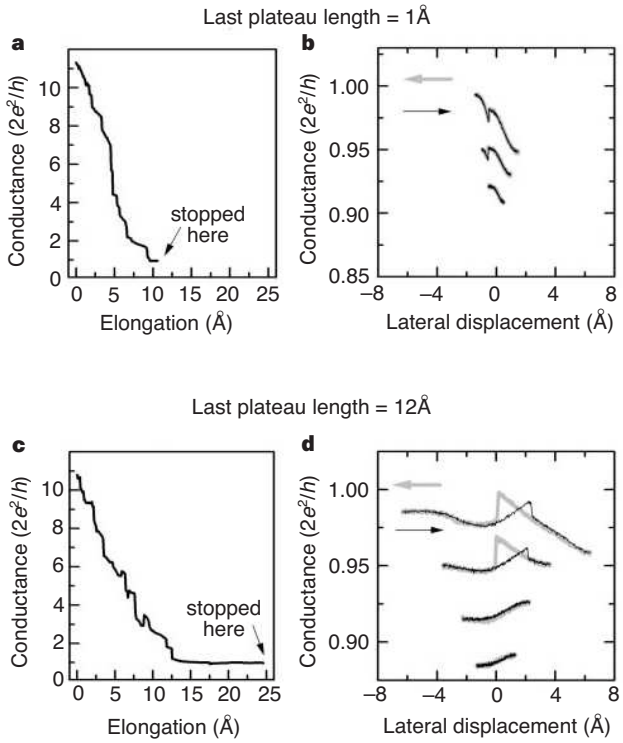

Figure 3.4: *Figure (b) shows the lateral displacement of the 1 Å long chain of figure (a). Figure (d) shows the displacement of the 12 Å long chain of figure (c). The lower two or three curves in (b) and (c), respectively, have been offset by steps of 0.05 $2e^2/h$ for clarity. Clearly the longer chain can laterally be displaced further. Data taken from Ref. [6]*

3.3 Investigation of atomic chains

The previous section gave extensive evidence for the existence of atomic chains of single atoms. Now a more quantitative investigation of the atomic chains is presented.

As illustrated in figure 3.2 every time the gold electrodes are pulled apart a chain of certain length can be formed. It is very interesting what the distribution of chain lengths will be when a few thousand breaking events are performed after each other. In subsection 2.5.2 is described how the length of an atomic gold wire, having a conductance close to 1 G_0 is measured. Now, the displacement of the electrodes is measured in an conductance window of [1.1-0.5] G_0. This means that from the moment the conductance of the contact drops below 1.1 G_0 the displacement of the electrodes starts to be measured. Once the conductance drops below 0.5 G_0 the length measurement is stopped. By repeating the chain forming, chain breaking and remaking contact sequence a few thousand times and subsequently plotting the number of times a certain

chain length is observed versus the chain length, a so-called length histogram is constructed. Figure 3.5 shows a length histogram for gold at T = 5 K, which gives the distribution of chain lengths at which rupture occurred in a large ensemble of chain formation events.

The length histogram shows a periodic sequence of peaks that occur at intervals of 2.5 $\pm$ 0.2 Å. These peaks identify lengths of atomic chains that have a higher probability of breaking. The periodic distance between the peaks has been interpreted as the interatomic distance of the atoms in the atomic wire [6, 47]. One can understand this in the following way. Upon thinning the contact a configuration is reached in which both electrodes end with a single gold atom and the conduction electrons travel through a channel that is a single linear bond between those two gold atoms. This is the configuration that has a conductance close to 1 G_0 [28] and is depicted in figure 3.6(a). Starting from that moment the displacement of the electrodes is measured. By elongation of the contact the gold-gold bond is being stretched up to the point that it can either break or pull out an additional gold atom from the bulk. When the bond breaks, the conductance drops into the tunneling regime and the length measurement is stopped. These events are represented by the first peak in the length histogram of figure 3.5. When an additional gold atom is pulled into the chain the bonds in the chain relax as has been seen in force measurements [44–46]. The atomic chain can then once again be stretched up until it

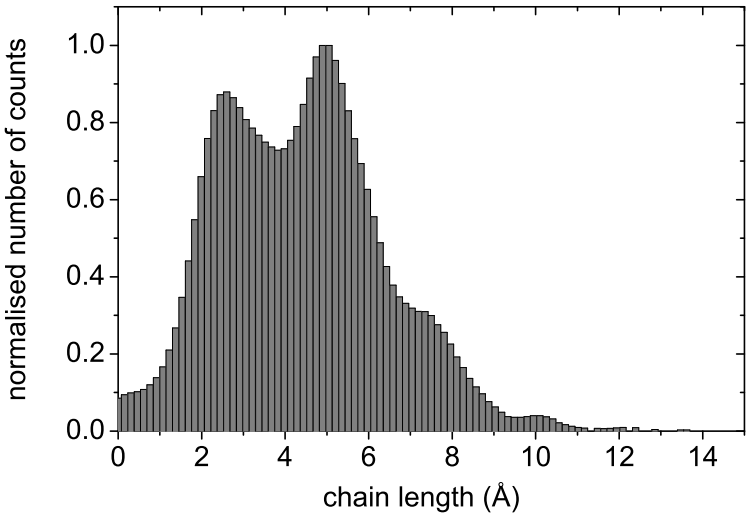

Figure 3.5: *Length histogram for gold at 5 K. The peaks indicate chain lengths that have a higher breaking probability. The histogram is built up from about 3000 breaking events and the bias voltage was 50 mV.*

reaches its critical stress as in configuration (b) in figure 3.6. Again a larger stress results in either a rupture or the addition of another atom from one of the electrodes into the chain. Upon breaking the length is recorded which adds to the second peak in the length histogram. This repeated build-up of critical stress and the consequent rupture of the chain or incorporation of another atom delivers the ensemble of atomic chains lengths that make up the length histogram. The peaks in the length histogram therefore indicate chain lengths in the maximally elongated configuration before rupture. The distance between the peaks signify the interatomic distance of a maximally stretched gold-gold bond in a gold chain, which is 2.5 ± 0.2 Å.

From the length histogram of figure 3.5 one can clearly see that chains of two and three atoms in length are very regularly formed. Longer chains have a rapidly decreasing probability to be formed and chains of seven atoms are hardly ever observed. Most probably this depends on the final configuration of the gold atoms that make up the apexes of the electrodes from the moment the chain formation starts. As was explained the chain elongation process is a repeated sequence of critical stress build-up in the chain and the consequent incorporation of additional atoms from the electrodes, which relaxes the stress. An atom will however only be incorporated in the atomic chain when it is weakly bound to the remainder of the bulk atoms. The linear bond is twice as large as a bulk bond, but when a gold atom is bound to more than two bulk bonds in the electrode, the linear bond at the position where the last atom of the chain is bound to the electrode will break. This ultimately means that the length of an atomic gold chain is pre-determined by the number of weakly bound atoms available at the apexes of the electrodes. Once the supply of weakly bound atoms is depleted the chain will break once the stress on the linear bonds increases beyond the maximal stress.

The phonon modes of these one-dimensional monatomic chains have been studied by Agraït *et al.* [43, 59] by means of point contact spectroscopy. This spectroscopic technique was discussed in chapter 2. Agraït *et al.* identified for short atomic chains a transversal mode in the range of 4 to 8 meV and a longitudinal mode in the range of 15 to 20 meV similar to what is observed in bulk

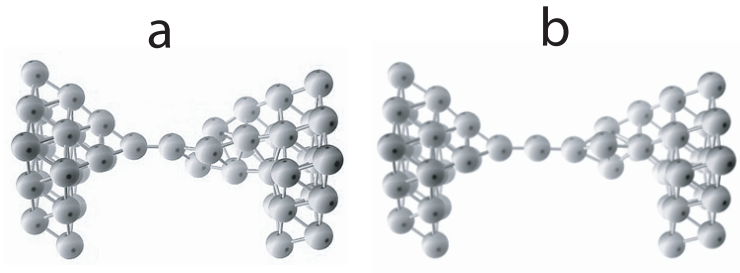

Figure 3.6: *Figures (a) and (b) show atomic chain configurations for the lengths around the first and second peak in the length histogram of figure 3.5.*

gold contact spectra [29]. For long chains consisting of about 6 or 7 atoms only the longitudinal mode is observed since the chain is a quasi one-dimensional structure. The conduction electrons passing through the chain have a very small perpendicular k-vector component and they therefore have a very small coupling to transverse phonons. The energy of longitudinal phonon modes will be reduced when the linear bond between the gold atoms is stretched due to weakening of the bond strength, since $E_{phonon} \propto \sqrt{\kappa/m}$ with κ the force constant and m the mass of the atom. This can be nicely seen from figure 3.7 in which a short 4.5 Å long gold chain in (a) is elongated for about 0.5 Å in (b). The energy of the longitudinal phonon mode decreases from about 20 meV in figure 3.7(a) to about 15 meV in (b).

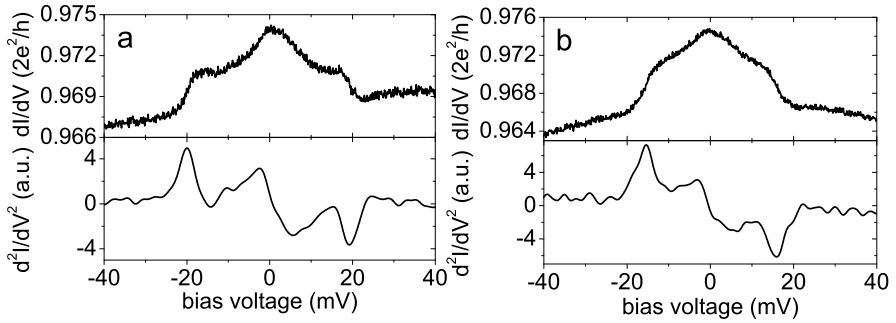

Figure 3.7: *Differential conductance (dI/dV) spectrum of a 4.5 Å long atomic gold chain is displayed in (a). The chain was elongated for 0.5 Å and the dI/dV spectrum for the stretched atomic chain is shown in (b).*

Only one longitudinal mode will be excited in a one-dimensional atomic chain. This is a consequence of the fact that in a monovalent metal like gold only one conductance channel, that is nearly fully transparent, is contributing to the conductance. Since the voltage drop takes place almost completely over the atomic chain, which is a ballistic conductor, the energy of the highest occupied forward and backward traveling electron states differ by an energy equal to the bias voltage eV. When an electron scatters inelastically with a phonon, the electron will lose energy equal to $\hbar\omega_{ph}$. Since all forward traveling electron states are fully occupied up to the Fermi level the electron has to scatter from a state with momentum $+\hbar k_F$ to a state with a negative k-vector $-\hbar k_F$, meaning that the electron is backscattered. Because of momentum conservation the phonon that is emitted in this scattering event needs to have a momentum close to $2\hbar k_F$, which selects the mode at the zone boundary.

3.4 Influence of oxygen on atomic gold chains

3.4.1 The effect of oxygen on the conductance and length of atomic gold chains

It has been discussed that atomic gold chains can be formed at cryogenic temperatures. As was already mentioned in the introductory section, calculations on gold chains with chemisorbed oxygen incorporated have shown that the linear gold-oxygen bond should be stronger than the linear gold-gold bond, which could lead to the formation of longer atomic chains consisting of gold and oxygen. The effects of oxygen on the formation of atomic gold chains has been studied by admitting a small amount of molecular oxygen to the vacuum can in which the gold sample is situated. The exact procedure is described in chapter 2. The first issue that has to be addressed is whether the conductance of a gold chain changes upon reaction with oxygen. Therefore the conductance of atomic gold chains is characterized before and after oxygen admission by means of conductance histograms.

Figure 3.8 shows a conductance histogram of a gold sample before and after oxygen admission. One can clearly see that in both cases a peak at 1 G_0 dominates the histogram. This indicates that a conductance of 1 G_0 occurs in a large number of intervals during the final thinning of the gold contact both with and without oxygen admitted. For clean gold similar histograms have been obtained not only in cryogenic environments but also in UHV at room

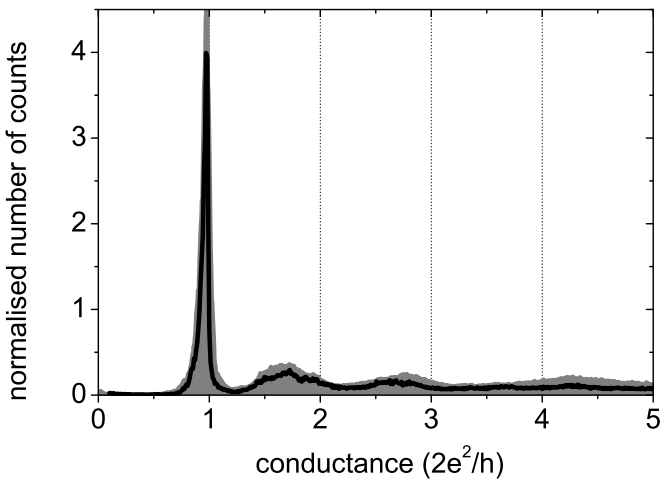

Figure 3.8: *Conductance histogram of clean gold (black curve) and gold with oxygen admitted (filled graph) at T = 5 K. The histograms have been normalized to the area under the curves. A bias voltage of 50 mV was used in both cases and each histogram consists of about 2000 traces.*

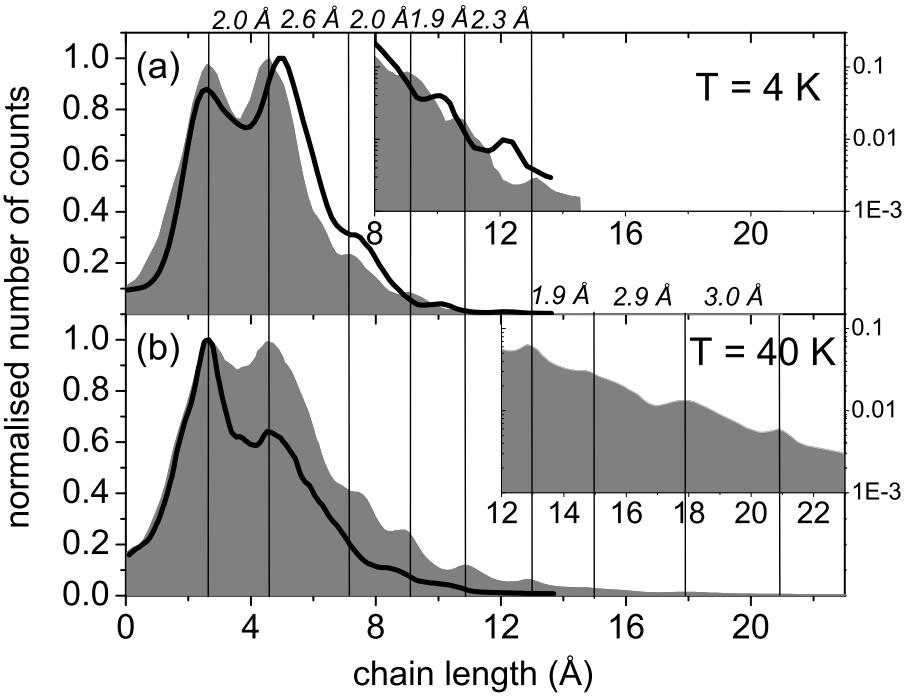

Figure 3.9: *Length histograms for clean gold (black curve) and gold with oxygen admitted (filled curve) at T = 5 K (a) and T = 40 K (b). The conductance window in which the length of the chains was measured was [1.1-0.5 G_0]. A bias voltage of 50 mV was used in all cases and each histogram consists of about 2000 traces.*

temperature using an STM [20,60,61] and even in air at room temperature [62]. The histogram demonstrates an almost 100% certainty of forming a single atom contact when thinning a contact and that the formation of atomic chains is responsible for the large and sharp peak at 1 G_0. The conductance histogram of gold with oxygen admitted at T = 5 K shows no noticeable difference to the clean gold histogram. From this observation two different conclusions could be drawn. First that at liquid helium temperature oxygen does not affect the conductance of a gold atomic contact and also not of a gold atomic chain. Or that oxygen does not react at all with atomic gold chains and therefore one does not see any difference between the two histograms of figure 3.8. To be able to draw a better conclusion about the influence of oxygen on atomic chain formation at 5 K let us take a look at the length histograms that have been measured for a gold sample before and after the admission of oxygen. In figure 3.9(a) a length histogram for clean gold (black curve) is compared to one for gold with oxygen admitted (filled graph). Indeed one can immediately see that the average chain length does not become longer once oxygen is admitted to the gold sample. But a remarkable change is observed when the distance between the

peaks in the length histogram is scrutinized. While the inter-peak distance for clean gold is 2.5 $\pm$ 0.2 Å between all peaks, for gold-oxygen one can clearly observe a distance of about 1.9 Å between the first two peaks. Taking a look at the other peaks results in the observation of two sets of inter peak distances, namely 2.5 $\pm$ 0.2 and 1.9 $\pm$ 0.2 Å. Previously it was concluded that the inter peak distances are in fact the interatomic distances or linear bond lenghs in the atomic chain. This would mean that two different linear bond lengths are present in gold atomic chains that have been exposed to oxygen. How can this be explained?

DFT calculations have predicted that atomic oxygen can be incorporated in an atomic gold chain [57]. The observation from the length histograms of figure 3.9(a) is the first experimental evidence that this is indeed the case. In order to back up this claim it should first be made clear how molecular oxygen can dissociate at such low temperatures on a gold atomic contact. This is indeed not at all trivial because gold is known to be a very inert element that in bulk form hardly reacts with any compounds. It should however be remembered that we are dealing here not with gold in its bulk form, and thus with bulk properties, but with gold on the atomic scale. Previous experiments have shown that bulk gold can indeed dissociate molecular oxygen, albeit at temperature far above room temperature [63]. Gold nanoparticles have displayed strong catalytic behavior at room temperature [64]. However, experiments with gold nanoclusters have not yet been done at cryogenic temperatures. Calculations suggest that upon lowering the coordination number of gold atoms in nanosystems the interaction energy of a gold nanocluster per oxygen molecule increases dramatically from -0.5 eV/molecule for gold atoms with a coordination number of 9 in a cluster, to -1.8 eV/molecule for an atomic chain [57]. It could therefore be possible that oxygen molecules dissociate even at cryogenic temperatures as long as they are able to react with a lowly coordinated gold system, preferably an atomic chain.

Recently, simulations have introduced yet another mechanism that could be responsible for dissociation of (oxygen) molecules at very low temperatures. The mechanical motion of the electrodes causes a forced motion of the atoms close to the apexes of the electrodes. This motion and consequent stress that is being exerted on the atomic and molecular bonds is shown to be so large that it can surmount the activation energy barrier and thus cause dissociation of the oxygen-oxygen bonds [65]. The energy for breaking an oxygen-oxygen bond is then supplied directly by the mechanical motion of the electrodes.

The chemical reaction of oxygen molecules with an atomic contact has an activation barrier that is difficult to surmount at 5 K but it should be easier at elevated temperatures. Therefore experiments were done in which the gold atomic contact was heated to higher temperatures. In figure 3.9(b) one can see a length histogram for clean gold and for gold with oxygen admitted at 40 K. In the case of clean gold it is clearly seen that the higher temperature hinders the chain formation process, because compared to 5 K less peaks are observed, the second peak of the histogram is severely suppressed, and the average chain length is shortened. This can be explained by the higher mobility

of the gold atoms in the electrodes and the larger thermal vibrations, which both cause the atomic chains to be intrinsically less stable and the higher mobility reduces the stability of the suspension points to the electrodes. After oxygen has been admitted the conductance of the atomic chains does not significantly change and the length recording was still done in the conductance interval G $\in$ [1.1,0.5]. The length histogram at 40 K is surprising because the average chain length is considerably larger. Up to nine peaks can be counted in the length histogram, which would mean that atomic chains consisting of up to ten atoms have been formed. This is even more than for clean gold at 5 K. Indeed, chains of more than 23 Å in length have been observed. When the temperature was increased further, the average atomic chain length was not observed to be enhanced further and at temperatures above about 60 K a slight decrease in the average chain length was observed, indicating that from about that temperature the thermal energy and mobility of the atoms became so large that it started to have a negative effect on the chain formation process. How to explain the seemingly contradictory observation that oxygen enhances atomic chain formation at 40 K, while it does not do so at 5 K?

As was mentioned before an activation barrier exists for dissociating oxygen molecules on the low coordinated gold contact or chain. Since the gold atoms in the atomic chain have a coordination number of only two, the effective activation barrier for dissociation will be smaller for oxygen molecules that land directly on an atomic chain than when they land on the contact apex, since the atoms are higher coordinated. It is very well possible that at 5 K the oxygen molecules can only overcome the barrier when they land on the chain, while when they land on the contact apex they will be physisorbed and stay immobile at their landing spot. The probability for those oxygen molecules to get dissociated at 5 K is therefore very small. However, the inter peak distances of the gold-oxygen length histogram that was recorded at 5 K can be understood by taking into account only one oxygen molecule that has been dissociated, resulting in two oxygen atoms. In order to make this clear it is best to look at table 3.1 in which the most probable atomic chain compositions at the observed peaks from the length histogram in figure 3.9(a) are given. The gold-gold distance is taken to be 2.6 Å, while the gold-oxygen distance is varied around the theoretical value of 1.9 Å [57]. From the table it can be concluded that, only two oxygen atoms are sufficient to explain all peak positions, meaning that the dissociation of only a single oxygen molecule could explain the experimental observation.

When taking a look at the gold-oxygen length histogram at 40 K on the other hand, it is clear that it takes more than two oxygen atoms to explain all possible chain configurations. The thermal energy at 40 K is already one order of magnitude larger than at 5 K, which could lead to easier dissociation of oxygen molecules, supplying more oxygen atoms that can be incorporated in the atomic chain. Additionally the thermally activated diffusion of oxygen atoms and molecules on the electrodes will be larger at 40 K than at 5 K, resulting in a higher probability of having an oxygen atom present at one of the apexes of the electrodes at the moment that the atom is pulled into the atomic chain. These

peak position (Å)	chain composition	number of Au-O bonds	length of Au-O bond (Å)
2.6	>Au-Au<	0	-
4.6	>Au-Au-O<	1	2.0
7.1	>Au-Au-Au-O<	1	1.9
9.1	>O-Au-Au-Au-O<	2	1.9
10.8	>Au-O-Au-Au-Au-O<	3	1.9
13.2	>Au-O-Au-Au-Au-O-Au<	4	2.0

Table 3.1: Gold-oxygen chain configurations that fit the experimental peaks positions from the length histogram of figure 3.9(a) recorded at 5 K. The left and right electrode are indicated by > and <, respectively.

differences can explain the observation that atomic gold chains after admission of oxygen become significantly longer when the sample temperature is in the range of 40-60 K and not at 5 K, because of the larger supply of dissociated oxygen at higher temperatures. At still higher temperatures the destabilizing effects due to higher atom mobility and thermal vibrations become dominant over the additional increase in linear bond strength and prevent longer chain formation.

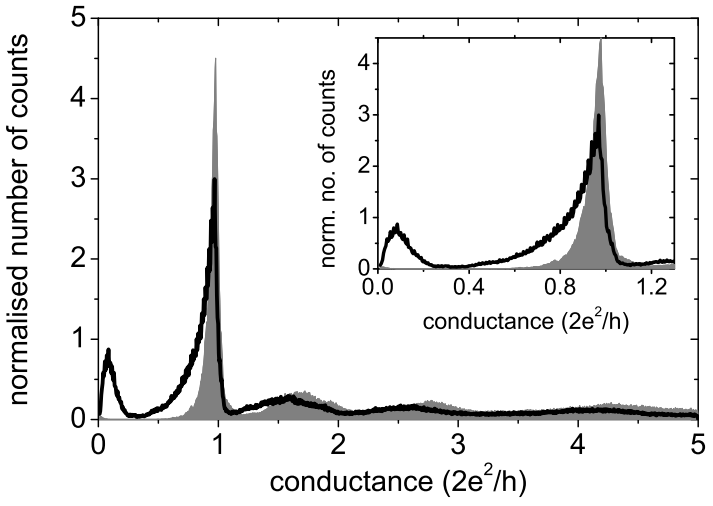

Figure 3.10: *Conductance histograms of gold with oxygen admitted at T = 5 K (filled graph) and at T = 40 K (black curve) normalized to the area under the curves. Both histograms consist of about 2000 breaking traces and a 50 mV bias was used in both cases.*

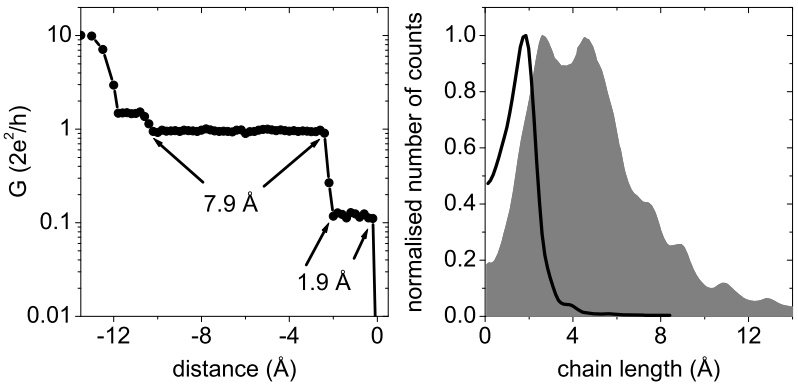

Figure 3.11: *Left panel: A typical breaking trace of a gold atomic chain in an oxygen rich environment at T = 40 K. The vertical conductance axis is in log scale, which enables a clear identification of the conductance plateau at 0.1 G_0. Right panel: Length histogram of gold with oxygen admitted at 40 K (filled graph). The conductance window in which the length was measured was $G \in$ [1.1,0.5] G_0. The black curve gives the length histogram of chain lengths that have been measured in the conductance window $G \in$ [0.2,0.05] G_0. Both histograms were recorded with 50 mV bias and each consists of about 2000 traces.*

The increase of the average chain length can also be concluded from the comparison of the conductance histograms that were obtained from gold- oxygen chains at 5 K and 40 K. In figure 3.10 a conductance histogram of gold contacts with admitted oxygen at 5 K and 40 K is shown. Integration of the area under the two histograms between conductance values of 0.5 and 1.1 G_0 yields a 15% larger area for the histogram at 40 K, indicating a larger contribution of atomic structures that have conductances between 0.5 and 1.1 G_0. This is consistent with the observation that the atomic chains in this conductance range are becoming longer.

Additionally, a peak at low conductance can be seen in the conductance histogram of gold with oxygen admitted at 40 K in figure 3.10. This peak is usually situated at a conductance of about 0.1 G_0 and is never observed at 5 K. It indicates that stable atomic structures are being formed regularly while pulling gold contacts apart in an oxygen rich environment. The left panel of figure 3.11 shows a typical breaking trace that has been recorded when a gold atomic chain was pulled in an oxygen rich environment at T = 40 K. After a chain with a conductance of 1 G_0 and a length of 7.9 Å was pulled the conductance suddenly dropped to a value of about 0.1 G_0. Upon further pulling the chain breaks after it was pulled an additional 1.9 Å. The jumps in conductance to plateaus around 0.1 G_0 are only observed after a plateau around 1.0 G_0 has already been pulled. Since the jump from a conductance of about 1.0 G_0 to the low conductance of about 0.1 G_0 occurs very abruptly additional length histograms for the low conductance plateaus were recorded. One of these histograms is displayed in the right panel of figure 3.11, compared to the

length histogram for "high" conductance values of gold-oxygen chains. It can be clearly seen that the length histogram consists of a dominant peak at about 1.9 Å followed by a small bump at about 4 Å. From this observation it can be concluded that from the moment that the conductance of the atomic chain suddenly drops to 0.1 G_0, hardly any additional atomic unit, being it a gold atom or oxygen, is being pulled in from the electrodes. The abrupt drop in conductance is due to the incorporation of an atomic unit that severely reduces the transmission of the atomic chain for conduction electrons. Not only does this atomic unit cause a drop in conductance, it also causes a large decrease in chain stability as can be concluded from the observation that the atomic chains can hardly be pulled longer once its conductance has dropped to about 0.1 G_0. Furthermore the low conductance plateaus have only been observed at temperatures of at least 40 K, at which temperatures oxygen is expected to be much more abundant and mobile around the atomic gold chain. Therefore, a likely explanation for the sharp drop in both conductance and chain stability could be the introduction of oxygen-oxygen bonds in the atomic chain. It could be that molecular oxygen is incorporated directly in the chain, but also the consecutive incorporation of two oxygen atoms leads to oxygen-oxygen bonds in the atomic chain. The reason why this apparently does not happen at 5 K is most probably due to the insufficient supply of oxygen atoms at the apexes of the electrodes.

3.4.2 Vibration-modes of gold-oxygen atomic chains

Up to now the conductance and length properties of gold-oxygen atomic chains have been investigated. Calculations predict that atomic oxygen can be incorporated in the atomic gold chain. Experimental evidence came from the ob-

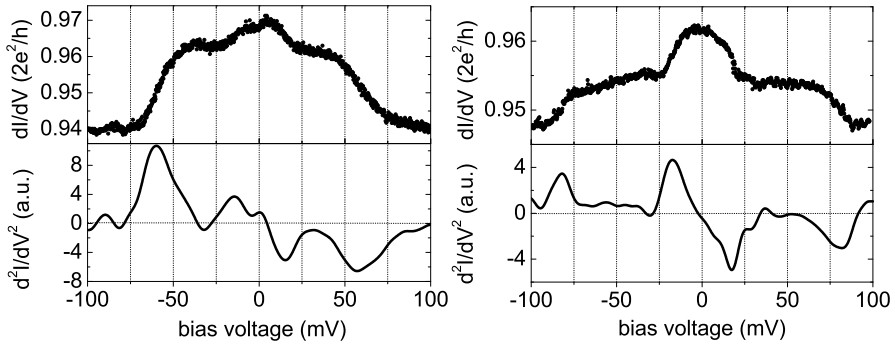

Figure 3.12: *dI/dV spectra (upper panels) for gold-oxygen chains at T = 5 K. The two spectra were taken on chains that were pulled to a length of about 7 Å. The lower panels show the second derivative, d^2I/dV^2, which is obtained by numerical differentiation of the measured dI/dV spectra.*

servation that the interatomic distances in the gold-oxygen chain changed and values of 1.9 Å were observed corresponding to a gold-oxygen bond length. It is, however, still possible that oxygen is not really incorporated into the atomic chain, but that it is chemisorbed on the side of the atomic chain resulting in different interatomic distances between the gold atoms that make up the atomic chain. Also there is no final conclusion about whether atomic or molecular oxygen is incorporated. When oxygen is incorporated in the atomic chain the one-dimensional structure will consist of two different elements, which would result in different energies of local vibration-modes of this diatomic chain. By means of differential conductance (dI/dV) spectroscopy the presence of oxygen in the chain could be verified when electrons are inelastically scattered by local vibration-modes. In figure 3.12 two spectra are shown that were obtained on gold chains that had been pulled to a length of about 7 Å, in the presence of oxygen. One can clearly see two downward steps in the dI/dV spectra indicating the excitation energies of two different vibration-modes of the atomic gold-oxygen wire due to backscattering of inelastically scattered electrons. The dI/dV spectrum of a clean atomic gold chain of reasonable length displays a single longitudinal phonon mode at an energy of about 15 meV [43]. In the left graph of figure 3.12 a low energy mode at 15 ± 2 meV and a high energy mode at 60 ± 4 meV are seen, while in the right graph the low and high mode have energies of 18 ± 2 meV and 83 ± 4 meV, respectively. All other spectra that have been obtained on the gold-oxygen chains that show a high energy step, were found at energies between 60 and 85 meV.

Let us now try to extract information regarding the incorporation of oxygen atoms in atomic gold chains. Since the spectra were obtained for chains of about 7 Å in length, this corresponds to structures that were created around the third peak of the length histogram of figure 3.9. According to the previous analysis this corresponds to a chain in which a single oxygen atom is present together with three gold atoms. For a qualitative indication of the energies of the observed vibration-modes, a simple classical spring-mass model is considered. The model consists of two gold atoms with mass M attached to solid walls and an oxygen atom with mass m sandwiched in between. Only the longitudinal eigenfrequencies are considered, because the probability of exciting transversal modes is small given the quasi one-dimensional geometry of the atomic chain. This model chain has three eigenfrequencies that can be obtained by solving the three equations of motion. For simplicity the spring constant between all

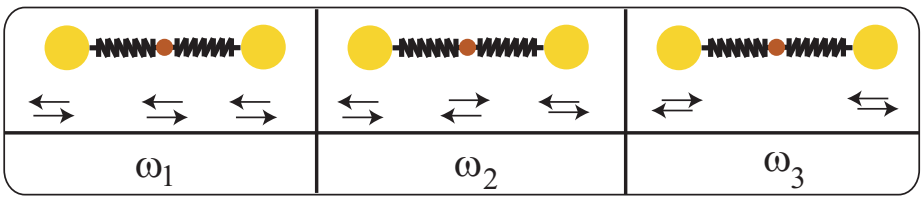

Figure 3.13: *The longitudinal vibration-modes of a Au-O-Au atomic chain.*

masses is taken to be k. The three eigenvalues are:

$$\begin{aligned} \omega_1^2 &= \tfrac{M+m-\sqrt{M^2+m^2}}{Mm}k \\ \omega_2^2 &= \tfrac{M+m+\sqrt{M^2+m^2}}{Mm}k \\ \omega_3^2 &= \tfrac{2}{M}k \end{aligned} \tag{3.1}$$

The three resulting modes are depicted in figure 3.13. The lowest frequency mode ω_1 corresponds to the in-phase motion of all atoms. The second mode ω_2 corresponds to the mode in which the oxygen atom moves in anti-phase to the two gold atoms. And ω_3 corresponds to the mode in which the oxygen atom is immobile and the gold atoms move in anti-phase, which has a slightly higher frequency than the first mode. By substituting the values of the masses M and m for gold and oxygen atoms respectively, it becomes clear that the two heavy mass modes (ω_1 and ω_3) differ a factor 1.4 with each other. The ratios ω_2/ω_1 and ω_2/ω_3 turn out to be 3.6 and 5.1 respectively. Since the two heavy mass modes have energies that are close together and in view of the width of the phonon steps in dI/dV it will be difficult to distinguish them in the experimental measurement. Assuming that the heavy mass modes would be around 15 ± 5 meV, close to the value of the phonon mode of a clean gold chain, the high energy vibration-mode can be expected at 65 ± 5 meV. Preliminary DFT calculations on gold-oxygen chains have resulted in a high energy longitudinal mode that has an energy in the range of 55 to 75 meV, depending on the stretching of the linear bonds [66]. From figure 3.12 one can see a high energy mode at 60 and 80 meV. This is close to the theoretical prediction and therefore it is claimed that the high energy modes observed in figure 3.12 are due to incorporated oxygen *atoms*. The possibility of an oxygen molecule being incorporated is less likely since the energy of such a mode would theoretically be about $\sqrt{2}$ lower at around 46 meV, which is well below the experimental value.

3.5 Oxygen induced atomic chain formation for silver and copper

3.5.1 Conductance of Ag and Cu atomic chains with oxygen admitted

In the previous section it was demonstrated that oxygen chemisorption has an reinforcing effect on atomic gold chains, resulting in longer chains. Gold in its pure form is known for its tendency to form atomic chains. The noble metals silver and copper are electronically very similar to gold, since they also have strong s-electron character. Contrary to gold, silver rarely forms chains, of at most three atoms, and copper forms no chains at all [67]. Bulk silver and copper are known to be more reactive with oxygen than gold. Therefore similar experiments as for gold in the previous section were performed on atomic contacts of silver and copper.

The upper panels of figure 3.14 show some individual breaking and return

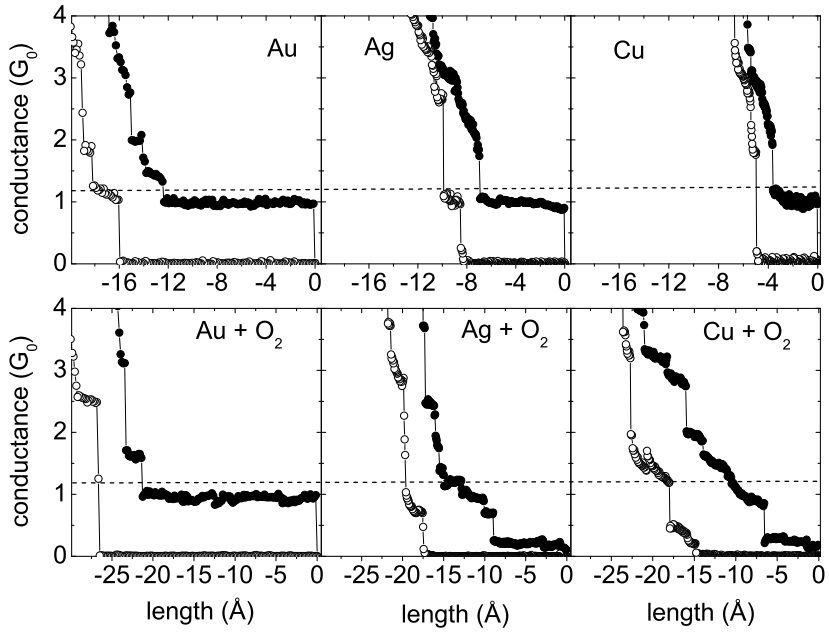

Figure 3.14: *Examples of individual breaking (filled circles) and return (open circles) traces for the metals gold, silver and copper with and without oxygen admitted. The dashed line indicates the contact-conductance of G = 1.2 G_0 that is taken as the starting point for measuring chain lengths.*

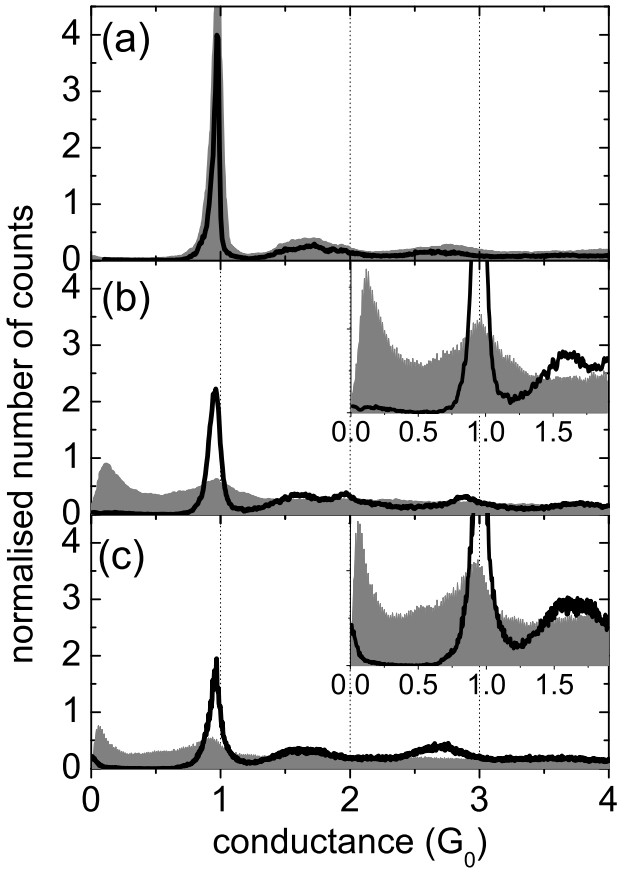

Figure 3.15: *Conductance histograms for clean gold (a) silver (b) and copper (c) (black curves) and with oxygen admitted (filled graphs). The conductance histograms have been normalized to the area. All histograms consist of about 1500 traces and a bias voltage of 50 mV was applied in all cases.*

traces for clean gold, silver and copper. In all cases the last plateau exhibits a conductance around 1 G_0 resulting from the *s*-electron character of the metals [4]. Individual traces in the lower panels are obtained after oxygen had been introduced to the vacuum can. A clear distinction between gold on the one hand and silver and copper on the other hand is that while gold-oxygen wires retain a conductance value close to 1 G_0 the conductance of silver and copper wires drops sharply to values of about one tenth of a conductance quantum. This conductance value is still much higher than when physical contact is broken, implying that the atomic chains are still intact. Additionally, the total length of stretching the contact from the point that the conductance is 1 G_0 un-

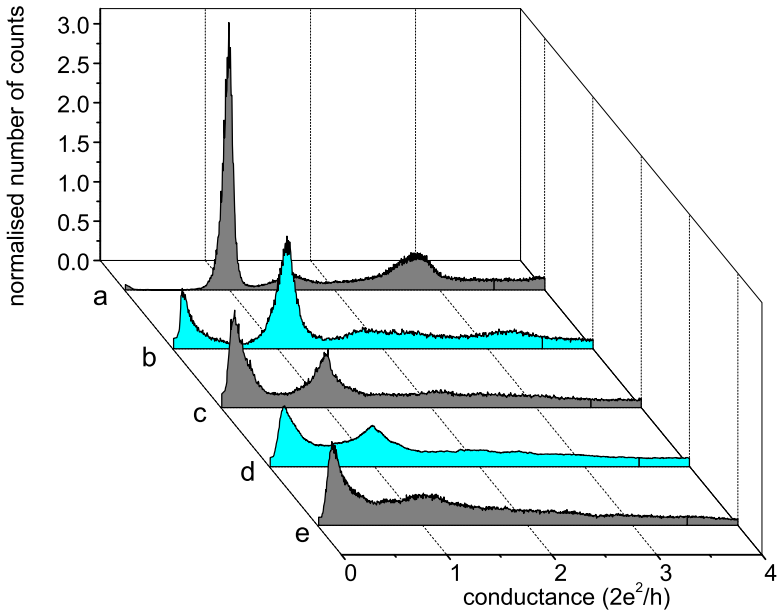

Figure 3.16: *Conductance histograms of clean silver at 50 mV bias (a) and silver with oxygen admitted at 200 mV (b), 100 mV (c), 50 mV (d) and 10 mV (e) bias.*

til the conductance drops deep into the tunneling regime is much longer than before oxygen is introduced to the atomic contact.

Conductance histograms for clean silver and copper in comparison to the histograms after oxygen had been admitted to the vacuum can, are displayed in figure 3.15. One can clearly see that after oxygen admission the dominant peak at 1 G_0 diminishes sharply and the weight is shifted to lower conductance values, in contrast to what was found for gold, which is also shown in the upper panel of figure 3.14. Especially around a conductance of about 0.1 G_0 a clear peak can be distinguished. Conductance values lower than 1 G_0 are likely due to atomic structures of only one atom in diameter since a single silver or copper atom contact has a conductance of 1 G_0. It is therefore expected that indeed atomic chains are being formed that have a conductance that is lower than the conductance quantum $2e^2/h$. In order to confirm this expectation length measurements on the atomic chains in the form of length histograms, similar to the measurements on the gold chains, have been done and are presented in the next section.

The ratio between the weight of the conductance peaks around 1 and 0.1 G_0 in the case of silver with oxygen admitted depends on the applied bias voltage as can be seen from figure 3.16. The conductance histograms have been normalized to the area under the graphs. P_{1G_0} and $P_{0.1G_0}$ are defined as

the areas under the curves between G=0.7-1.1G_0 and G=0-0.3G_0, respectively. As a function of bias voltage the ratio $P_{1G_0}/P_{0.1G_0}$ changes from 0.77 for 10 mV bias to 1.02 for 50 mV to 0.83 for 100 mV and finally to 2.36 for 200 mV bias. The reason why the ratio is much higher for the case of 200 mV bias is most probably the local heating of the junction by the high current passing through the contact, causing the oxygen to be desorbed from the junction. This results into a lower probability for oxygen to be incorporated in the chain.

3.5.2 Oxygen enhanced atomic chains for silver and copper

Since the conductance of oxygen induced atomic silver and copper chains can be as low as 0.1 G_0, as can be determined from figure 3.14 and 3.15, the lower value of the conductance at which the length measurement is stopped, is lowered from 0.5 in the case of gold to 0.05 G_0 in the case of silver and copper. The resulting length histograms are displayed in figure 3.17. The length histograms of the three clean noble metals are compared to the histograms after oxygen was admitted. The difference between the length histograms of clean silver and copper and after the contacts had reacted with oxygen are dramatic. While clean silver has the tendency to occasionally form very short atomic chains and clean copper not at all, the lengths of the chains reaches lengths of many atomic distances after oxygen is admitted to the vacuum can. From figure 3.17(c) one can see that silver chains up to 18 Å in length have been measured, corresponding to a length of seven silver atoms given an interatomic distance of 2.5 Å as in the case of gold. The longest observed copper chains have a length of about six copper atoms, given a theoretical bond length of about 2.3 Å [68]. The observation of these exceptionally large lengths of atomic chains is very much related to the interaction of the metal atoms with oxygen molecules that have landed on the atomic contact. Because of the similarity in electronic structure between silver and copper on the one hand and gold on the other hand and the fact that silver and copper are known to be much more reactive with oxygen it is tempting to suggest that silver-oxygen and copper-oxygen atomic chains are being formed, which apparently have a lower conductance than gold-oxygen chains.

By taking a look at the inter-peak distances in the length histogram for silver-oxygen chains of figure 3.17(c), the spacing between the major peaks is determined to be 1.5 $\pm$ 0.1 Å. One would be tempted to interpret this distance as being the interatomic distance between the silver and oxygen atoms present in the chain. This interatomic distance is much smaller than the distance between gold and oxygen atoms, which was found to be 1.9 $\pm$ 0.1 Å. DFT calculations of the total energy have shown that the latter distance for stretched gold-oxygen chains agrees very well with the experimental results [57,68]. The interatomic distance in stretched silver-oxygen chains is calculated to be also around 1.9 Å, which clearly does not match the inter-peak distance. In the gold-oxygen case the 1.9 Å inter-peak distance was observed, probably due to only very few gold-oxygen bonds being present in the gold-oxygen wires. The shoulder at the left of the first major peak is at exactly the same position as

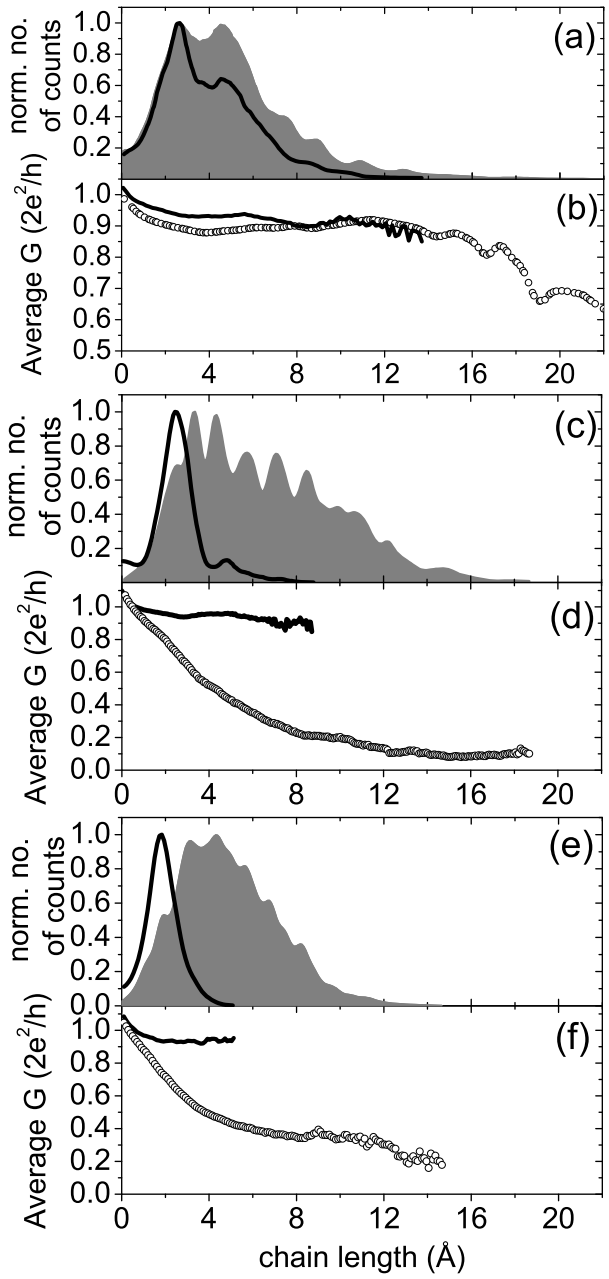

Figure 3.17: *Figures (a), (c) and (e) display length histograms of clean gold, silver and copper (black curves) and with oxygen admitted (filled graphs). Figure (b), (d) and (f) display the average conductance as a function of atomic chain length for the clean metals (black curves) and the metals with oxygen admitted (open circles). The histograms for Au were taken at T = 40 K, while the other histograms were recorded at T = 5 K*

peak position (Å)	chain composition	number of Ag-O bonds	length of Ag-O bond (Å)
3.3	>Ag-O-Ag<	2	1.7
4.3	>Ag-Ag-O<	1	1.8
5.7	>Ag-O-Ag-O<	3	1.9
7.1	>Ag-O-Ag-O-Ag<	4	1.8
8.5	>Ag-O-Ag-O-Ag-O<	5	1.7
9.9	>Ag-Ag-O-Ag-O-Ag<	4	1.9
10.7	>Ag-O-Ag-O-Ag-O-Ag<	6	1.8
12.2	>Ag-O-Ag-O-Ag-O-Ag-O<	7	1.7
14.7	>Ag-O-Ag-O-Ag-O-Ag-O-Ag<	8	1.8

Table 3.2: Silver-oxygen chain configurations that fit the experimental peaks positions from the length histogram of figure 3.17(c). The number and length of the silver-oxygen bonds are also given.

the main peak in the pure silver length histogram. Therefore it is most probably caused by the breaking of a >Ag-Ag< contact. A similar analysis as in the case for the gold-oxygen chains is performed. All peak positions as observed in figure 3.17(c) are listed in table 3.2. With every peak position the possible chain composed of silver-silver and silver-oxygen bonds is shown. In determining these chain compositions the silver-silver bond was fixed to 2.5 Å, while the silver-oxygen bond was allowed to vary slightly around 1.8 Å. From this simple analysis it can be concluded that the silver-oxygen bond in silver-oxygen atomic chains is 1.8 $\pm$ 0.1 Å, very close to the theoretical value of 1.9 Å. Additionally, the chain compositions of table 3.2 indicate that chains that include a Ag-Ag-Ag part, i.e. two consecutive silver-silver bonds, do not occur. Even the appearance of a single silver-silver bond in a long atomic chain is very rare and is only present in the silver-oxygen chain composition with 9.9 Å length. This is expected since pure silver chains consisting of two silver-silver bonds are hardly ever observed, as seen from the length histogram in figure 3.17(c), and the silver-silver bond is about 2.4 times weaker than the silver-oxygen bond [68].

A similar analysis was made on the copper-oxygen length histogram of figure 3.17(e). The single peak in the histogram of pure copper has its center at 1.9 Å, which is significantly smaller than the theoretical value of 2.3 Å for an atomic chain of copper atoms. Since copper does not show any indication of atomic chain formation at all, the likely explanation for the shorter experimental value of the bond length of a copper-copper bond is a more rapid rupture because of its relative weakness. In the analysis of the length histogram of the copper-oxygen chains the theoretical value of 2.3 Å was used and this yields a copper-oxygen bond length of 1.7 $\pm$ 0.1 Å. DFT calculations predict a minimum in the total energy of a stretched infinite copper-oxygen chain at a bond

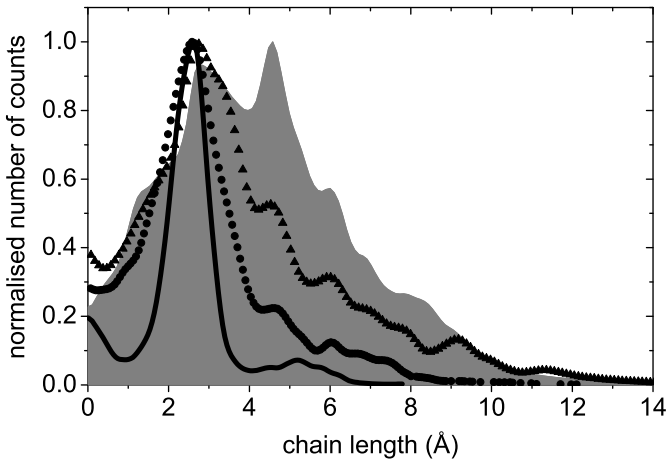

Figure 3.18: *Length histograms obtained from silver-oxygen chains at T = 5 K with different conductance windows for chain length measurement: Filled graph: G ∈ [1.1,0.5 G_0]; Triangles G ∈ [1.1,0.6 G_0]; Bullets G ∈ [1.1,0.7 G_0]. For comparison a length histogram for clean silver is also plotted (black curve). All length histograms consist of about 2000 traces and a bias voltage of 50 mV was used in all cases.*

length of 1.8 Å [68], again very close to the experimental value. Therefore it can be concluded that there is very reasonable agreement between the experimental bond lengths in the metal-oxygen atomic chains and the values that have been calculated by DFT.

From figure 3.17(d) and (f) it is very clear that the average conductance of the silver-oxygen and copper-oxygen chains drops sharply from the point that a single atom contact is formed and chain formation sets in. In the case of silver the conductance drops to a value of about 0.1 G_0 upon increasing chain length and stabilizes around that value for chain lengths of more than about 12 Å. Also the conductance of copper-oxygen chains decreases upon increasing chain length. Eventually the conductance of the longest copper-oxygen chains is about 0.2 G_0.

Length histograms of silver-oxygen chains have been studied as function of the lower stop conductance value. Since the conductance of the chains drops below 0.5 G_0 once the length of the chain on average reaches a value of 5 Å, it is expected that the length histograms display a much smaller amount of long chains when low conductance values are not included in the chain length measurement. Figure 3.18 shows the evolution of the length histograms of silver-oxygen chains when the stop conductance values for the length measurement is increased from 0.5 G_0 (filled graph) to 0.6 G_0 (triangles) to 0.7 G_0 (bullets). For comparison a length histogram of clean silver (black curve) is also plotted. From the figure it is obvious that upon increasing the lower conductance

values for stopping the length measurement, the average measured lengths of the atomic chains decreases, as expected. In fact, the length histogram recorded with a conductance window of G $\in$ [1.1,0.7 G_0] starts to resemble the histogram of clean silver. This indicates that indeed chains with a conductance very close to the quantum unit $2e^2/h$ consist solely of silver atoms. Once a single oxygen atom is pulled into the chain the conductance drops considerably. From figure 3.18 some more interesting observations can be made. Firstly the second peak in the silver-oxygen length histograms at a length of about 4.5 Å is present in all three histograms but is absent in the histogram for clean silver, which displays the second peak at about 5.1 Å. This peak is therefore attributed to the presence of oxygen in the chain. Also the third peak at about 6 Å turns out to be present in all length histograms recorded on the silver-oxygen chains. The peaks at longer lengths are somewhat smeared out compared to each other and a comparison with clean silver is irrelevant since such long atomic silver chains are never being created. Secondly the above mentioned peaks at 4.5 and 6 Å were also present in the length histogram for silver-oxygen chains that is plotted in figure 3.17(c), indicating once more that these peaks arise due to oxygen admission to the atomic silver wires. Thirdly and finally it seems that upon increasing the lower conductance value for the chain length measurement the first major peak in the length histogram shifts from a values of about 3 Å, which is related to oxygen incorporation since it is also present in figure 3.17(c), towards the first major peak in the clean silver histogram, which is located at a length of about 2.5 Å. This observation leads to the conclusion that the number of clean >Ag-Ag< chains that were broken and counted in the length histogram with 0.7 G_0 as a stop value for length measurement (circles curve of figure 3.18) has increased compared to the histogram with 0.5 G_0 as a stop value (filled graph of figure 3.18). This makes sense since the chains with several incorporated oxygen atoms, having a lower conductance and on average a longer length due to the enhanced linear bond strength, are excluded from the ensemble of lengths that make up the histogram. The silver-oxygen chains length histograms have been studied in more detail by investigating the lengths of the chains at a lower conductance.

A length histogram for silver-oxygen chains that display a conductance between 0.5 and 0.05 G_0 is recorded and is displayed in figure 3.19. One can immediately distinguish six peaks in the length histogram, which are fitted by a multiple Gaussian. The multiple Gaussian fit is shown as the black curve, while individual six Gaussian curves are drawn in white. From the fit the inter-peak distance is determined to be 1.5 $\pm$ 0.1 Å. This measurement gives a strong indication that indeed when the conductance of silver-oxygen chains decreases, the elongation of the wires continues by the incorporation of additional atomic units.

More evidence for the formation of long silver-oxygen and copper-oxygen atomic chains comes from the average return lengths of the contacts after physical contact of the chains to the electrodes has been broken. The average return lengths for gold, silver and copper with oxygen admitted are displayed in figure 3.20. As in the case of clean gold (see figure 3.3) the average return length

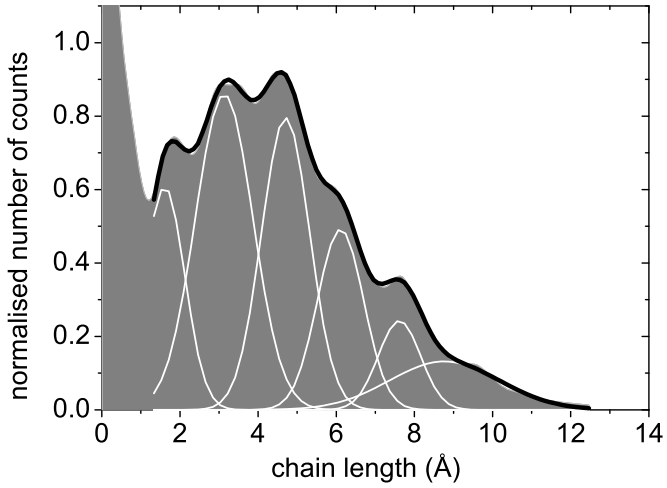

Figure 3.19: *Length histogram taken on silver-oxygen chains. The conductance value to start chain length measurement was 0.5 G_0 and stop conductance value was 0.05 G_0. The graph is fitted with a multiple Gaussian curve fit (black curve), consisting of six individual Gaussian curves .*

increases more or less linearly with increasing length of the atomic chain. This is the expected behavior: Metal and oxygen atoms are being pulled out of the electrodes to form a suspended atomic chain, that exists only as long as it is physically contacted to the electrodes. At the moment that the wire snaps the atoms collapse back to the electrodes and the electrodes have to be moved back by about the distance equal to the chain length of the previously existing chain.

3.5.3 Point Contact Spectroscopy on silver-oxygen chains

Point Contact Spectroscopy (PCS) was performed on the silver-oxygen atomic chains in order to determine local vibration modes of these the one-dimensional structures. Regular use of PCS in order to determine vibration-modes of a single atom or molecule contact is usually only feasible when the conductance of the junction is determined by a single conductance channel that is completely transparent, as was explained in chapter 2. This yields a conductance of 1 G_0 as in the case of clean gold or silver chains. As we have seen in section (3.4.2) PCS could also be performed on the gold-oxygen chains that have a conductance near 1 G_0. However, the silver-oxygen chains, are different in the sense that the conductance for these chains drops very fast with increasing length of the chains. Normally dI/dV spectra are very much distorted by random conductance fluctuations when the conductance is below 1 G_0 [36,37]. This makes the observation of small bias-symmetric changes in the conductance difficult.

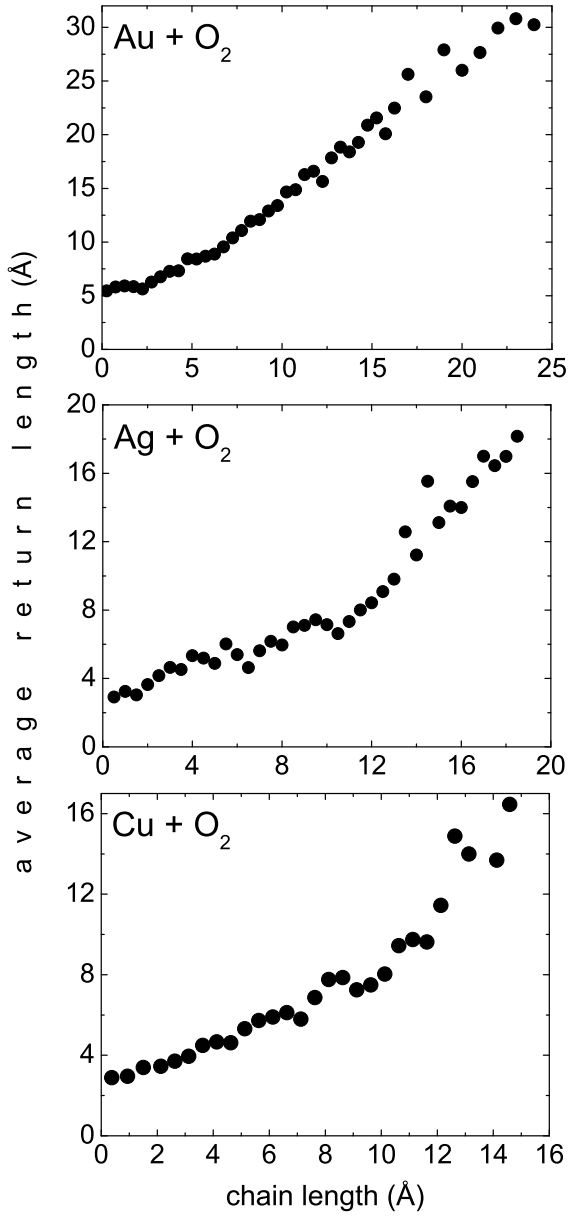

Figure 3.20: *Average return lengths for gold, silver and copper with oxygen admitted. The corresponding length histograms are displayed in figure 3.17.*

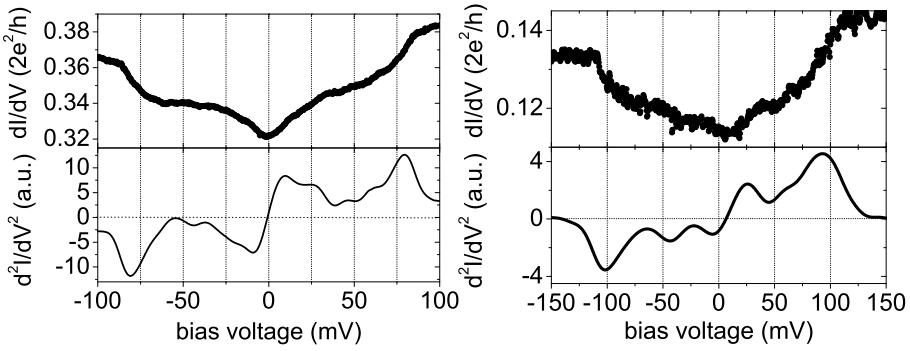

Figure 3.21: *Two dI/dV spectra obtained from low-conducting silver-oxygen atomic chains. The left spectrum was taken on a 7 Å long chain. The right spectrum was taken on a 11 Å long chain.*

Still it has been possible to obtain a few dI/dV spectra on the low-conducting silver-oxygen chains that showed bias-symmetric spectroscopic features. In figure 3.21 two of these spectra are shown. One can clearly see a high energy feature that is located at around 80 meV in the left graph and around 100 meV in the right graph. Very striking is the fact that a step-like increase of the conductance is observed, opposed to the the decrease in conductance, which is observed in dI/dV spectra on contacts that display a conductance near $2e^2/h$.

Recently it has been predicted that the correction in the conductance of an atomic wire, due to electron-phonon interaction depends on the transmission of the conductance channel [40,41,69]. It was demonstrated for a single channel conductor that by inelastic scattering, when exciting a vibration-mode, electrons become 100% backscattered when the transmission of the channel is one. When the transmission is very low, all electrons get forward scattered as in the case of a tunneling contact. The calculations suggest that when the transmission of the channel is 0.5, the amount of forward and backward scattered electrons is the same and no correction on the conductance will be noticed. The silver-oxygen chains of figure 3.21 have a conductance that is lower than $0.5\,G_0$, which would indeed result in a net amount of forward scattered conduction electrons. In infinite pure silver chains the conductance is determined by a single fully transparent conduction channel that is formed by the s-orbital of the silver atoms crossing the Fermi level, which results in a conductance close to $1\,G_0$. The following section will deal with calculations that will disclose more about the conduction channels involved in silver-oxygen atomic chains and the physical mechanism that is responsible for the enhanced linear bond strength in the metal-oxygen chains. From experiments is clear that the transmission of the conduction channels is very low and the upward steps seen in the spectra of figure 3.21 can be interpreted as inelastically forward scattered electrons. The observed energies of 80 and 100 meV are in the range of the expected vibrational energies of oxygen atoms in a one-dimensional chain, albeit somewhat

high compared to the energies observed for gold-oxygen chains. Preliminary calculations on a simple model system consisting of a oxygen atom contacted between two silver atoms yield a somewhat higher vibrational frequency for the high frequency mode, than for the Au-O-Au wire [66]. It is therefore very likely that the observed mode is indeed caused by a local vibration-mode in an silver-oxygen chain.

3.6 Calculations

The previous sections provided evidence that oxygen dissociates by reacting with atomic junctions of the noble metals gold, silver and copper, and can be incorporated such that atomic chains form. A striking difference between gold and silver-oxygen atomic chains is the very different conductances that the two wires display. Whereas the average conductance of gold-oxygen chains remains close to 1 G_0, only decreasing towards 0.6 G_0 for chains of lengths longer than 16 Å, the average conductance of silver-oxygen chains decreases rapidly as a function of chain length. The band structures for infinite atomic silver and gold chains look very similar (see the calculations for Ag in the upper panel in figure 3.22), with a single s-band crossing the Fermi level. Aan de Brugh *et al.* [68] calculated the band structure for infinite alternating silver-oxygen atomic chains as shown in the lower panel of figure 3.22. The solid and dashed lines represent the bands for infinite wires with a silver-oxygen distance of 2.0 Å and 2.2 Å respectively. Only the $d-p$ hybrid bands change considerably upon straining the wire, indicating that these bands are relevant for covalent bonding.

From the band structure it can be seen that also in the case of infinite silver-oxygen atomic chains the Fermi level is crossed by a single band, which is spin-degenerate. Novaes *et al.* [58] showed that the covalent bond between gold and oxygen atoms in a wire is mainly due to the bonding between the Au $5d_{z^2}$ and O $2p_z$ orbitals. This corresponds with calculations done on silver-oxygen wires performed here.

To investigate the conduction properties a Greens function method has been used [70]. Figure 3.23 displays the transmission function for -Ag-O- and -Ag-O-Ag-O- (a) and -Au-O- and -Au-O-Au-O- (b) junctions contacted by semi-infinite silver and gold chains on both sides. For silver the total conductance is nearly zero when two oxygen atoms are present. A single oxygen atom reduces the conductance of the chain to 0.2 G_0. For the case of gold the conductance becomes 0.1 G_0 and 0.7 G_0 for two and one oxygen atoms, respectively. For the single oxygen atom contacted by infinite silver wires the conductance is carried by a single transmission channel at the Fermi energy, originating from the $2p_z$ orbital of oxygen. The same holds for the case of gold, but electrons scatter much less onto this channel resulting in a higher transmission. Finally, it has to be remarked that these calculations are performed by using semi-infinite atomic wires as electrodes. When coupling the system to more realistic surface electrodes a finite coupling between higher angular momen-

tum (m=$\pm$1) -Ag-O- or -Au-O- $d-2p$ hybrid states and d states in the metal electrodes can be expected. Strange *et al.* [71] have found that this indeed leads to the opening of more eigenchannels, resulting in a higher conductance. They found furthermore that the conductance of -Ag-O- wires contacted by more realistic electrodes should oscillate as a function of the number of -Ag-O- units in the wire. According to their calculations the conductance reaches a minimum at four -Ag-O- units and starts to increase again when more units are incorporated in the atomic wire. Four -Ag-O- units would correspond to a chain length of about 15 Å which is very close to the bottom of the conductance vs. chain length that is shown in figure 3.17(d). Unfortunately it is experimentally not possible to create much longer chains in order to verify that the conductance

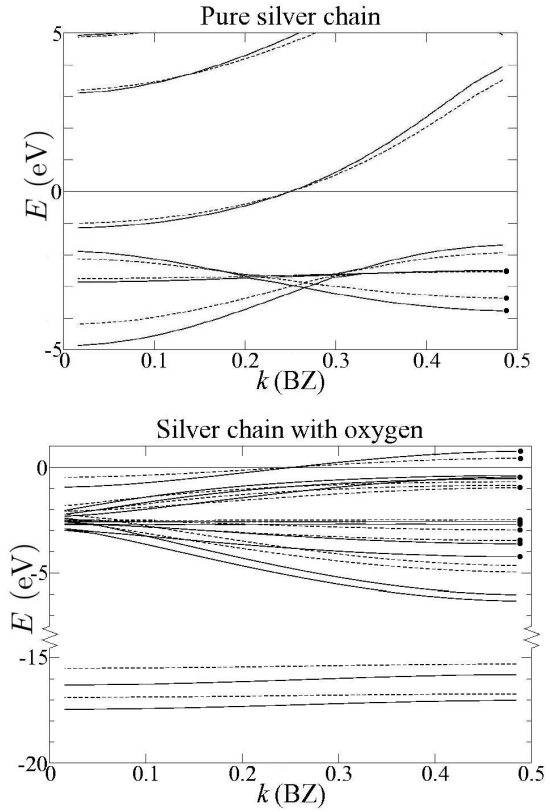

Figure 3.22: *Top panel: Calculated band structure of an infinite silver chain with an interatomic distance of 2.6 Å (continuous lines) and 2.8 Å (dashed lines). Bottom panel: Calculated band structure of an infinite alternating silver-oxygen chain with an interatomic distance of 2.0 Å (continuous lines) and 2.2 Å (dashed lines). Bands are spin-degenerate. The marked bands are twice degenerate. k runs from the* Γ*-point to the end of the Brillouin Zone. The unit cell contains one silver atom (top) or one silver and one oxygen atom (bottom). Taken from Ref. [68].*

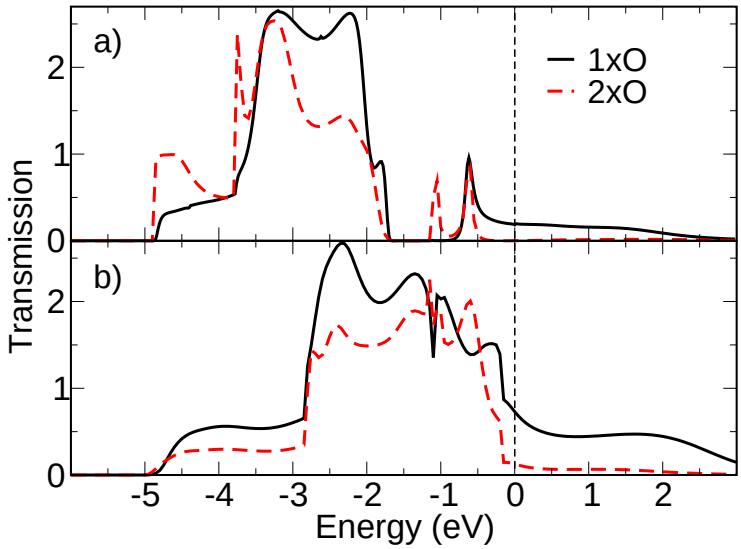

Figure 3.23: *(a) Transmission function for a -Ag-O- (full curve) and -Ag-O-Ag-O- (dashed curve) junction contacted by semi-infinite silver atomic wires. (b) Transmission function for a -Au-O- (full curve) and -Au-O-Au-O- (dashed curve) junction contacted by semi-infinite gold atomic wires. Data provide by M. Strange et al.*

would increase again.

Isolated noble metal atoms like gold, silver and copper have a full d-shell and a single s-electron in the highest orbital. In a one-dimensional atomic chain, the d-states form a band, which is energetically situated below the highest half-filled s-band, resulting in completely filled d-bands. In the case of a linear gold chain the d-band is situated very close to the Fermi level. For gold a lowering of the Fermi level caused by a relativistic correction to the energy of the s-bands partly depletes the d-band, resulting in additional bonding of the d-bands. The d-band for a silver chain is energetically situated further below the Fermi level and does not become depopulated, causing no additional bonding. When silver binds to oxygen, the $2p$-orbitals of oxygen hybridize with the $4d$-orbitals of silver that have the same symmetry with respect to the chain-axis and split in a bonding and anti-bonding state (see figure 3.22). From figure 3.22 is seen that when a silver-oxygen chain with an interatomic distance of 2.0 Å is stretched to one with 2.2 Å the anti-bonding states remain roughly at the same energy, but the bonding states rise considerably in energy. This indicates that a larger force is required to pull the linear bond apart, or in other words the bonding $p-d$-hybrids are strongly bonding. The number of bonding electrons is only one higher than the number of anti-bonding electrons as in a pure silver chain. The stronger linear bonds in silver-oxygen wires compared to pure silver wires originate from the difference in strength of the bonding states for pure silver and silver-oxygen.

3.7 Conclusions

Oxygen has been shown to react strongly with atomic contacts of the noble metals gold, silver and copper. Whereas gold is known for its tendencies to form atomic wires the other two noble metals silver and copper do not. But oxygen enhances the linear bonds sufficiently such that silver and copper-oxygen atomic wires can be formed. While for the clean noble metals a contact with a diameter of a single atom yields a conductance of about 1 G_0, oxygen suppresses the conductance severely for silver and copper. The presence of oxygen in the linear wires is nicely demonstrated using differential conductance spectroscopy, which led to the observation of a high energy vibration-mode that cannot be due to any mode of the heavy metal atoms, since it is far above the Debye energy. Both the bond-reinforcing and the conductance-suppressive effect of incorporated oxygen atoms are in agreement with calculations. It should also be mentioned that it has been claimed before that an interesting connection exists between atomic chain formation and spontaneous surface reconstructions for gold, platinum and iridium [47]. Silver and copper surfaces do not show these reconstructions, but upon reaction with oxygen they do [72, 73]. A renewed connection between surface reconstruction and atomic wire formation appears here, because oxygen enhances the physical mechanism of depopulating the anti-bonding states of the metal's d-bands. By using oxygen as an atomic glue it is possible to create new atomic wires. Nickel-oxygen atomic wires have also been observed and their properties will be discussed in detail in chapter 5. Since oxygen-induced surface reconstructions have be observed for other metals as well, it is possible that these metals will also form atomic chains upon incorporation of oxygen.

4

Vibrationally induced two-level systems in single-molecule junctions

It is found that differential conductance characteristics of single-molecule junctions and atomic chains with small molecules incorporated display positive or negative peaks at bias voltages located around energies of local vibration-modes. These spectroscopic features are observed for a wide variety of metal-molecule contacts, pointing to a general feature of single-molecule junctions. A theoretical approach in the form of vibrationally induced two-level systems is made in order to quantify the physical mechanism responsible for the observed features. A molecule in an atomic junction can be bonded in two (or more) geometrically different configurations, with slightly different binding energies. The molecular configurations yield slightly different conductances for the junction. The states are separated by a large barrier and only by exciting the molecule vibrationally, transitions between the configurations are possible, resulting in a sudden jump in conductance and thus a peak in differential conductance. This interpretation opens the possibility to use the peaks as a new tool for identifying local vibration-mode energies of single-molecule junctions. [1]

[1] Parts of this chapter have been published in: W.H.A. Thijssen, D. Djukic, A.F. Otte, R.H. Bremmer and J.M. van Ruitenbeek, Phys. Rev. Lett. **97**, 226806 (2006)

4.1 Introduction

A nanowire can be thinned down until only a single atom is bridging the gap between the two electrodes. As discussed before the metals gold, platinum and iridium have the tendency that upon further stretching of the contact additional atoms can be pulled out of the electrodes, forming an atomic chain of single atoms. With the mechanically controllable break-junction technique it is possible to move the electrodes in two directions. This makes it possible to remake physical contact between the electrodes after the last atomic bond has been broken in the elongation process. Very small displacements of order 10 pm are possible, which offers the possibility to investigate the mechanical and electronic properties as function of the amount of stress applied to the atomic bonds. Due to these unique experimental conditions it has become possible to measure the conductance of atomic chains as function of their length [74–77]. Also the increase in conductance upon stretching a single atom contact of e.g. aluminum [14] or the stretch of the linear bonds in an atomic chain of gold atoms with hydrogen incorporated have been studied [78].

Additionally, it is possible to measure the conductance of the single atom or molecule junction differentially (dI/dV). This is done using a lock-in amplifier as was described in chapter 2. dI/dV measurements are very sensitive and have resulted in the observation of conductance fluctuations that originate from the interference of electron waves that have scattered with impurities and defects near the contact [36–38]. The amplitude of these fluctuations are typically of order of a few percent, which makes them difficult to distinguish in normal I-V measurements. It has been demonstrated that the amplitude of conductance fluctuations is severely suppressed when the current through the single atom or molecule junction is exclusively carried by a single fully transparent conductance channel. A single conductance channel with 100% transparency reduces the standard deviation of the conductance by more than one order of magnitude [8, 36]. This reduction in the amplitude of conductance fluctuations opens possibilities to detect more delicate features in the dI/dV spectrum that are usually shrouded by fluctuations. The observation of local vibration-modes of an atomic chain have been discussed in detail in the previous chapter. But also vibration-modes of molecules contacted with leads have been observed. Park *et al.* [7] have measured very low vibration-mode energies of a C_{60} molecule contacted by gold electrodes by means of an electro-migrated break junction. The C_{60} molecule is weakly coupled to the electrodes, making it behave as a quantum dot and the electronic transport is incoherent. The experiments that are described in this chapter are done with small molecules that are chemisorbed to the electrodes, which causes the electron transport to be coherent. In previous work a hydrogen molecule has been contacted by platinum leads and the vibration-modes of the Pt-H-H-Pt junction have been measured in detail [8, 22]. The contacted hydrogen molecule was found experimentally to have a conductance near 1 G_0, which agrees with DFT calculations [79–81]. The drop in the conductance due to inelastic scattering of the conduction electrons is typically of order 1%. With the mechanically controlled break-junction

technique it is even possible to investigate the stretching dependence of the molecular vibration modes. Depending on whether the mode is longitudinal or transversal, the energy of the vibration mode is decreasing or increasing upon stretching the linear bonds, respectively [22].

This chapter deals with a novel phenomenon in the dI/dV spectra of single-molecule junctions and atomic chains: Sharp positive and negative peaks at well defined energies. A spike in the dI/dV spectrum indicates a step in the I-V measurement, implying a sudden change of the conductance of the junction. This basic ingredient forms the basis for a simple model that will be derived in this chapter in order to explain these remarkable observations.

4.2 Observation: Spectroscopic anomalies

This chapter presents differential conductance measurements for several metal-single-molecule-metal junctions. Metal junctions for gold, silver, platinum and nickel with molecules like hydrogen, deuterium, oxygen, acetylene, benzene, carbon-monoxide and water have been studied. In all cases similar spectroscopic anomalies have been observed. Positive or negative peaks in dI/dV spectra are found to be located at energies of order of a few tens of meV. In figure 4.1 two typical dI/dV spectra are shown that display anomalous spikes.

The spectrum displayed in figure 4.1(a) was taken for a single CO molecule

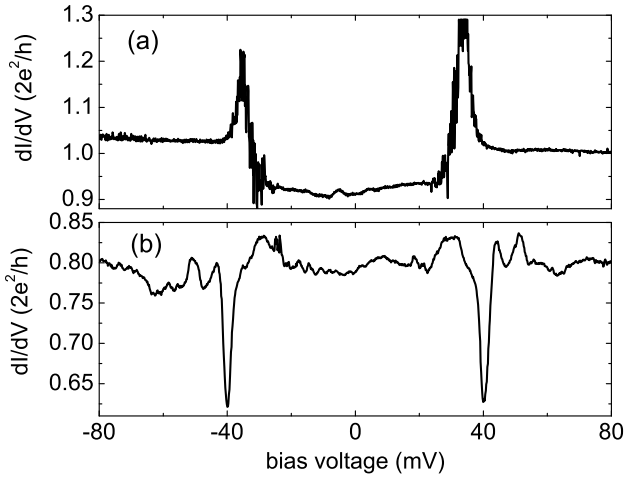

Figure 4.1: *Two examples of dI/dV spectra in which anomalous spectroscopic peaks (a) and dips (b) are present. The spectrum of figure (a) was taken on a single CO molecule contacted by platinum electrodes. Figure (b) shows a spectrum taken from an atomic gold chain with hydrogen admitted.*

contacted by platinum electrodes and shows bias voltage symmetric peaks at about $\pm$ 35 mV. The spectrum of figure 4.1(b) was taken for an atomic gold chain, which reacted with hydrogen. The spectrum shows sharp negative peaks at about $\pm$ 40 mV. It has to be mentioned that these spectra are just examples and that a single CO molecule also displays sometimes negative peaks and atomic gold chains with hydrogen display positive peaks.

In the literature a few measurements displaying anomalous peak-like structures have been published. In the early 1990's Ralph *et al.* [82, 87]. developed a technique to create nanoscopic holes with diameter of about 3-10 nm in a silicon nitride membrane. The holes are subsequently filled by evaporation of metal from both sides in order to create metal nano-constrictions. In their dI/dV measurements the authors observed anomalous extremely sharp negative peaks at energies around 10 meV. Figure 4.2 shows those sharp negative

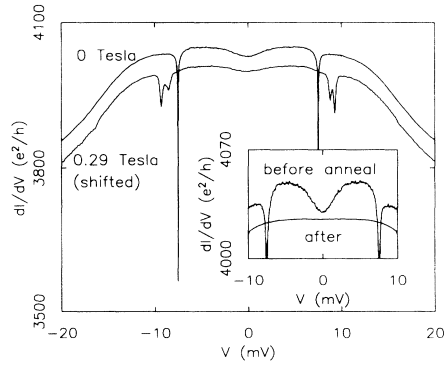

Figure 4.2: *dI/dV spectrum recorded for a copper nano-constriction at T = 4.2 K. See text for more details on experiments. Taken from Ref. [82].*

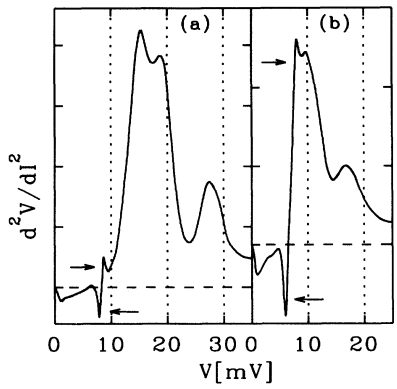

Figure 4.3: *d^2I/dV^2 spectrum taken on copper (a) and gold (b) microscopic junctions created by MCBJ at T = 1.3 K. Taken from Ref. [83].*

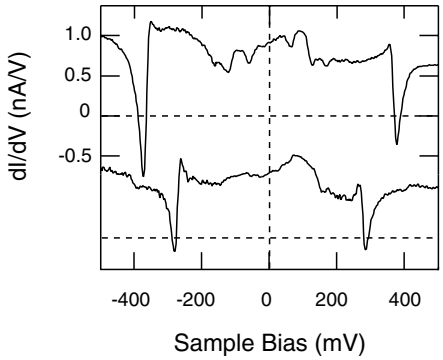

Figure 4.4: *Upper dI/dV spectrum taken with an STM for a single pyrrolidine molecule on a Cu(001) surface at T = 7 K. The lower spectrum was taken for a deuterated molecule. Taken from Ref. [84].*

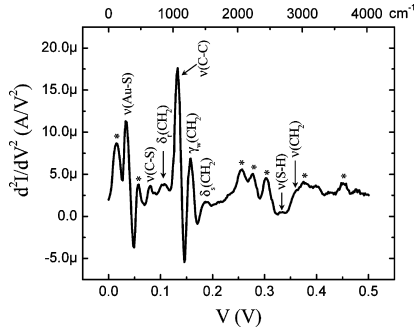

Figure 4.5: *d^2I/dV^2 spectrum taken on a self-assembled monolayer of alkanedithiol molecules in a nanopore contacted by evaporated gold from both sides. The experimental temperature was 4.2 K. Taken from Ref. [85].*

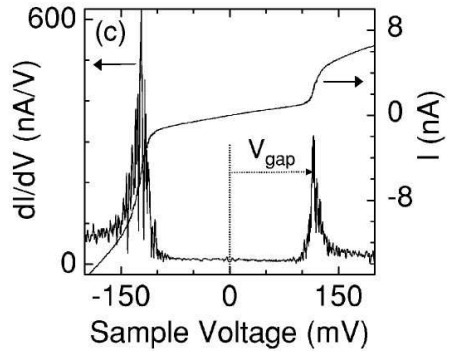

Figure 4.6: *dI/dV spectrum taken on a hydrogen covered Cu(111) surface. The position of the peaks was found to be coverage dependent. The experimental temperature was 2.5 K. Taken from Ref. [86].*

peaks that were measured on a nano-constriction of copper. Upon applying a small external magnetic field the amplitude of the negative peaks decreased dramatically and they were observed at a somewhat larger bias voltage. Furthermore the anomalies were only observed after copper was evaporated and immediately cooled down to T = 4.2 K. After annealing the sample at room temperature for one week the anomalous peaks had disappeared.

In 1995 Keijsers *et al.* measured anomalies in MCBJ experiments on gold, silver, copper and platinum constrictions [83]. So-called S-shaped features were observed in d^2I/dV^2 spectra accompanied by zero-bias anomalies which, as in the case of Ralph *et al.*, have been explained in terms of two-level Kondo systems. The S-shaped features can be seen in figure 4.3. These S-shaped features correspond to peak-like features in the dI/dV spectrum, similar to the observations by Ralph *et al.* and the observations displayed in figure 4.1. The peak-like anomalies have never been explained quantitatively.

More recently very similar spectroscopic negative peaks have been observed in very different measurements, namely when measuring differential conductance of a single pyrrolidine molecule on a Cu(001) surface by means of STM [84]. At an energy of about $\pm$ 380 meV sharp negative peaks are observed (see figure 4.4) and at the same time the conformation of the molecule changed in the STM image. By substituting the hydrogen atoms on the carbon ring with deuterium atoms they were able to observe a downward shift of the bias voltage at which the peak occurred, as can be seen in the second spectrum of figure 4.4. The authors drew the conclusion that by exciting an internal vibration-mode of the molecule, it can change its conformation which changes the conductance of the tunnel junction.

Yet another recent example comes from IETS measurements on a self assembled monolayer (SAM) of alkanedithiol molecules in a nanopore, contacted by gold from both sides [85]. S-shaped features were measured in d^2I/dV^2 and appeared to be very close to the known energies of the Au-S and C-C stretching modes and the CH_2 wagging mode.

Finally, Gupta *et al.* [86] have observed positive and negative peaks in IETS measurements on a hydrogen covered Cu(111) surface. They found that the position in energy of the peaks depends on the hydrogen coverage. By means of a phenomenological model, involving different conductance paths for electrons that do and do not scatter inelastically in the tunnel junction, it was possible to obtain good fits of the experimental data.

4.3 Physical mechanism causing the anomalies

Let us summarize the observations: In differential conductance measurements a positive or negative peak is observed. A peak in dI/dV implies a step in I-V and a S-shaped feature in d^2I/dV^2. A step in a I-V measurement indicates a sudden change of the total conductance of the contact as the bias voltage is swept through a small voltage window. This is the first ingredient of the physical mechanism that needs to be found.

Gaudioso *et al.* [84] and Wang *et al.* [85] presented evidence that the spectroscopic anomalies are related to vibration-modes of the molecule. Figure 4.7 shows a sequence of differential conductance spectra of a single deuterium molecule contacted by platinum leads. A regular spectrum displays voltage-symmetric downward steps at the voltage where a vibration-mode of the Pt-D-D-Pt junction is excited [22]. The top spectrum of figure 4.7 displays vibration-mode steps, but it features also a small bump just before the step down occurs. The middle spectrum of figure 4.7(b) was taken on the same contact but the electrodes had been pulled about 0.1 Å apart compared to figure 4.7(a). One can see that the bumps have evolved into clear peaks indicating a change in the junction. A careful look at the zero-bias conductance indicates a small increase from 1.02 G_0 to 1.03 G_0. The conductance at $\pm$ 80 mV is unchanged at 1.00 G_0. Figure 4.7(c) was obtained for the same contact that had been stretched another 0.1 Å. Here one can see the complete disappearance of the peaks and a regular vibration-mode spectrum featuring downward steps is displayed.

The observations displayed in figure 4.7 give a strong indication that the anomalous peaks are strongly related to local vibration-modes for the single-molecule junction. In order to obtain more evidence that the anomalies are indeed related to local vibration modes the effect of the isotope substitution has been studied. If the energies at which the anomalous peaks occur, correspond

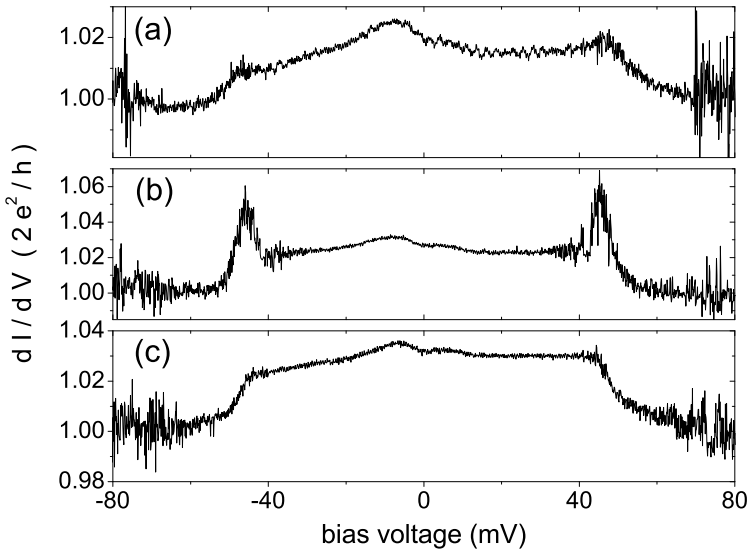

Figure 4.7: *Differential conductance spectra taken for a single deuterium molecule contacted by platinum electrodes. The electrodes were moved apart 0.1 Å and 0.2 Å in figure (b) and (c) respectively, compared to figure (a). The experimental temperature was 5 K.*

to the energies of local vibration-modes, then by increasing the mass of the molecule, the energy at which the anomaly is observed has to decrease with the square root of the mass increase, assuming that the vibration of the molecule behaves to a good approximation as a harmonic oscillator.

The isotope substitution effect was tested for single molecules of hydrogen and deuterium contacted by platinum electrodes as well as hydrogen and deuterium incorporated in atomic gold chains. The top graph of figure 4.8 shows a typical differential conductance spectrum for an atomic gold chain with hydrogen admitted. A peak around 45 meV is clearly visible. All energies at which a positive or negative peak was observed were collected for many different contacts and four different MCBJ samples. The voltage at which the peak maximum or minimum was found in a given spectrum was collected and stored

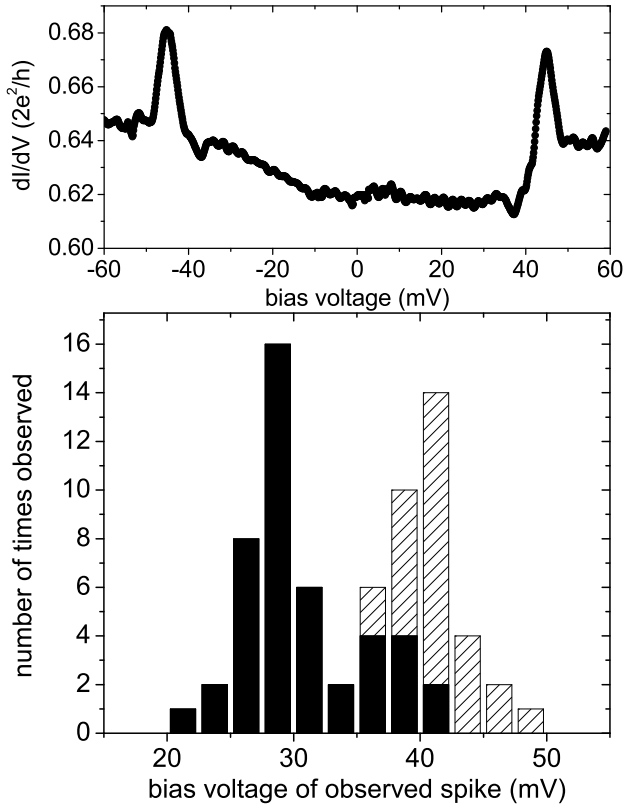

Figure 4.8: *Top graph shows a dI/dV spectrum obtained for an atomic gold chain with hydrogen admitted. The histogram in the bottom graph shows the energies at which the peak anomalies in the spectra for gold chain with admitted hydrogen (hatched bars) and deuterium (filled bars) have been observed.*

in a histogram and the contact was broken. Then the contact was remade by pushing the electrodes far back into each other to make sure that all atoms have enough possibilities to reconfigure. Subsequently, a new atomic chain was sought for that displayed peaks in the dI/dV spectrum. This was done for two different gold MCBJ samples to which hydrogen was admitted and two different samples for the case of deuterium admission. The various samples showed no differences in behavior so that we can rule out artifacts related to a specific MCBJ sample.

One can clearly see from the histogram in the bottom graph of figure 4.8 that the maximum in the distribution of energies has shifted from about 41 to about 29 meV. This is exactly the $\sqrt{2}$ shift in energy that is expected when vibrational excitations of hydrogen or deuterium atoms or molecules are causing the anomalous peaks to occur. But how does a local vibration-mode cause peaks in differential conductance, or in other words, how can a local vibration induce a sudden, albeit sometimes small, change in the conductance of the single-molecule junction? Is it possible that the transparency or the number of conductance channel(s) changes when the molecule is in its vibrationally excited state? From the width of the vibration-mode step in the differential conductance spectrum of figure 4.7 it is possible to make a rough estimate of the lifetime of the vibration-mode. Assuming that the spectroscopic broadening is dominated by lifetime broadening the lifetime is of order of a femtosecond. The number of electrons that pass through a single-molecule junction having a conductance close to 1 G_0 at a 50 mV bias voltage is about 2×10^{13} per second, meaning that the average time that the molecule spends in its excited state is only about 1% of the total time. This makes it very unlikely that the anomalous peaks are due to a different conductance of the vibrationally excited state.

From figure 4.7 one may conclude that whether or not a peak is measured depends strongly on the amount of stress applied to the molecular bonds that bind the molecule to the electrodes. Apparently, the sudden change in junction-conductance depends strongly on how the molecule is configured in the junction. It is known that the conductance of a single-molecule junction depends on the conformation, orientation and position of the molecule. This was seen by Gaudioso *et al.* [84] in their STM experiments on single pyrrolidine molecules. In other experiments it was found that e.g. an oxygen molecule on a platinum(111) surface can be rotated by exciting the molecule vibrationally [88]. Rotational motion was also found for C_2H_2 on Cu(100) [89]. Komeda *et al.* [90] were able to observe an increase in the lateral hopping rate of CO molecules on a Pd(110) surface by exciting an internal vibration-mode of the CO molecules. These experiments show that it is possible to induce molecular motion by exciting an internal vibration-mode of the molecule. This could also happen in a single-molecule junction, in which a bonded molecule is located in a shallow potential well and may jump to another geometrical configuration by exciting it internally. When the other geometric configuration results in a different junction-conductance, then a jump in the conductance of the junction will be observed once the molecule is vibrationally excited. The conductance of another geometrical configuration is likely to be different because the conduc-

tance of the metal-molecule-metal junction depends on the degree of coupling of the molecule to the electrodes. Displacements of the molecule on length scales less than λ_F (~ 5 Å) can furthermore cause different interference effects for conduction electrons, which can change the actual conductance in the order of 1%.

4.4 Modelling a vibrationally induced two-level system

Let us now quantify the physics responsible for the anomalous peaks in single molecule dI/dV spectra. The conductance of the junction formed by the molecule depends on the geometrical configuration of the molecule in the junction. Suppose that there are two geometrically different configurations with a slightly different binding energy for the molecule. An energy barrier separating the two states can be overcome by exciting the molecule vibrationally. In figure 4.9 the energy landscape of the molecule in the junction is schematically drawn. Ψ_0 and Ψ_1 are the two ground states of the molecule in the two local energy minima. The molecule can be vibrationally excited with energy $\hbar\omega_v$ to an excited state Ψ^e. This excited state is energetically located above the barrier that separates the two ground states. Only via this excited state it is possible to displace the molecule from Ψ_0 to Ψ_1 since the barrier is too high to allow tunneling between the two ground states to take place. The direction of vibration has to be in the direction of the reaction coordinate (i.e. the movement of the molecule) [91] in order to make a displacement of the molecule possible, unless internal relaxation from one mode to another is taken into account. Here the simplest model is used and the latter possibility is ignored, as well as higher excited states. Support for the idea that the vibrational mode needs to be transversal is obtained experimentally on single-molecule junctions of deuterium molecules contacted by platinum electrodes. A transversal and a longitudinal vibration-mode around 45 meV and 90 meV, respectively, have been found [22, 92]. The transversal mode does regularly show anomalous peaks, as was demonstrated in figure 4.7, while for the longitudinal mode around 90 meV anomalous peaks have never been observed. This indicates that the direction of a transversal vibration is the correct reaction coordinate for a geometrical displacement of the molecule. Given the symmetry of the junction this is understandable since the molecule that is displaced in the perpendicular-to-current direction has many more possibilities of finding a position in which it can be bonded to both electrodes and form a bridge. In the direction of the current there are simply much less possible binding sites given the geometry and the requirement of maintaining contact to both sides. Now it is easily understood that the two different local energy minima can result into two different conductances of the single-molecule bridge. Due to the displacement of the molecule it is most probably bonded to a different site at the apex of one of the electrodes, resulting in a small change of the total conductance of the junction.

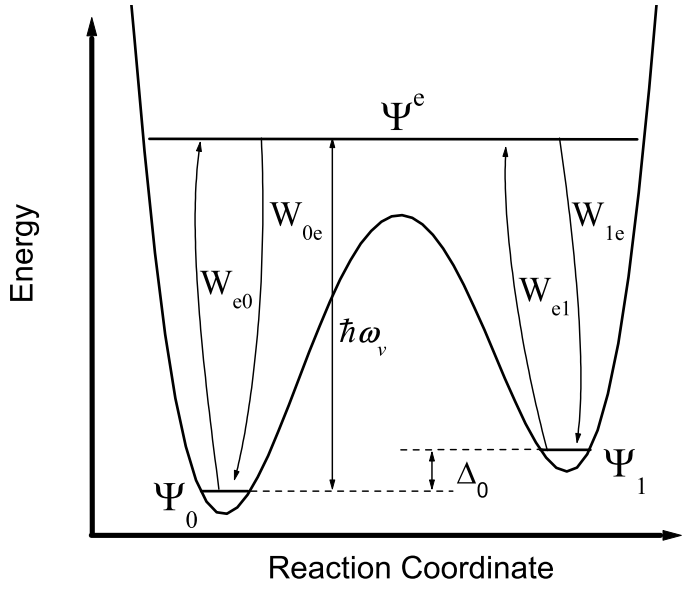

Figure 4.9: *Schematic drawing of the energy landscape of a molecule bridging two electrodes. The molecule experiences two local energy minima, with two ground states Ψ_0 and Ψ_1, separated by a large barrier that can be overcome by exciting the molecule vibrationally with energy $\hbar\omega_v$. Δ_0 is the difference in binding energy between the two ground states, representing the two configurations. The transition rates W_{fi} between all involved states are also shown.*

Now all basic physical ingredients have been introduced and the model of a Vibrationally Induced Two-Level System (VITLS) can be elaborated. The total current passing through the junction can be written as:

$$I(V) = \left(n_0(V)\sigma_0 + n_1(V)\sigma_1 + n_e(V)\frac{(\sigma_0 + \sigma_1)}{2} \right) V, \tag{4.1}$$

in which $n_0(V)$, $n_1(V)$ and $n_e(V)$ represent the voltage dependent occupation numbers of the three states involved in the VITLS. And σ_0 and σ_1 are the conductances of the junction in the local geometrical ground states. For simplicity the conductance of the excited state is taken to be the average of the ground state conductances. Later it will follow that the value of the conductance of the excited state is not very important for the shape of the peak in the differential conductance. In order to determine the shape of the dI/dV spectrum one needs to know the voltage dependence of the occupation numbers $n_0(V)$, $n_1(V)$ and $n_e(V)$.

A dynamic equilibrium between of the three states involved can be de-

scribed in terms of the transition rates between the states:

$$\begin{aligned}\frac{dn_0}{dt} &= -W_{e0} + W_{0e} = 0 \\ \frac{dn_1}{dt} &= -W_{e1} + W_{1e} = 0 \\ \frac{dn_e}{dt} &= -W_{0e} - W_{1e} + W_{e0} + W_{e1} = 0\end{aligned} \tag{4.2}$$

Here W_{fi} represent the transition rates from initial states i to final states f. The total occupation of all three states have to add up to 1:

$$n_0 + n_1 + n_e = 1 \tag{4.3}$$

The equations (4.2) and (4.3) form four coupled equations with three unknown occupation numbers. In order to solve these equations one needs to calculate the rates W_{fi}. The difference in binding energy between the two configurations of the molecule in the junction is the energy difference between the two local ground states and is defined as Δ_0 (see figure 4.9). The vibration-mode energy $\hbar\omega_v$ is assumed to be much larger than Δ_0 and $k_BT \leq \Delta_0$ in order to keep the VITLS well defined in ground state Ψ_0 for low bias voltages.

The rates W_{fi} can be calculated as the integral over energy of the product of available occupied electron states and available unoccupied electron states after exchange of energy with the vibration-mode of the molecule. Furthermore the rate is proportional to the electron-vibration-mode coupling strength γ_{e-v}. It is assumed here that γ_{e-v} is independent of energy. This assumption is valid when the electron conduction band is much wider than the energy-width of the localized vibration-mode, which is usually the case. For simplicity it is additionally assumed that the value of γ_{e-v} is the same in both potential wells. Finally, the rates are proportional to the initial occupation of state i. Therefore the four rates can be written as follows:

$$\begin{aligned}W_{e0} &= n_0 \int_{-\infty}^{+\infty} \gamma_{e-v} f(E, eV)\left[1 - f(E - \hbar\omega_v, eV)\right] dE \\ W_{0e} &= n_e \int_{-\infty}^{+\infty} \gamma_{e-v} f(E, eV)\left[1 - f(E + \hbar\omega_v, eV)\right] dE \\ W_{e1} &= n_1 \int_{-\infty}^{+\infty} \gamma_{e-v} f(E, eV)\left[1 - f(E - \hbar\omega_v + \Delta_0, eV)\right] dE \\ W_{1e} &= n_e \int_{-\infty}^{+\infty} \gamma_{e-v} f(E, eV)\left[1 - f(E + \hbar\omega_v - \Delta_0, eV)\right] dE\end{aligned} \tag{4.4}$$

It is assumed that the density of states is flat over the considered energy window. The non-equilibrium electron distribution functions $f(E, eV)$ can be written in terms of the Fermi-Dirac distribution functions $f_{FD}(E)$:

$$f(E, eV) = \tfrac{1}{2} f_{FD}(E + \tfrac{1}{2}eV) + \tfrac{1}{2} f_{FD}(E - \tfrac{1}{2}eV) \tag{4.5}$$

$$f_{FD}(E) = \frac{1}{1 + \exp\left(\frac{E - E_F}{k_B T}\right)} \tag{4.6}$$

In order to evaluate the integrals let us set $E_F = 0$ and define the new variables $u = E/k_B T$ and $\nu = \frac{1}{2}eV/k_B T$ so that equation (4.5) can be written as:

$$f(E, eV) = \frac{1}{2}\left[\frac{1}{1 + e^{u+\nu}} + \frac{1}{1 + e^{u-\nu}}\right] \tag{4.7}$$

The main part of the expression for the transition rates consists of the integrals of equation (4.4), which are of the form $\int f(E, eV)\left[1 - f(E + \Delta E, eV)\right] dE$, in which ΔE is $(\pm\hbar\omega_v \pm \Delta_0)$. After a new variable is introduced, $\varepsilon = \Delta E/k_B T$, the integrals can be evaluated:

$$\int_{-\infty}^{+\infty} f(E, eV)\left[1 - f(E + \Delta E, eV)\right] dE = \tag{4.8}$$

$$\frac{k_B T}{4} \int_{-\infty}^{+\infty} \left[\frac{1}{1 + e^{u+\nu}} + \frac{1}{1 + e^{u-\nu}}\right]\left[2 - \frac{1}{1 + e^{u+\varepsilon+\nu}} + \frac{1}{1 + e^{u+\varepsilon-\nu}}\right] du =$$

$$\frac{k_B T}{4} \int_{-\infty}^{+\infty} \left[\frac{1}{1 + e^{u+\nu}} + \frac{1}{1 + e^{u-\nu}}\right]\left[\frac{1}{1 + e^{-u-\varepsilon-\nu}} + \frac{1}{1 + e^{-u-\varepsilon+\nu}}\right] du$$

By using the following integral,

$$\int_{-\infty}^{+\infty} \frac{1}{1 + e^{x}} \frac{1}{1 + e^{-x-a}} dx = \frac{\alpha}{1 - e^{-\alpha}} \equiv g(\alpha), \tag{4.9}$$

the integrals can be separated into four similar terms and be evaluated:

$$\frac{4}{k_B T} \int_{-\infty}^{+\infty} f(E, eV)\left[1 - f(E + \Delta E, eV)\right] dE =$$

$$[g(\varepsilon)+g(\varepsilon-2\nu)+g(\varepsilon+2\nu)+g(\varepsilon)]= \\ \frac{2\varepsilon}{1-e^{-\varepsilon}}+\frac{\varepsilon-2\nu}{1-e^{\varepsilon+2\nu}}+\frac{\varepsilon+2\nu}{1-e^{-\varepsilon-2\nu}} \tag{4.10}$$

The solution (4.10) can be further simplified when considering the low temperature limit, with $\frac{\hbar\omega_v}{k_BT}, \frac{(\hbar\omega_v-\Delta_0)}{k_BT} \gg 1$, and by limiting the discussion to positive bias voltage only, $eV > 0$. Then (4.10) simplifies to:

$$\int_{-\infty}^{+\infty} f(E,eV)\left[1-f(E+\Delta E,eV)\right]dE = \\ \begin{cases} \Delta E+\dfrac{1}{4}\dfrac{\Delta E-eV}{e^{(\Delta E-eV)/k_BT-1}}, & \text{when } \Delta E>0, \\ \dfrac{1}{4}\dfrac{-\Delta E-eV}{e^{(-\Delta E-eV)/k_BT}-1}, & \text{when } \Delta E<0 \end{cases} \tag{4.11}$$

The results of (4.11) can now be inserted into the expressions for the transition rates of equation (4.4), which become:

$$\begin{aligned} W_{e0} &= n_0\gamma_{e-v}\frac{1}{4}\left(\frac{\hbar\omega_v-eV}{e^{(\hbar\omega_v/k_BT)}-1}\right)dE \\ W_{0e} &= n_e\gamma_{e-v}\left(\hbar\omega_v+\frac{1}{4}\frac{\hbar\omega_v-eV}{e^{(\hbar\omega_v/k_BT)}-1}\right)dE \\ W_{e1} &= n_1\gamma_{e-v}\frac{1}{4}\left(\frac{\hbar\omega_v-\Delta_0-eV}{e^{(\hbar\omega_v+\Delta_0)/k_BT}-1}\right)dE \\ W_{1e} &= n_e\gamma_{e-v}\left(\hbar\omega_v+\Delta_0+\frac{1}{4}\frac{\hbar\omega_v+\Delta_0-eV}{e^{(\hbar\omega_v+\Delta_0)/k_BT}-1}\right)dE \end{aligned} \tag{4.12}$$

These transition rates can now be inserted in the set of linear equations (4.2) in order to find the voltage dependent expressions for the occupation numbers of the three states of the VITLS. The set of equations can be solved analytically but since the solutions are very lengthy they are not displayed here.

The shape of the dI/dV spectrum is determined by the five parameters that enter the VITLS model, namely the conductances σ_0, σ_1, the energy difference Δ_0 between Ψ_0 and Ψ_1, the vibration-mode energy $\hbar\omega_v$ and the temperature T. Figure 4.10 shows how the shape of a dI/dV spectrum changes when a certain parameter is modified. The vibration-mode energy is fixed at 50 meV in all shown spectra. In figure (a) a peak is seen caused by the fact that σ_1 is 10% larger than σ_0. It is clear that the peak maximum is more than 30% higher than the average of σ_0 and σ_1. The evolution of the occupation numbers is shown in the bottom graph of figure (a). It is clearly seen that at zero bias voltage Ψ_0 is more than 90% occupied while Ψ_1 less than 10%. Ψ_e is unoccupied because the bias voltage is far below the vibration-mode energy. When the temperature is raised from 5 to 20 K the peak becomes very much suppressed and broadened as is shown in figure 4.10(b), in which all other parameters are kept the

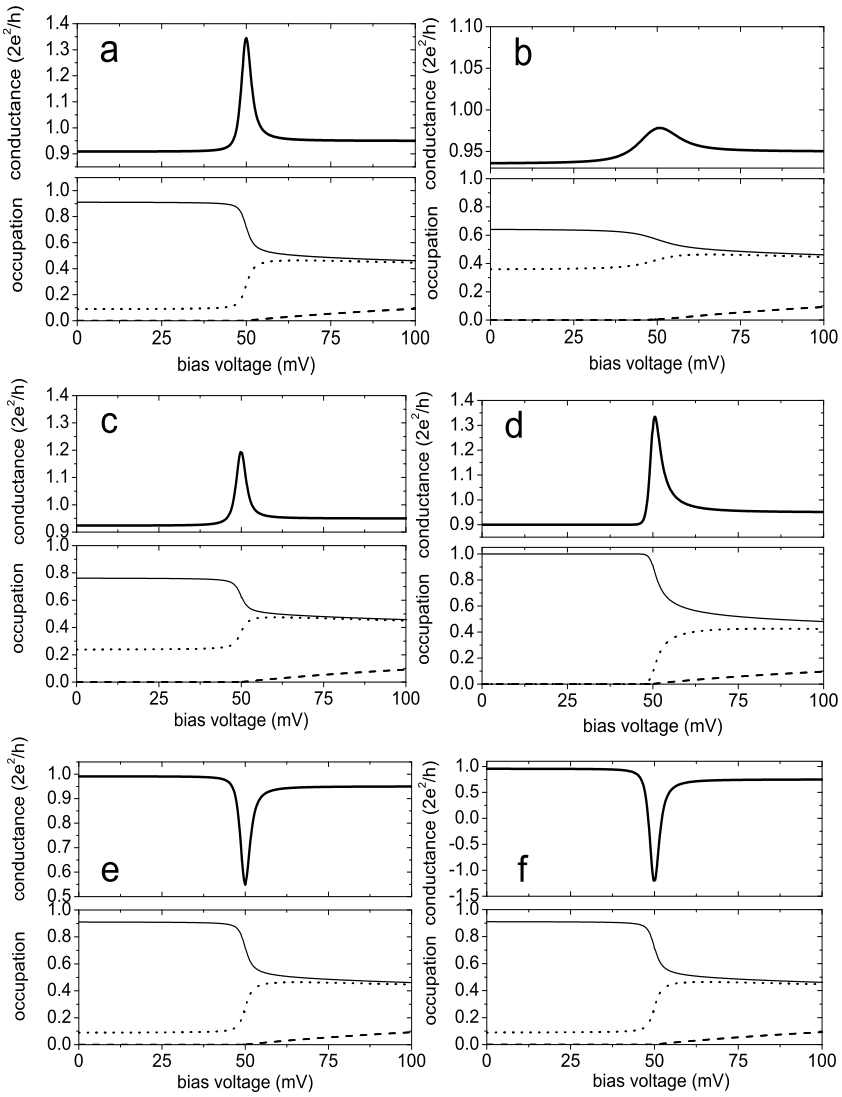

Figure 4.10: *Dependence of the calculated dI/dV spectrum and occupation numbers on different sets of parameters. Upper graphs show dI/dV spectra and lower graphs show occupation numbers n_0 (solid line), n_1 (dotted line) and n_e (dashed line). The energy of the vibration-mode is fixed at 50 meV. Fig.(a)* $\Delta_0 = 1.0meV$, $\sigma_0 = 0.9G_0$, $\sigma_1 = 1.0G_0$, $T = 5K$; *Fig.(b)* $\Delta_0 = 1.0meV$, $\sigma_0 = 0.9G_0$, $\sigma_1 = 1.0G_0$, $T = 20K$; *Fig.(c)* $\Delta_0 = 0.5meV$, $\sigma_0 = 0.9G_0$, $\sigma_1 = 1.0G_0$, $T = 5K$; *Fig.(d)* $\Delta_0 = 4.0meV$, $\sigma_0 = 0.9G_0$, $\sigma_1 = 1.0G_0$, $T = 5K$; *Fig.(e)* $\Delta_0 = 1.0meV$, $\sigma_0 = 1.0G_0$, $\sigma_1 = 0.9G_0$, $T = 5K$; *Fig.(f)* $\Delta_0 = 1.0meV$, $\sigma_0 = 1.0G_0$, $\sigma_1 = 0.5G_0$, $T = 5K$.

same as in figure (a). Here the peak maximum is only a few percent higher than $\frac{\sigma_0+\sigma_1}{2}$. The bottom graph shows that the reduction of the peak is due to a more equilibrated occupation of n_0 and n_1 at low bias voltage. This causes the effect of decrease and increase of n_0 and n_1, respectively, upon exciting the vibration-mode to be reduced. Additionally, the higher temperature causes the energy window, in which the repopulation of Ψ_0 and Ψ_1 mainly occurs, to be larger, which also has a reducing effect on the strength of the peak. This has serious consequences for experiments where higher temperatures can reduce the peak so much that it can not be resolved anymore. Reducing Δ_0 also results in a decrease of the peak maximum as is shown in figure (c), but the broadening of the peak is almost unaffected. Increasing Δ_0 on the other hand causes more asymmetry in the peak-shape, but the peak height remains more or less the same as can be seen in figure 4.10(d). The asymmetry can also be seen in the occupation numbers of the bottom graph of (d). Since Δ_0=4meV is much larger than the temperature (k_BT = 0.43meV at T = 5 K) there is a nearly full occupation of Ψ_0 at low bias voltage. Furthermore the thermal smearing of the vibration-mode energy is less effective due to the larger Δ_0. This causes a more abrupt repopulation of the two local ground-states once the bias voltage comes close to $\hbar\omega_v$. In figure 4.10(e) a negative peak is shown, resulting from σ_1 being smaller than σ_0. When $\frac{\sigma_1}{\sigma_0}$ is small enough the minimum of the dI/dV peak can become negative, resulting in negative differential conductance as displayed in figure 4.10(f).

4.5 Fitting experimental data with the VITLS model

The model for a VITLS as formulated and calculated in the previous section is applied to experimental differential conductance spectra for single-molecule junctions. Figure 4.11 shows the positive bias part of a differential conductance spectrum for a single hydrogen molecule contacted by platinum electrodes. At about 47 meV a clear positive peak is observed. One can also observe a difference in conductance between the low and high bias side of the peak, where the latter is higher in accordance with the model for a positive peak. The solid curve is a fit to the experimental data using the first derivative of equation (4.1). The lower graph of figure 4.11 shows the evolution of the occupation of the three states involved in the VITLS as a function of bias voltage. The graph shows that for low bias voltages ($V << V_{\hbar\omega}$) the molecule is practically for 100% of the time in state Ψ_0. When the bias voltage is increased and comes close to the value $V_{\hbar\omega}$, the time averaged population of state Ψ_0 decreases sharply while the time averaged population of state Ψ_1 increases sharply. Since the geometrical configuration of the molecule in the junction represented by state Ψ_1 has a slightly higher conductance, a sudden change in the time averaged conductance is the result. The fit of figure 4.11 was generated with a difference of only 2.5 % in conductance between the two states in order to obtain a clearly distinguishable peak in the differential conductance spectrum. This small difference in conductance is not easily observed in the

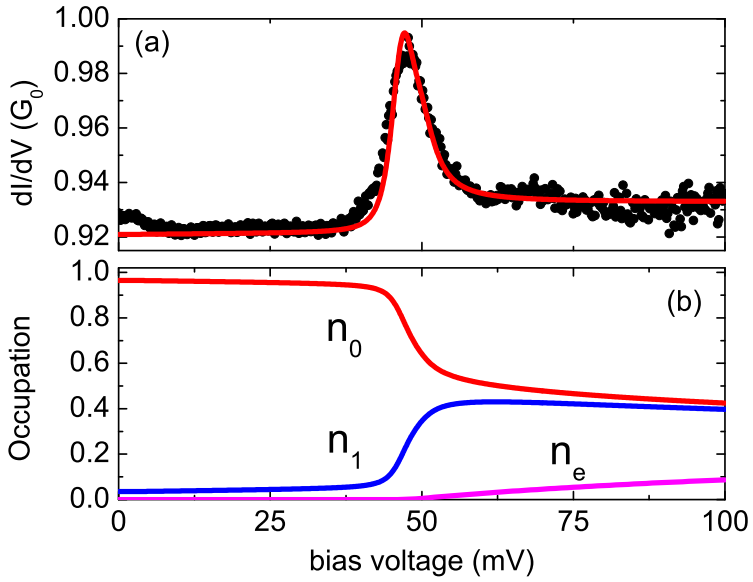

Figure 4.11: *Figure (a) shows the positive bias part of a dI/dV spectrum (black dots) taken for a single H_2 molecule clamped by Pt electrodes. Clearly the peak at about 47 mV is resolved and nicely fitted by the VITLS model (solid curve). Fit parameters are: $\Delta_0 = 3.0meV$, $\sigma_0 = 0.923G_0$, $\sigma_1 = 0.946G_0$, $\hbar\omega_v = 47meV$, $T = 8K$. Figure (b) shows the evolution of the three occupation numbers as a function of bias voltage.*

I-V measurement.

As was mentioned earlier in this chapter the anomalous peaks in differential conductance spectra do appear in single-molecule junctions of many different molecules and electrode metals. Figure 4.12 shows some more examples plus VITLS fits of positive and negative peaks in dI/dV spectra. Figure (a) was taken on an atomic gold chain with hydrogen admitted. The hydrogen molecules can either be physisorbed or chemisorbed on the side of the gold chain or even be incorporated into the chain. More on this subject can be found in the next chapter of this thesis. In this case clear negative peaks are seen at a bias voltage around $\pm$ 40 mV. Also the conductance fluctuates a lot as a function of bias voltage and the mean conductance of the atomic wire is around 0.8 G_0 instead of 1 G_0 as in the case for clean gold wires. These fluctuations are more pronounced when the conductance of the junction is lower than 1 G_0. The conductance fluctuations are attributed to the interference of electron waves that scatter on impurities and defects in the electrodes close to the junction [93] and are suppressed when the junction conductance is due to a single fully transparent channel [36]. These conductance fluctuations often mask regular vibration-mode steps in dI/dV spectra. The difference in conductance

between σ_0 and σ_1 is only 5%, but the peaks clearly show in the spectrum.

Figure 4.12(b) displays another differential conductance spectrum for an atomic gold chain with hydrogen admitted, at an elevated sample temperature of 20 K. The VITLS-peaks at about $\pm$ 42 mV can still be seen, but they do not stand out as much, due to thermal smearing. A 3% difference in conductance between the two geometrical states results in a peak that lifts itself just 1% above the average conductance of the atomic chain. Another nice feature of this spectrum is the, equally smeared, regular longitudinal phonon mode for a gold atomic chain around $\pm$ 15 mV. Note that the temperature of the fit agrees very well with the experimental value.

Figure (c) shows a dI/dV spectrum for a single CO molecule bridging two platinum electrodes. Large positive peaks are seen at about $\pm$ 33 mV and

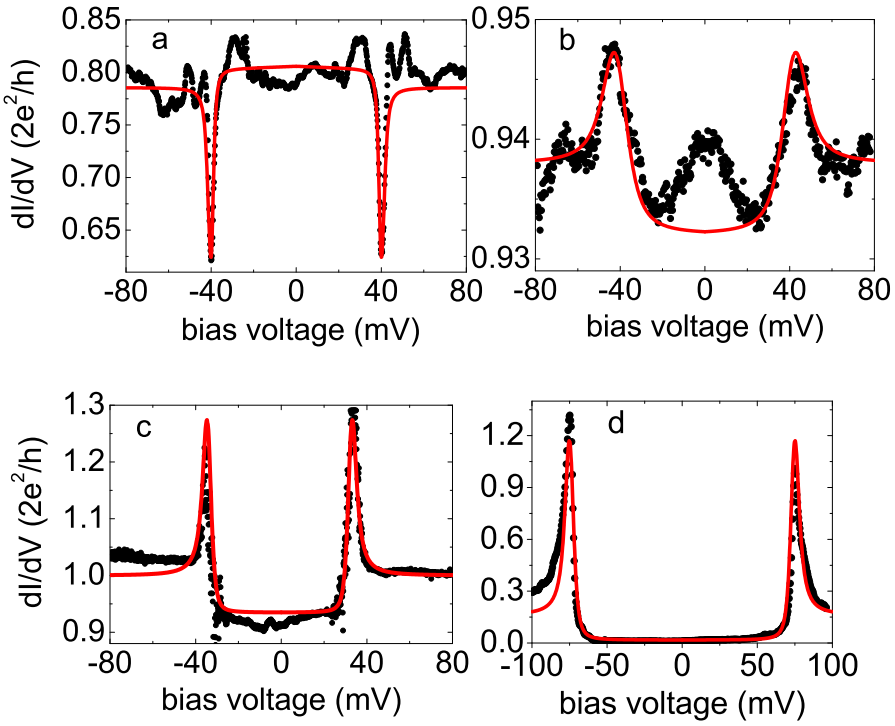

Figure 4.12: *VITLS fits for different molecule-metal combinations: (a) Atomic gold chain with hydrogen admitted at T = 5 K; (b) atomic gold chain with hydrogen admitted at T = 20 K; (c) CO molecule contacted by platinum electrodes at T = 5 K; (d) Oxygen contacted by nickel electrodes at T = 5 K. The fit parameters of the VITLS model [σ_0, σ_1, $\hbar\omega_v$, Δ_0, T] are: (a) [0.803G_0, 0.765G_0, 40meV, 1.0meV, 4K]; (b) [0.924G_0, 0.954G_0, 42meV, 1.5meV, 20K]; (c) [0.93G_0, 1.07G_0, 33meV, 2.5meV, 6.5K]; (d) [0.01G_0, 0.33G_0, 75meV, 2.5meV, 8.5K]. Note that all fits have been performed on the positive bias side of the spectrum, which in general also yield good fits for the negative bias side.*

the VITLS fits yield a difference of 15 $\%$ in conductance between Ψ_0 and Ψ_1, larger than for the hydrogen experiments discussed above. In case of oxygen in a nickel contact the difference in conductance is typically much larger. The VITLS fit of figure 4.12(d) resulted in a difference of as much as 100$\%$, but even larger differences have been measured.

For all fits the value of Δ_0, which is the difference in binding energy for the molecule in the two geometrical configurations, has a value between 1 and 4 meV. This is very small compared to the total binding energy of the molecule, which is typically of the order of eVs. For a very small molecule like hydrogen this small difference in binding energy apparently results in also a small difference in conductance. The bigger molecules like CO and oxygen seem in general more sensitive to the difference in binding energy, since difference in conductance of the two configurations is larger. CO is a non-symmetric molecule, which makes it probably more sensitive on the exact binding sites and the strength of the bonds. Of all studied molecules, oxygen contacted by nickel electrodes displayed by far the largest VITLS peaks and consequently also the largest difference in conductance between the two configurations. Chapter 6 deals with the case of Nickel-oxygen contacts in more detail.

In most cases the VITLS fits of differential conductance spectra yield a somewhat higher temperature than the bath temperature. The maximum fitted temperature for a bath temperature of about 5 K is about 8 K. The reason for this discrepancy is possibly due to poor thermal anchoring of the metal MCBJ-wire. A thermometer mounted close to the sample typically reads a temperature between 5 and 9 K depending on the insert used. Another reason can be that due to the very high current density near the contact the local electron temperature in the junction is somewhat higher. The higher temperature is probably not an artifact of the VITLS model, since also in regular vibration-mode spectra the width of the conduction step is broader than expected given a bath temperature of 5 K [8, 22, 92].

4.6 Exceptional curves and multiple levels

In the VITLS-model the molecule can be bonded in two geometrically different configurations. When the molecule has a different binding energy to the electrodes in these two configurations and the junction displays different conductances, then a peak in dI/dV can be observed. But it is of course also possible that the molecule has more binding sites due to a more complicated potential landscape involving more local minima, which can be accessed once the potential barrier is overcome by vibrationally exciting the molecule. This can explain other features that have been observed in differential conductance spectra, albeit on a much less regular basis. The most prominent of these features is a combination of two peaks in opposite direction, closely resembling an S-shaped feature. In figure 4.13 an example of such S-shaped feature is displayed together with a fit. The fit was made by introducing a third local ground state Ψ_2 in the model, making it in essence a Three-Level model, consisting of an ab-

solute ground state Ψ_0, a slightly elevated local ground state Ψ_1 and a second even higher elevated local ground state Ψ_2. The geometrical configuration of the molecule in the junction represented by Ψ_1 has a lower conductance than the geometry of Ψ_0. The third geometry of Ψ_2 has a higher conductance than Ψ_0. Since the difference in binding energy of the molecule to the electrodes between Ψ_2 and Ψ_0 is somewhat larger than between Ψ_1 and Ψ_0 the population of state Ψ_2 starts to increase at a slightly higher bias voltage as can be seen in the bottom graph of figure 4.13, where the evolution of the voltage dependent occupation numbers is displayed. This evolution results in the fit that is shown in the upper graph of figure 4.13.

The difference in binding energy between the two geometrical excited state configurations ($\Delta_1 - \Delta_0$) is only 1.1 meV, but it has a dramatic result on the eventual shape of the fitted dI/dV spectrum. The sensitivity to the value of the difference in binding energy ($\Delta_1 - \Delta_0$) on the shape of the fit of the differential conductance spectra is displayed in figure 4.14. In figure 4.14(b) the S-shaped structure has disappeared and is replaced by a single negative peak. This is caused by increasing the value of Δ_0 from 1.5 to 2.2 meV, which decreases the

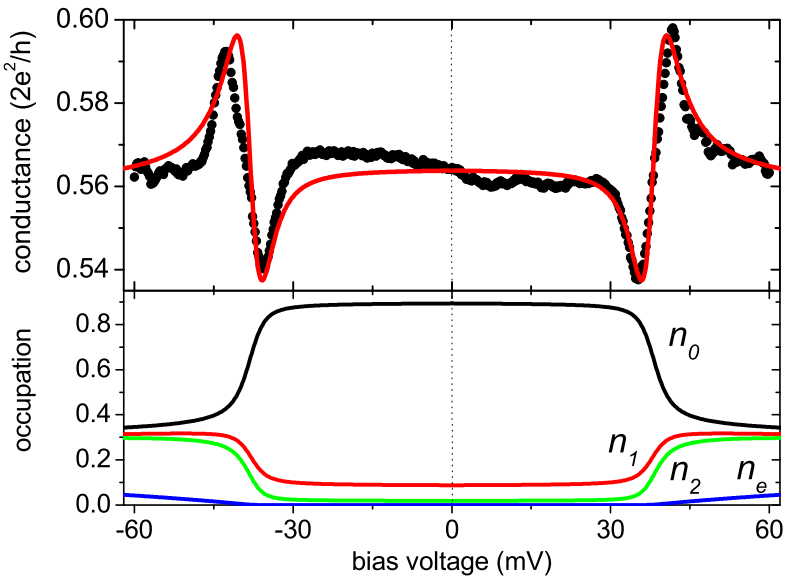

Figure 4.13: *Three level fit of a dI/dV spectrum taken on an atomic gold chain with hydrogen admitted at T = 5 K. The top graph shows a clear negative peak rapidly followed by a positive peak in the spectrum. The bottom graph shows the voltage dependent occupation numbers n_0, n_1, n_2 and n_e. The fit parameters are: [σ_0=0.574G_0, σ_1=0.435G_0, σ_2=0.702G_0, $\hbar\omega_v$=38.5meV, Δ_0=1.5meV, Δ_1=2.6meV, T=7.5K]. Note that the positive bias side of the spectrum was fitted.*

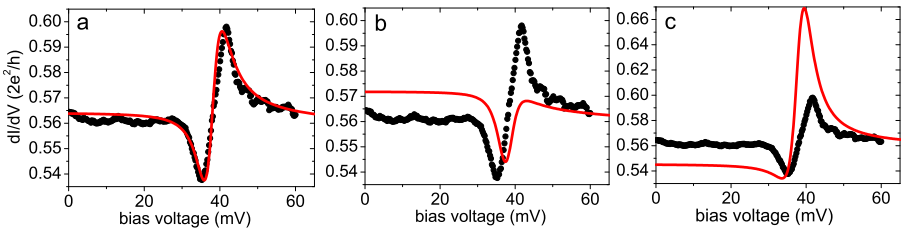

Figure 4.14: *Changing the difference in binding energy between the two states Ψ_1 and Ψ_2 and the effect on the resulting dI/dV spectra: (a) shows the same fit as in figure 4.13. In (b) Δ_0=2.2meV and in (c) Δ_0=0.8meV.*

difference in binding energy of the two states Ψ_1 and Ψ_2. When (Δ_1 - Δ_0) is increased, as was done for the fit in figure 4.14(c), the S-shaped feature is lost and a large positive peak remains. These results indicate that the exact value of Δ_0 and Δ_1 is extremely important for the eventual shape of the differential conductance curve that is obtained, compared to when only two levels are involved. In the latter case the shape of the spectrum is much less sensitive to the value of Δ_0.

4.7 Relationship with previous observations

Let us finally discuss the relationship between the VITLS model and dI/dV peaks from the literature that were mentioned earlier in this chapter in figures 4.2 to 4.6. For the experiment on a single pyrrolidine molecule on Cu(001) the relationship between the dI/dV peaks, vibration-mode energies and different molecular conformations was clearly demonstrated [84]. It is therefore very likely that the origin of the peaks is a sort of VITLS. The IETS experiment by Wang *et al.* [85] were performed at T = 4.2 K on a self-assembled monolayer of alkanedithiols consisting of hundreds of molecules. Some of the broadened peaks in dI/dV spectra are located at known energies of internal vibration-modes of alkanedithiol and have been discussed in view of their unexpected shape [42, 94]. It is also possible that they are caused by exciting VITLSs in the monolayer. The strong broadening of the peaks can be attributed to inhomogeneous broadening in the ensemble of molecules measured and because a higher modulation amplitude was used. The STM measurements on a hydrogen covered copper surface have yielded similar anomalous dI/dV spectra in largely the same energy range (10-100 meV) as discussed here [86]. Although the peaks look very similar and are probably related, the peaks have not been found at known vibrational excitations of hydrogen on copper and were furthermore hydrogen-coverage dependent. It could be that for different hydrogen-coverage, certain different hydrogen-copper clusters are formed with different vibrational properties. Moreover, the system was observed to remain in the σ_1-state above the threshold voltage. Possibly the geometry of

the experiment allows the molecules to be excited into locations away from the STM tip, after which they are slow to return. Another explanation could be that it is due to a asymmetric electron-phonon coupling of the two levels involved in the two-level system as was recently proposed by Halbritter *et al.* [95]. In the two-level model described in this thesis the electron-phonon coupling is assumed to be equal for both geometrically different states. A large asymmetry not only results in huge peaks in differential conductance but also that at high bias the system remains in the state that has the weakest electron-phonon coupling.

This leaves the two older experiments by Ralph *et al.* [82, 87] and Keijsers *et al.* [83] to be discussed. Both studies investigated large contacts with resistances of order 1-10 Ω and observed the anomalous peaks at bias voltages below the Debye energy of the metal under study. These low energies rule out that the anomalies are due to impurities in the form of small molecules. Although there are similarities there are also main differences between those observations. Ralph *et al.* found a dependence on applied magnetic field, while Keijsers *et al.* did not. The former authors also found that the spikes were sometimes much narrower than what thermal broadening would allow (see figure 4.2), while Keijsers *et al.* did not. The latter study found a $\sqrt{R}$ dependence of the energy at which the S-shaped anomaly was observed. In both investigations the anomalies have been brought in connection with two-level systems in the contact, since they were often observed together with zero-bias anomalies, which have been very well understood in terms of the excitation of two-level systems. The exact physical mechanism driving the anomalies, nevertheless, remains elusive.

4.8 Conclusions

Anomalous positive and negative peaks in differential conductance spectra have been regularly observed for single-molecule junctions. These peaks are observed for many different molecules and different metal electrodes making them a general feature. It was found from previous experiments and from the isotope substitution effect that the peaks are related to local vibration-modes of the molecule in the contact. The basic assumption behind the anomalous peaks is that a molecule in the atomic junction does not have one unique binding site but that there can be one or more other configurations, which the molecule can access when it is vibrationally excited. A model of a vibrationally-induced two-level system (VITLS) has been mathematically elaborated and fits the experimental differential conductance spectra very well. Because the VITLS peaks are also observed for single-molecule junctions having a much lower than $2e^2/h$ conductance and are typically much better visible than "regular" vibration-mode steps in the spectrum, they can be used as a new tool for identifying local vibration-mode energies in single-molecule junctions. With this conclusion it can shed a new light on previous experiments in which similar features have been observed.

5

Physical properties of gold-hydride atomic chains

The properties of gold atomic chains under the influence of hydrogen are investigated. Evidence is supplied that gold atomic chains react with hydrogen molecules resulting in the incorporation of hydrogen into the wires. Hydrogen incorporation modifies the conductive and vibrational properties of these atomic wires. A simultaneous study of the conductance and vibration-modes of the gold-hydride wires as a function of stretching of the wire is performed. The results are compared with previous experimental and theoretical investigations on gold-hydride chains and provide additional evidence that hydrogen is preferably incorporated as a molecule into atomic gold chains.

5.1 Introduction

In chapter 3 the properties of metallic atomic chains with oxygen incorporated were discussed. Substantial evidence was provided that atomic oxygen can be incorporated in atomic chains of the noble metals gold, silver and copper reinforcing the linear bond in order to create longer chains. The large interatomic distances in atomic gold chains created in UHV by means of TEM, which were observed by Ohnishi *et al.* [5] and Rodrigues *et al.* [96] have been analyzed in terms of the incorporation of oxygen atoms in gold atomic chains [57, 58]. But another very interesting candidate as contaminant in atomic gold chains is hydrogen. It is the smallest and lightest molecule and hydrogen is always present in a (UHV) vacuum chamber at room temperature. Hydrogen is the most heavily studied element as impurity in atomic gold wires by computational methods [53–55, 97–100]. These investigations deal with the incorporation of both molecular and atomic hydrogen and do not produce a unique picture about which form is preferred. Also experimentally the effects of hydrogen on atomic gold wires have been investigated [78,101]. It was found that atomic gold wires in a hydrogen environment display next to the regular conductance of 1 G_0 also a preferential conductance of about 0.5 G_0 [101]. This half-conductance quantum was interpreted as being the result of the onset of a dimerization in the gold chain, induced by the embedding in several mono-layers of hydrogen molecules that stabilize the one-dimensional structure. More recent calculations show that the observation of a half-conductance-quantum can also be due to the chemisorption of atomic hydrogen to the side of an atomic gold chain [99]. The authors claim that the reactivity of atomic gold chains increases substantially when the chain is stretched, making the dissociation of molecular hydrogen possible. A stabilization of atomic gold wires due to incorporated atomic hydrogen was claimed by Skorodumova *et al.* [54]. Experiments have shown that atomic gold chains also display conductances lower than 0.5 G_0 when they are exposed to hydrogen [78]. Sometimes an interesting alternating pattern was observed of a gradual conductance increase from less than 0.1 G_0 to above 0.2 G_0 upon stretching the wire. This phenomenon is attributed to incorporated molecular hydrogen that is stretched into a parallel-to-wire configuration, which should have a higher conductance compared to a perpendicular-to-wire configuration according to calculations [97].

Various experiments and calculations have resulted in different values for the conductance of gold-hydride atomic wires. A value of about 0.6 G_0 has been calculated and found experimentally and it has been attributed to the adsorption of atomic hydrogen [99, 101]. Another calculation found the conductance of a gold wire with incorporated atomic hydrogen to be less than 0.1 G_0 [97]. The conductance of an incorporated hydrogen molecule was calculated to be higher, namely around 0.25 G_0. Yet in another calculation both the conductance of incorporated atomic and molecular hydrogen was calculated to be much higher, namely about 0.8 G_0 [100]. These contradicting and confusing results make it hard to draw a firm conclusion about whether atomic or molecular hydrogen is preferably incorporated into atomic gold wires. In this

chapter the combined results on the conductance and mechanical properties of gold-hydride atomic chains will be presented providing additional information to clarify this issue.

5.2 Conductance of gold-hydride atomic wires

The conductance of atomic gold-hydride wires is analyzed by constructing conductance histograms as was first done for this system by Csonka *et al.* [101]. The results from their experiments are shown in figure 5.1. The conductance histograms were taken at T = 20 K and in figure (a) one can clearly see a peak around 0.5 G_0. The peak at half conductance quantum was not observed at lower temperatures and also not when a high bias voltage was applied over the gold wires, as can be seen in figure (b). The experiments of Csonka *et al.* were repeated for the investigation described in this chapter. Figure 5.2 shows conductance histograms taken at 20 K on clean gold at 50 mV bias (a), gold with hydrogen admitted at 150 mV bias (b), gold with hydrogen admitted at 50 mV

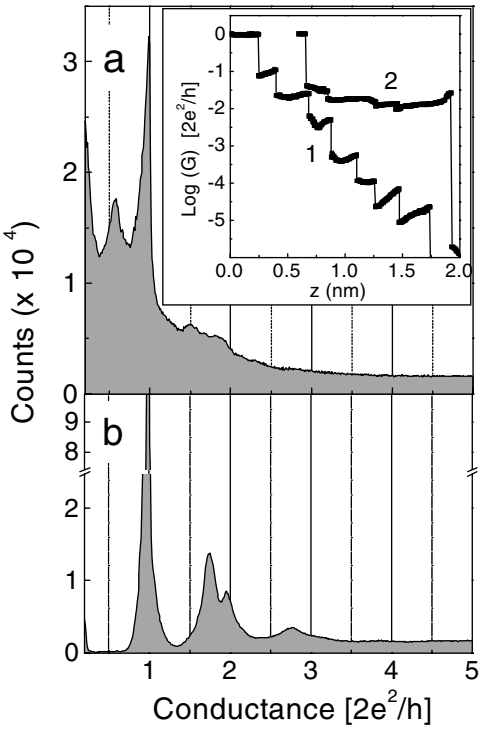

Figure 5.1: *Conductance histograms taken for gold with hydrogen admitted at T = 20 K with different bias voltages. In figure (a) a bias voltage of 65 mV was used and (b) 240 mV. Taken from Ref. [101].*

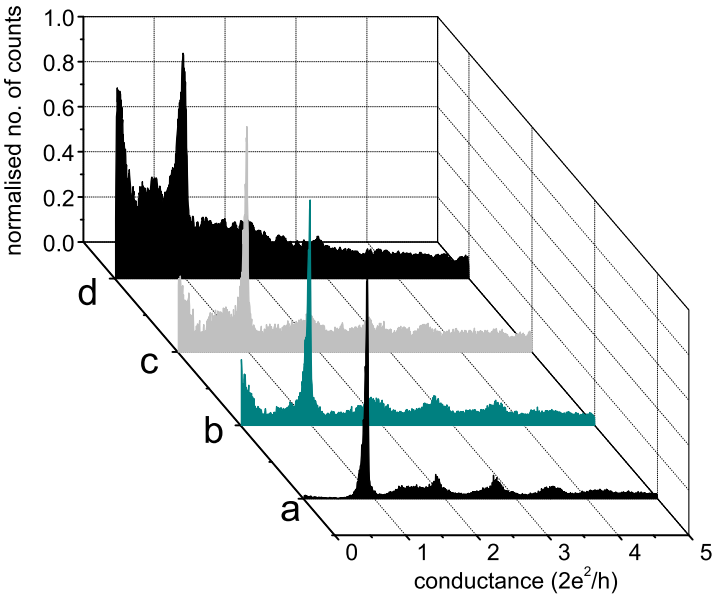

Figure 5.2: *Conductance histograms taken for gold with hydrogen admitted at T = 20 K for different bias voltages: (a) clean gold at 50 mV bias; (b) gold with hydrogen admitted at 150 mV bias; (c) gold with hydrogen admitted at 50 mV bias; (d) gold with hydrogen admitted at 20 mV bias.*

bias (c) and gold with hydrogen admitted at 20 mV bias (d). Clean gold shows no anomalies, as expected, and the conductance histogram is dominated by the large peak located around 1 G_0. There are hardly any counts for conductance values below 0.8 G_0. When hydrogen is admitted to the vacuum chamber and the bias voltage is kept at 50 mV the most evident change is the observation of conductance values lower than 1 G_0. Especially for very low conductance values a clear increase is seen and around 0.5 G_0 one can see a broad peak, although it is not as clear as was seen by Csonka *et al.* Upon increasing the bias voltage to 150 mV one can clearly see that the number of counts for conductances lower than 1 G_0 decreases compared to the histogram taken with 50 mV bias. This phenomenon was also observed by Csonka *et al.* and also in measurements of hydrogen with platinum [92]. The most probable explanation is that due to the higher bias voltage the contact becomes locally heated, since the power dissipated in the contact increases linearly with increasing current. The higher temperature causes a shorter average lifetime of the contact due to larger thermal motion of the atoms and eventually the local desorption of hydrogen. In other words the probability that a hydrogen molecule is stably chemisorbed to the electrodes at the moment that it needs to bridge the gap between the electrodes becomes lower at higher bias voltages. The hot spot formed by the junction will cause hydrogen to diffuse away from it and even

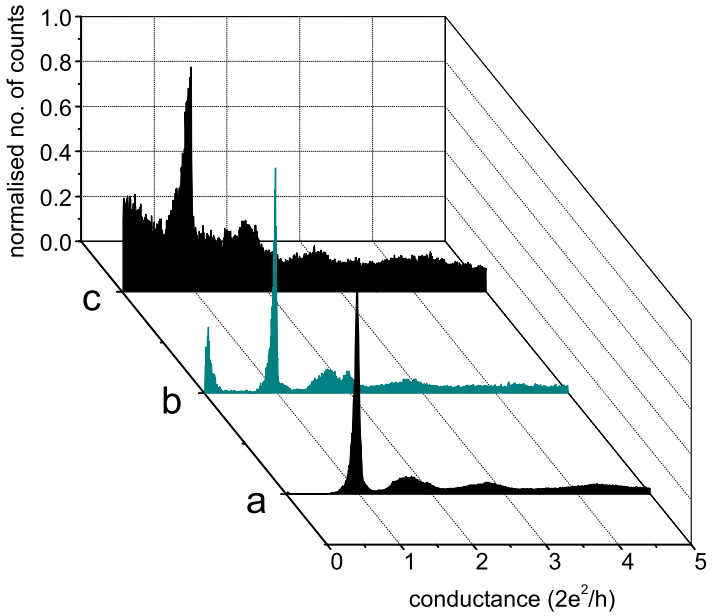

Figure 5.3: *Conductance histograms taken for gold with hydrogen admitted at T = 5 K for different bias voltages: (a) clean gold at 50 mV bias; (b) gold with hydrogen admitted at 150 mV bias; (c) gold with hydrogen admitted at 50 mV bias.*

evaporate into the vacuum. By lowering the bias voltage to 20 mV the number of counts for conductances between 0 and 0.8 G_0 increases quite dramatically and a peak around 0.5 G_0 is resolved as seen in figure 5.2(d). Due to a lower bias voltage and thus lower local heating more adsorption sites for hydrogen molecules are possible that would not be stable at higher bias.

All measurements presented in figure 5.2 have been performed with a junction temperature of 20 K, since this is the temperature at which Csonka *et al.* observed the peak at half quantum [101]. Conductance histograms for clean atomic gold wires and with hydrogen admitted at the base temperature of 5 K are shown in figure 5.3. Without having any hydrogen admitted to the junction, the regular conductance histogram for gold is obtained without any conductance counts below the dominant peak at 1 G_0 (see figure 5.3(a)). By keeping the bias voltage at 50 mV when hydrogen is admitted, more conductance counts are recorded below 1 G_0 but no peak at 0.5 G_0 is resolved in contrast to the measurements at 20 K, which corresponds with the observations of Csonka *et al.* When hydrogen is admitted to the vacuum chamber and the bias voltage is raised to 150 mV the number of counts between 0 and 1 G_0 dramatically decreases, leaving only some conductance counts close to zero conductance. Likely, this is again due to more thermal instability at the apexes of the electrodes.

5.3 Length histograms for gold-hydride wires

One way to obtain more information about the composition of gold-hydride atomic wires is to study the evolution of the conductance of individual traces while pulling the electrodes apart. In figure 5.4 four individual traces are shown, which were recorded at the final stages of breaking gold atomic contacts in a hydrogen rich environment at T = 5 K. All contacts reach a stable conductance value of about $2e^2/h$, indicating that a contact with a diameter of only a single gold atom is reached. Upon further stretching the conductance drops considerably and varies between 1 and 0 G_0 upon further stretching until the wire eventually breaks. Csonka *et al.* [78] have investigated individual traces in detail and they found sometimes a repeating sequence of increasing conductance from about 0.1 G_0 to 0.25 G_0 upon stretching, followed by a jump in conductance back to 0.1 G_0 and an increase again. This pattern was attributed to the presence of a hydrogen molecule in the atomic gold chain that is stretched resulting in a higher conductance as was predicted by calculation [97]. Once the stress that is built up in the wires reaches its maximal value, the wire breaks or pulls another gold atom into the wire. When the latter happens the atomic

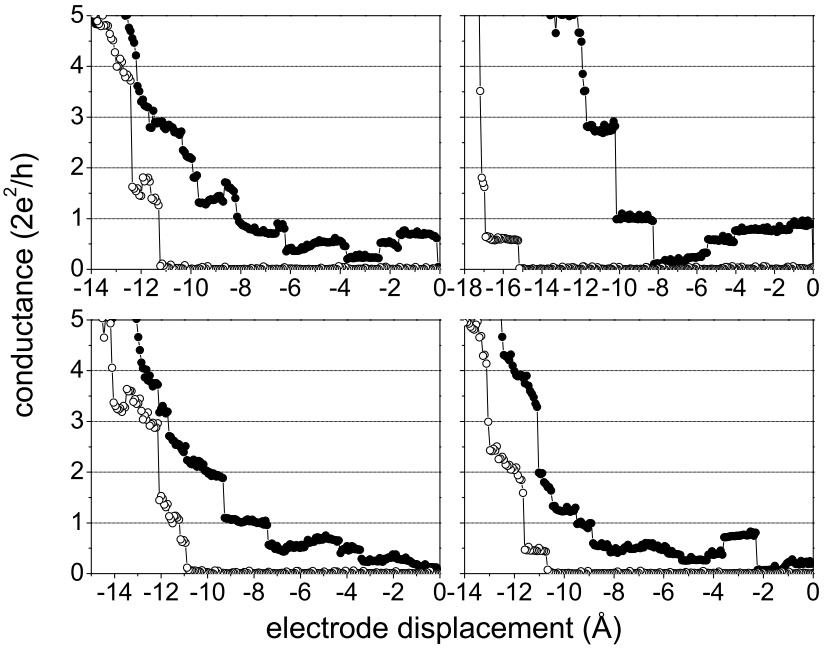

Figure 5.4: *Individual breaking (black circles) and return traces (open circles) of gold atomic wires with hydrogen admitted. All traces were recorded at T = 5 K and with 50 mV bias voltage.*

bonds in the wire relax and the hydrogen molecule switches from an elongated position back to a tilted configuration that has the lowest energy. This observation provides evidence that molecular hydrogen is present in atomic gold chains.

Length histograms for gold with hydrogen admitted have been recorded and in figure 5.5 two histograms are shown: The filled gray graph is a length histogram for bare gold, as has been shown before. One can nicely distinguish the equidistant peaks situated at a distance of about 2.5 Å from each other. The black curve was recorded after a small amount of hydrogen was admitted to the vacuum can. Two important results can be derived. First, the overall length of the wires does not change significantly. Measurements at elevated temperatures up to 20 K show very similar results. This would mean that a hydrogen atom or molecule adsorbed on or incorporated in the gold chain does not substantially increase or decrease the linear bond strength. It agrees with molecular dynamics simulations, which found the maximal strain force of a clean gold wire and wire with atomic or molecular hydrogen incorporated to have similar values around 1.1 nN [97]. DFT calculations performed by Skorodumova *et al.* [54] also found a nearly equivalent but higher force of 1.8 nN. Force measurements would therefore not result in conclusive evidence

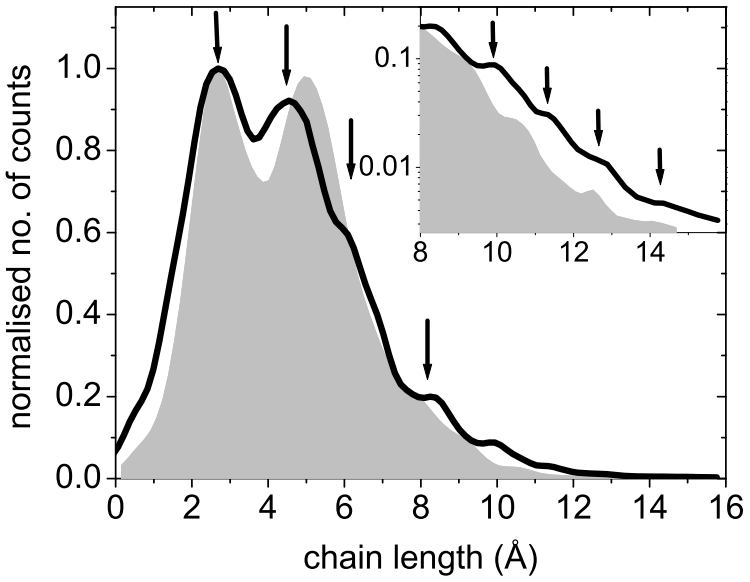

Figure 5.5: *Length histograms of clean gold (filled graph) and with hydrogen admitted (black curve). Both histograms were recorded at T = 5 K and a bias voltage of 50 mV was applied. The conductance window in which the length was measured was 1.1 $G_0 > G > 0.8\ G_0$ for clean gold and 1.1 $G_0 > G > 0.1\ G_0$ for gold with hydrogen admitted.*

whether hydrogen is present in atomic or molecular form in the wire.

The second interesting observation of figure 5.5 is the fact that the position of the peaks in the histogram have shifted somewhat as in the case of oxygen in chapter 3. This could indicate that hydrogen is often incorporated in the atomic wires. This is most clearly seen when looking at the distance between the first and the second peak of the histogram. The inter-peak distance decreases from about 2.6 Å for bare gold to about 1.8 Å with hydrogen admitted. The length of 1.8 $\pm$ 0.1 Å is very close to what calculations predict for both atomic and molecular hydrogen present in the chain [54, 97, 100].

The analysis using length histograms gives an indication that hydrogen interacts with atomic gold wires and most probably can be incorporated into the wires. However, it cannot lead to any conclusions about whether hydrogen is dissociated when it reacts with the gold wires or whether the molecules remain intact when they are pulled into wires. In order to clarify this issue the vibrational properties of the gold-hydride atomic chains are investigated.

5.4 Vibrational properties of gold-hydride wires

5.4.1 Experimental observations

Gold-hydride wires display only very rarely "regular" bias-symmetric downward steps in differential conductance spectra. But as was demonstrated in chapter 4, gold-hydride atomic chains do feature bias symmetric positive and negative peaks in dI/dV spectra, which are interpreted as due to a vibrationally induced two-level system (VITLS) in the junction. With this interpretation the peaks can be used as a new tool to identify the energy of local vibration-modes in single-molecule junctions.

As was seen in figure 4.8 in chapter 4 gold-hydride chains feature a local vibration-mode around 41 $\pm$ 5 meV for hydrogen and 29 $\pm$ 5 meV for deuterium. It has been previously demonstrated by Djukic *et al.* [22] that the nature of a local vibration-mode of a single hydrogen molecule in a platinum contact can be determined by measuring the stretching dependence of the vibration-mode energy. They were able to distinguish between transversal and longitudinal vibration-modes of a single hydrogen molecule by observing an increase and a decrease in vibrational energy, respectively. By means of a combined measurement of the elongation dependence of the vibration-mode energy and the zero-bias conductance of gold-hydride chains, it may be possible to gain more insight into whether atomic or molecular hydrogen is present in the atomic chains.

Figure 5.6 shows a sequence of three dI/dV spectra that were taken from a series of stretching a gold-deuterium atomic wire at T = 5 K. It is clear that upon stretching the wire the energy of the VITLS-peaks maxima increases from about 40 meV to about 50 meV, while the zero-bias conductance sharply decreases from about 0.4 G_0 to 0.05 G_0. In figure 5.7(a) the VITLS-peak-maxima and zero-bias conductances of the spectra of figure 5.6, completed with addi-

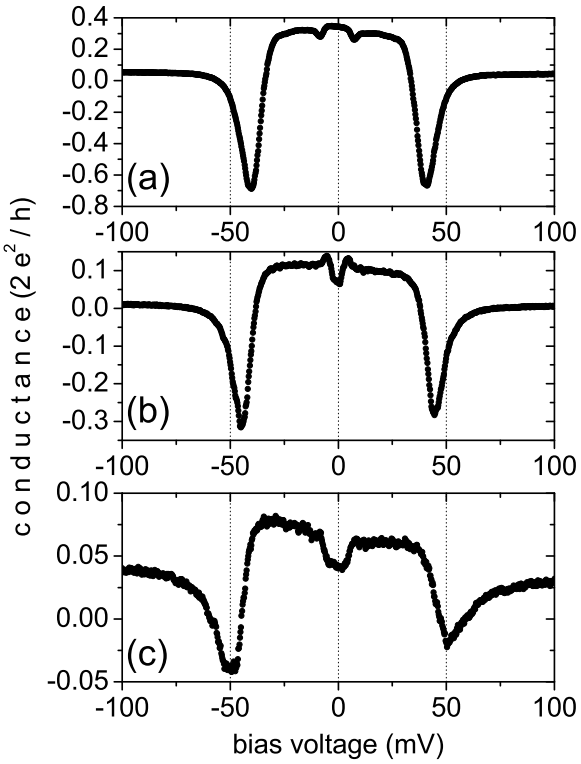

Figure 5.6: *A sequence of three dI/dV spectra displaying VITLS peaks for a gold-deuterium wire at T = 5 K. Spectrum (b) was stretched about 0.3 Å compared to (a). Spectrum (c) was stretched about 0.7 Å compared to (a).*

tional spectra, are plotted. From this graph it is clear that upon increasing the distance between the two gold electrodes, the VITLS-peak-maxima, representing local vibration-mode energies of the atomic wire, increase as well. It can be concluded from this observation that the vibration-mode that gives rise to the VITLS-peaks in this case, is likely a transversal mode.

From the many experiments on the stretching behavior of gold-deuterium atomic wires four trends in the combined zero-bias conductance and VITLS-peak energy evolution have been found as shown in the four graphs of figure 5.7. The first trend was discussed just above and an example is shown in figure 5.6 and 5.7(a). The conductance is typically below 0.4 G_0 and decreases upon elongating the wire, accompanied by an increase in the energy of the VITLS-peaks. The peaks have been observed in quite a large energy window between 30 and 70 meV. The increase in vibrational energy suggests that the mode observed in this trend is a transversal mode.

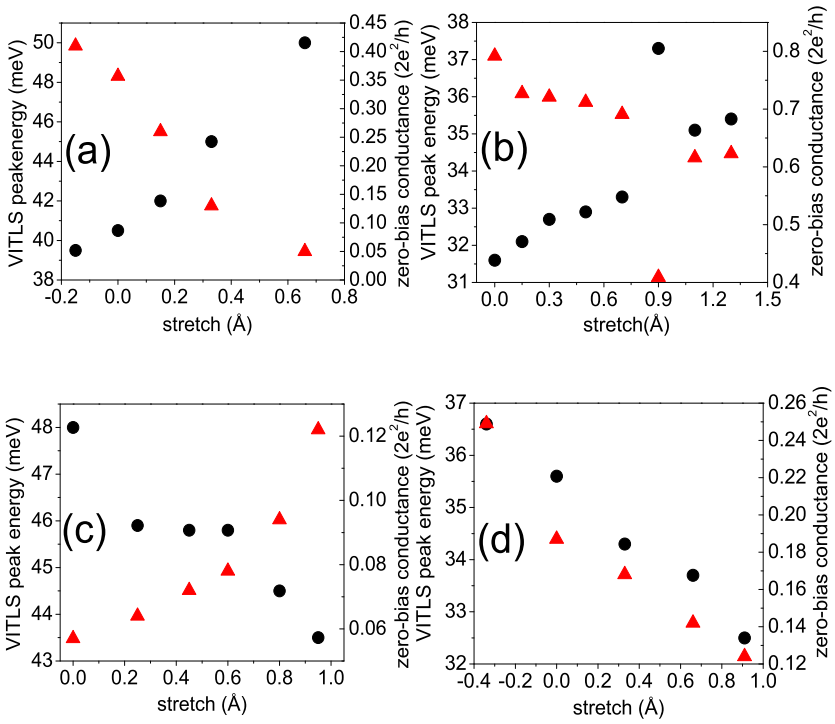

Figure 5.7: *Simultaneous measurement of the VITLS-peak energy and zero-bias conductance for gold-deuterium atomic wires at T = 5 K. Four trends have been observed while stretching gold-deuterium wires, which are described in the text. For each trend an example is plotted in the four windows (a), (b), (c), (d). The dots represent the vibrational energies extracted from the VITLS-peak maxima and the triangles the zero-bias conductance.*

In the second trend dI/dV measurments for a gold-deuterium wire display VITLS-peaks in the high conductance regime (i.e. G $>$ 0.6 G_0). The conductance is observed to be decreasing upon stretching the wire while simultaneously the energy of the VITLS-peaks is increasing. The energies at which the VITLS-peaks are observed are roughly between 30 and 40 meV for this trend. In figure 5.7(b) an example is shown. Clearly a decrease in conductance can be seen together with a simultaneous increase of the VITLS-peak energies. When this specific atomic wire was stretched for 0.9 Å a sudden sharp increase of the VITLS-peak energy together with a sharp decrease in conductance occurred. Likely the linear atomic bonds in the wire where stretched to their maximum, resulting in a severely weakened coupling between the atoms in the wire and a maximal stress on the bonds. Upon further stretching an additional atom is pulled into the wire, resulting in a relaxation of the linear bonds, causing the conductance to restore itself and the vibrational energy to come down. Finally,

the wire was broken upon pulling beyond 1.3 Å.

In the third trend the zero-bias conductance of the gold-deuterium wires is low (i.e. G$<$ 0.25 G_0). Upon stretching the atomic wire the conductance increases, while the energy of the VITLS-peaks decreases. The latter observation indicates that the vibration-mode, which causes the VITLS is a longitudinal mode. The peaks are always observed between 40 and 65 meV. Figure 5.7(c) shows an example for the third trend. Interestingly, one can see that while stretching in a small region between 0.3 and 0.6 Å the energy of the VITLS-peak remains at a stable value, while the zero-bias conductance of the wire increases. The latter observation confirms that the bonds in the atomic wire are being affected by the displacement of the electrodes. It has more often been observed that the energy of the VITLS peaks is not changing upon displacing the electrodes, while the zero-bias conductance of the junction does change. This is possible when the displacement of the electrodes is not equally distributed over all bonds in the atomic wire, which can happen when the bonds are not equally strong and the wire is not symmetric, in the sense that the molecule is located close to one of the two electrodes.

The fourth and last trend that is regularly observed is when the atomic gold-deuterium wire displays a low conductance below 0.3 G_0 and it decreases upon stretching simultaneously with a decreasing VITLS-peak energy, indicating a longitudinal mode. In figure 5.7(d) an example for trend 4 is given. The energies at which the VITLS-peaks are observed lie between 25 and 40 meV.

Sometimes the inelastic features of two different vibration-modes can be observed simultaneously in differential conductance spectra and it is possible to follow the energy dependence of these modes as a function of stretching the wire. In figure 5.8 a nice but rare example is shown. The bottom graph of the figure displays a dI/dV and numerically derived d^2I/dV^2 spectrum taken for a gold-deuterium chain. At about $\pm$48 meV the peak maxima of the VITLS-peaks are seen, while at about $\pm$70 meV the bias symmetric upward steps can be seen due to inelastic electron scattering with a local vibration-mode.

In the upper graph the position in energy of the VITLS-peak maxima and the d^2I/dV^2 peak maxima for the higher vibration mode steps are plotted as function of displacement of the electrodes. Interestingly, both modes behave longitudinally in the range of 0.9 to 1.2 Å, while the conductance of the wire increases.

5.4.2 Comparison between experiments and calculations

In the literature three studies are published, in which the stretching dependence of the conductance and/or vibrational properties for gold-hydride atomic wires were investigated. Jelinek *et al.* [99] have calculated that the chemisorption of a single hydrogen atom to the side an atomic gold chain results in a suppression of the conductance of the wire to about 0.6 G_0 and that when this structure is being stretched the conductance slightly decreases. During the stretching the hydrogen atom remains bonded to the side of the atomic chain.

Calculations on a single hydrogen molecule and a single hydrogen atom incorporated in a gold wire performed by Barnett *et al.* [97] displayed low conductances in both cases. While the conductance for a single hydrogen atom remains below 0.1 G_0, the conductance for a single molecule incorporated in a gold wire rises from about 0.1 G_0 to 0.25 G_0 when it is stretched. They also cal-

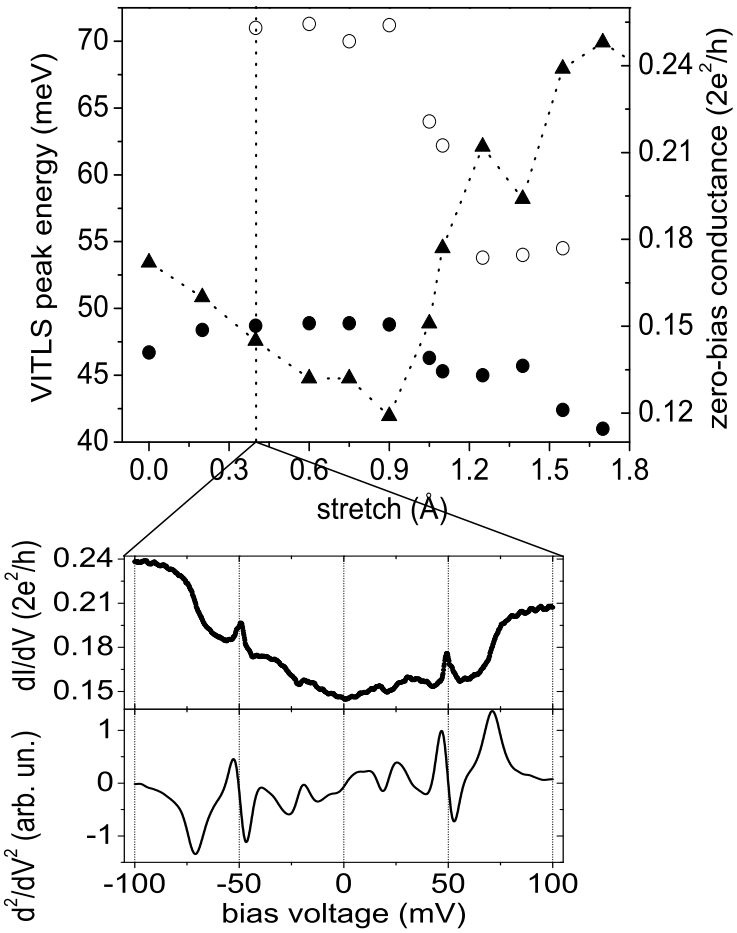

Figure 5.8: *Observation of two vibration-modes in differential conductance spectra for a gold-deuterium atomic wire. The upper graph indicates the evolution of the two vibration-mode energies (black and white dots) as a function of stretching. The bottom graph is one dI/dV spectrum taken from the series where one mode exhibits itself through a VITLS, while the other displays regular bias-symmetric upward steps in conductance.*

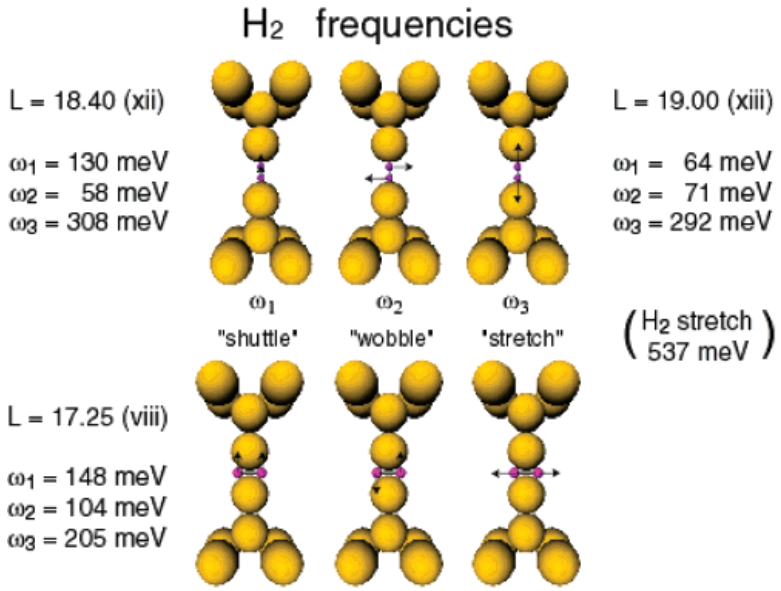

Figure 5.9: *Snapshots of a simulation stretching a single hydrogen molecule, which is incorporated in a short atomic gold chain. The top graph displays three modes for the molecule in the "parallel-to-wire" configuration, while the bottom graph displays the modes for the "perpendicular-to-wire" configuration. For three lengths of the atomic chain three vibration-modes of the hydrogen molecule are calculated. Taken from Ref. [97].*

culated vibration-mode energies for a single hydrogen molecule incorporated in a short atomic gold chain. Two calculated vibration-modes have energies that fit in the experimental energy window of 0 to 100 meV (see figure 5.9). The first is the so-called "shuttle" mode, which is the simultaneous movement of both hydrogen atoms of the molecule parallel to the wire axis. For a deuterium molecule this mode decreases from 105 meV to 92 meV upon 1.15 Å stretch and to 45 meV upon an additional 0.6 Å stretch. The other mode is the so-called "wobble" mode, which is the simultaneous movement of the two atoms in the opposite direction. In the relaxed position the atoms move in the direction parallel to the wire axis, whereas in the stretched position the atoms move perpendicular to the wire axis. The energy of this mode for a deuterium molecule first decreases from 74 meV to 41 meV upon 1.15 Å stretch and then increases again to 50 meV when the molecule is stretched 0.6 Å more.

A third investigation on the stretching dependence of the vibrational energy for a single hydrogen atom and single molecule incorporated in a short atomic gold chain was performed by Frederiksen *et al.* [100], as shown in figure 5.10. They found for a single atom in a linear gold chain a longitudinal mode between 156 and 106 meV depending on stretching, corrected for the

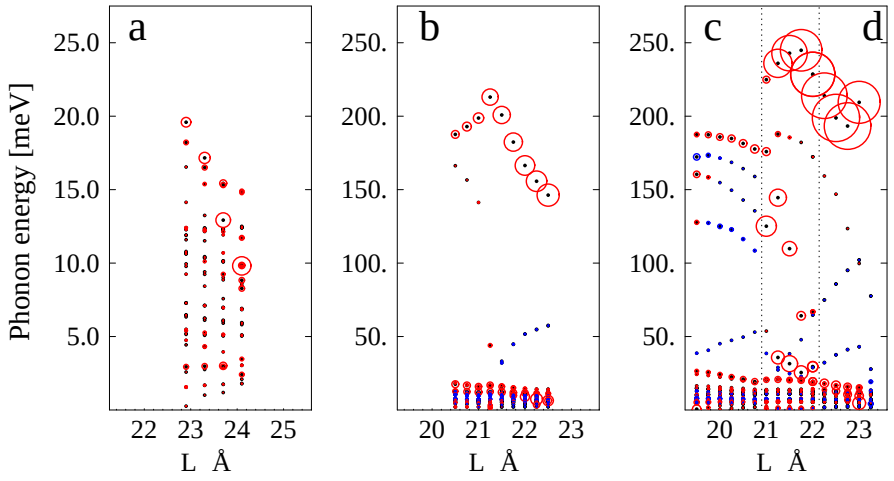

Figure 5.10: *Calculated stretching dependence of local vibration-mode energies for (a) a bare four atom long gold wire; (b) four atom gold wire with a single hydrogen atom incorporated; (c) four atom gold wire with a single hydrogen molecule incorporated. The circles about the dots indicate the strength of the electron-phonon interaction for that mode. Taken from Ref. [100].*

twice larger mass of a deuterium atom. Next to this longitudinal mode also a transversal mode was found with an energy between 43 and 22 meV depending on stretching, again corrected for deuterium. An important difference between these modes is that the longitudinal mode has a large coupling with conduction electrons (slightly larger than for the longitudinal mode of a clean atomic gold chain). The transversal mode on the contrary has a very small coupling, which would make the observation of this mode in differential conductance spectroscopy very difficult. For a single hydrogen molecule both longitudinal and transversal modes have been found. Most importantly two active modes (i.e. with a reasonably large coupling to conduction electrons) were found in the energy window between 105 and 20 meV (corrected for deuterium), which overlap with the experimental window. One longitudinal mode that sharply decreases from about 90 meV to about 45 meV upon stretching for about 1 Å, as can be seen from figure 5.10(c). Another mode behaves longitudinally at first while decreasing from about 30 to 18 meV upon stretching by 0.5 Å, but then increases again to 30 meV upon stretching by about 1 Å (corrected for deuterium). Both modes are observed in the regime where the molecule is in its "tilted" position, i.e. between the perpendicular-to-wire and the parallel-to-wire orientation. Interestingly, the stretching behavior of these two modes is very similar to the results obtained by Barnett *et al.* that were described above, albeit that the vibration-mode energies are not fully overlapping.

Turning back to the experimental observations and comparing them with calculations the following conclusions can be drawn:

In trend 1 a high conductance ($G > 0.5\ G_0$) of the gold-hydride wire is observed, which decreases when stretching the wire. In this regime mostly a transversal mode is seen. These observations could indicate that atomic deuterium is present in the atomic wire since the conductance values correspond to wire calculations done by Jelinek *et al.* and Frederiksen *et al.* for a single hydrogen atom in a gold wire. Furthermore, from Jelinek's investigation also follows that the conductance decreases upon stretching the wire, in accordance with experimental observations. But Jelinek's calculations were done on a hydrogen atom that is chemisorbed to the side of the gold chain, without breaking any gold-gold bond. They found furthermore that even in that case the conductance of this wire was carried by the suppressed transmittance of the s-channel of the linear gold bonds. This would make a coupling of a vibration mode of the hydrogen atom to the conduction electrons extremely small. Taking into account that Frederiksen *et al.* found for both the atomic and molecular hydrogen incorporated a transversal mode in the experimental energy window of 30-40 meV, it is hard to confirm that trend 1 is uniquely due to incorporated *atomic* hydrogen.

Both trend 2 and 3 have been observed in the low conductance ($G < 0.25\ G_0$) regime. While in trend 2 a longitudinal mode is accompanied with an increase in conductance, in trend 3 a transversal mode has been observed while the conductance was decreasing upon stretching. Barnett *et al.* calculated that a single molecule incorporated in an atomic gold wire can display both longitudinal as well as transversal behavior when it is being pulled through the "tilted" configuration. The conductance first increases upon pulling accompanied by a longitudinally behaving "wobble" mode. Once the hydrogen molecule is in it's parallel-to-wire configuration the conductance starts to decrease and the "wobble" mode behaves transversally. Also Frederiksen *et al.* calculated a similarly behaving mode at lower energies when the molecule "passes through the tilted" configuration. Therefore trend 2 and 3 are very likely to be caused by incorporated *molecular* deuterium.

Trend 4 involves a decreasing conductance upon stretching in the low conductance ($G < 0.25\ G_0$) regime. A longitudinal mode between 30 and 40 meV is observed. The longitudinal mode energy as calculated by Frederiksen *et al.* [100] for atomic deuterium present in an atomic gold chain is far above the observed energies between 30 and 40 meV, ruling out atomic deuterium. Molecular deuterium on the other hand is calculated to have a longitudinal mode in range where the modes of trend 4 are seen. It is therefore very likely that also trend 4 is a sign for incorporated molecular hydrogen in atomic gold wires.

The simultaneous observation of two longitudinal vibration-modes for a gold-deuterium wire as was displayed in figure 5.8 can be explained when one or more molecules are present. From figure 5.10(b) it is seen that for a single deuterium atom only a transversal mode can be simultaneously observed together with a longitudinal mode. From figures 5.9 and 5.10(c)-(d) it becomes clear that two longitudinal modes can be excited when a single molecule is incorporated in the atomic gold chain. When stretching the molecule through its

tilted configuration both the "shuttle" (ω_1 in figure 5.9) and "wobble" (ω_2 in figure 5.9) modes behave longitudinally. From the upper graph of figure 5.8 is seen that the zero-bias conductance of the gold-deuterium wire increases simultaneously with the decrease of the two vibration-mode energies while stretching between 0.9 Å and 1.2 Å. This is another indication that a molecule is incorporated in the wire, since stretching the molecule through its tilted configuration should increase the conductance according to Barnett *et al.* [97].

5.5 Conclusions

This chapter aimed to provide more information on the interaction of atomic gold wires with hydrogen. Previous work already provided evidence in the form of a change in conductance of the wire upon hydrogen incorporation that hydrogen can be incorporated in a gold wire. It was however not evident whether it is in atomic or molecular form. The results presented on the stretching behavior of local vibration-mode energies of gold-hydride chains give substantial evidence that hydrogen molecules are mostly incorporated in molecular form at T = 5 K. This conclusion corresponds with previous experiments [78] on gold-hydride wires. The interpretation of the experiments done at T = 20 K, where a preferential conductance near 0.5 G_0 is seen, could be that due to the higher temperature hydrogen is more easily dissociated. Chemisorbed atomic hydrogen could be the origin of the half-conductance quantum as predicted by the calculations of Jelinek *et al.*

6

Nickel-oxygen atomic chains

Nickel is a 3d-metal, which also has the property of being ferromagnetic. In the periodic system of the elements nickel is located two rows above platinum. The transport properties of bare nickel atomic contacts are very similar to the intensively studied properties of platinum atomic contacts. Platinum is known for its atomic chain-forming tendencies, while the lighter element nickel is not. As was shown in chapter 3, oxygen has a reinforcing effect on the linear bonds in atomic chains, making chains of silver and copper with oxygen possible. The experimental results in this chapter will demonstrate that also nickel reacts with oxygen resulting in the formation of nickel-oxygen atomic chains. Besides inelastic signals in differential conductance spectra due to local vibration-modes of the oxygen in the atomic chains, there is evidence that under proper conditions a nickel-oxygen wire becomes a Kondo-system.

6.1 Introduction to ferromagnetism

Cobalt, iron and nickel are the only three elements that are ferromagnetic in bulk form at room temperature. A piece of material is ferromagnetic when it can have a spontaneous magnetic moment in zero applied magnetic field. A finite magnetic moment indicates that the net sum of all magnetic moments of the atoms in the material has a preferential direction. The magnetic moments interact with each other via the so-called exchange field. In a ferromagnetic material the exchange energy is negative when two neighboring atoms have a magnetic moment in the same direction and is positive when they are in opposite direction. The total magnetic energy of a ferromagnetic material is given by the sum of the magnetic field energy and the exchange interaction energy.

$$E_{tot} = E_{field} + E_{exchange} \tag{6.1}$$

The exchange interaction originates from the fermionic nature of electrons that implies when two electrons are brought together two parallel aligned spins cannot occupy the same location. For the two-electron system a symmetric (both spins parallel) and antisymmetric (both spins anti-parallel) wave function exists. The interaction energy resulting from the symmetric wave function is lower than from the anti-symmetric wave function because of a lower Coulomb repulsion, which makes the two parallel aligned the energetically most favorable configuration. In a ferromagnetic material this results in an energy minimization when all spins align parallel. But the magnetic field created by all the parallel aligned spins in the material will increase the field energy, which grows with the square of the field. In order to minimize the total energy the material will create magnetic domains. Magnetic domains are regions inside the ferromagnetic material that have all the magnetic moments inside aligned, thus being a single magnetic object. The size of these domains depends on the purity of the material and how the material was synthesized (e.g. how the metal was annealed). The domain size of single crystal nickel can be of order of a few μm [102].

When cooling a ferromagnetic material down from the high temperature paramagnetic phase through the Curie temperature (627 K for bulk nickel [9]) into the ferromagnetic phase domains form. The magnetization directions of these domains which will be randomly oriented and the total magnetization of the material will be zero. Applying an external magnetic field will align the domains parallel to the field and the material will become magnetized. After removing the external magnetic field a large share of the magnetic domains remain oriented in the direction of the external magnetic field. As a result, the material retains a net magnetization. When the ferromagnet is heated above the Curie temperature the domain structure is destroyed due to thermal energy. The externally applied magnetic field should be sufficiently large in order to orient all domains into the same direction parallel to that field. The magnetic field at which all magnetic domains are aligned is called the saturation field H_s and it depends on the shape of the material. For bulk nickel the

saturation field is about 150 mT. Once all domains are aligned parallel to the external applied magnetic field, one can rotate the field 180^o in order to reverse the magnetization direction. The external field needed to reduce the net magnetization to zero is called the coercive field H_c. For bulk nickel the coercive field is about 10 mT. When the dimensions of a ferromagnet are shrunk to a few hundred nanometers or less, shape anisotropy starts to play a significant role and it alters the value of both H_s and H_c compared to the bulk values. The dimensions of the ferromagnet have become similar to the size of the magnetic domains, meaning that the small ferromagnet consists of only a few domains or is a single domain. Consider for example the case of an elliptically shaped ferromagnet. When the external magnetic field is applied parallel to the major axis (easy-axis) the saturation field is smaller, but the coercive field is larger than when the magnetic field is applied parallel to the minor axis (hard-axis) and vice versa. The larger the aspect ratio of the ellipse is, the larger the difference of H_s and H_c in the easy- and hard-axis directions. See for a review Ref. [103].

6.2 Magnetic properties of atomic contacts

In this chapter the transport properties of nickel atomic contacts with oxygen admitted are investigated. Let us therefore take a brief look at transport through junctions of single ferromagnetic atom contacts. Chapter 2 explained that the actual conductance of a single atom or molecule contacted by two macroscopic leads is determined by the overlap of the Fermi energy of the bulk material with the LDOS of the atom in the contact. This also holds for a ferromagnetic atom, like nickel, contacted by nickel electrodes. Since nickel is located above platinum in the periodic table of the elements, its electronic properties are very similar to those of platinum. Both elements have partially occupied s and d-orbitals, which cause the conductance of a single atom to consist of several partially opened channels. According to a recent theoretical analysis a nickel dimer configuration (i.e. both electrodes ending in a single atom and a single bond bridging the electrodes) supports four conductance channels [104]. Because spin degeneracy is lifted, in bulk nickel the density of states for the different bands does not have an equal filling for spin up and spin down electrons. It has been speculated that the exchange interaction would be strong enough to suppress transport for one spin direction resulting in half-integer conductance quantization. Indeed several groups have reported experimentally conductance values of half-integer value for ferromagnetic metals [62, 105–110]. Although this interpretation is tempting the evidence is only based on the observation of conductance and a more detailed analysis would need to consider many partially filled conduction channels [111]. Another intriguing feature related to spin-dependent transport is the potential of gigantic magneto-resistance for a ferromagnetic single-atom contact. When the transmission of the conduction channels of the ferromagnetic atom in the contact is very different for the different electron spins, then the single atom could func-

tion as a spin valve, transmitting for instance spin up electrons but blocking spin down electrons. By controlling the magnetization of the electrodes, the spin of the conduction electrons could be regulated when the spin of conduction electrons is polarized parallel to the magnetization of the electrode. Enormous magneto-resistance values have been reported for ferromagnetic atomic contacts [112–117].

As for the half-integer conductance, MCBJ experiments done on all three ferromagnetic metals under cryogenic circumstances, with and without applied magnetic field, have not revealed any sign of half-integer conductance values [118]. This casts doubts on the conclusion of previous experiments claiming the effects being due to bare nickel. The experiments were conducted mainly under ambient conditions and could therefore be prone to contaminants. Untiedt *et al.* [118] have taken conductance histograms for nickel that yielded a broad peak centered around a value of about 1.6 G_0, in agreement with results previously reported for an STM contact study under cryogenic conditions [119].

Calculations suggest that the spin-dependent transport of a bare single-atom contact of nickel influences the conductance in the order of 20-30% [120]. This suggests that the observation of enormous magneto-resistance cannot be due to the conduction properties of nickel alone. The conduction of single nickel atom contacts are discussed in more detail in the next section. The magnetic moment of a ferromagnetic atom in a contact is proportional to the integral from zero to E_F of the projected LDOS for the majority spin d-band. The conductance of the atomic contact is determined by the LDOS at E_F, which is situated at the minority spin d-band, while the conductance has only a small contribution from the high energy tail of the majority spin d-band [120–123]. For the sp-orbitals the majority and minority spin states have a nearly equal LDOS at E_F. If the current through a single atom nickel contact is mainly carried by conduction channels formed by d-orbitals, the conductance would be very much dependent on the magnetization of the two electrodes. However, calculations have demonstrated that the conductance of a single nickel atom contact is mainly carried by sp-orbitals and the d-orbitals are poorly conducting or even blocked [104, 120, 121]. This would rule out any half-quantum conductance or enormous magneto-resistance from a theoretical point of view. Interestingly, some calculations have suggested that the presence of oxygen in the contact could cause large magneto-resistance due to transport through oxygen p-orbitals [124] or pd-hybridized orbitals in a nickel-oxygen atomic chain [125].

6.3 Observation of nickel-oxygen atomic chains

6.3.1 Conductance of nickel-oxygen atomic contacts

The conductance properties of nickel atomic contacts have been studied experimentally. In figure 6.1 a conductance histogram of clean nickel at T = 5 K is shown. It displays a broad peak around 1.5 G_0 as in the case for clean plat-

inum. The peak consists actually of two peaks, which are thought to originate from two different atomic configurations as for platinum. The configuration in which a single nickel atom bridges the electrodes has a conductance just below 2 G_0, while the dimer configuration, has a somewhat lower conductance close to 1.5 G_0. It corresponds with what has been reported in earlier experiments [118,119] as well with calculations [104,120]. The conductance of 1.5 G_0 is carried by five spin-degenerate conductance channels that are all partially transmitting. According to Pauly *et al.* [104] the majority-spin component of the electron current is carried in the dimer configuration by a single *sp*-orbital channel that has conductance of close to e^2/h. The minority-spin component is carried by four channels, adding up to a total conductance of about $2e^2/h$. This results in a total conductance close to 1.5 G_0. Jacob *et al.* [120] arrive at a very similar conductance for the configuration in which the bulk electrodes have a parallel magnetization. They find a slightly lower conductance (1.4 G_0) when the magnetization of the electrodes is anti-parallel.

When oxygen is admitted to the nickel junction and conductance traces are measured the large peak around 1.5 G_0 in the histogram disappears in a featureless background of conductance counts. But around 1 G_0 a clearly resolved peak can be distinguished that remains distinguishable for different bias voltages as can be seen in figure 6.2. This result is very similar to the case of hydrogen admission to a platinum junction [8,22], in which the 1 G_0 conductance

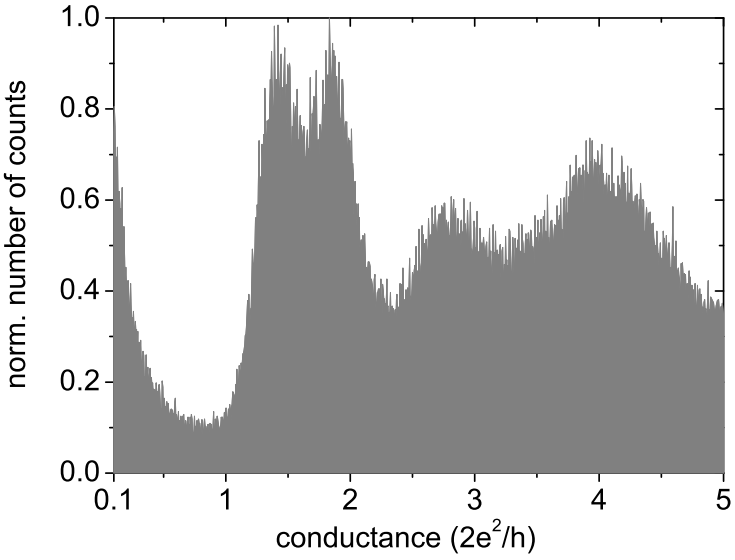

Figure 6.1: *Conductance histogram taken for clean nickel at T = 5 K. A bias voltage of 50 mV was used and the histogram consists of about 1000 traces.*

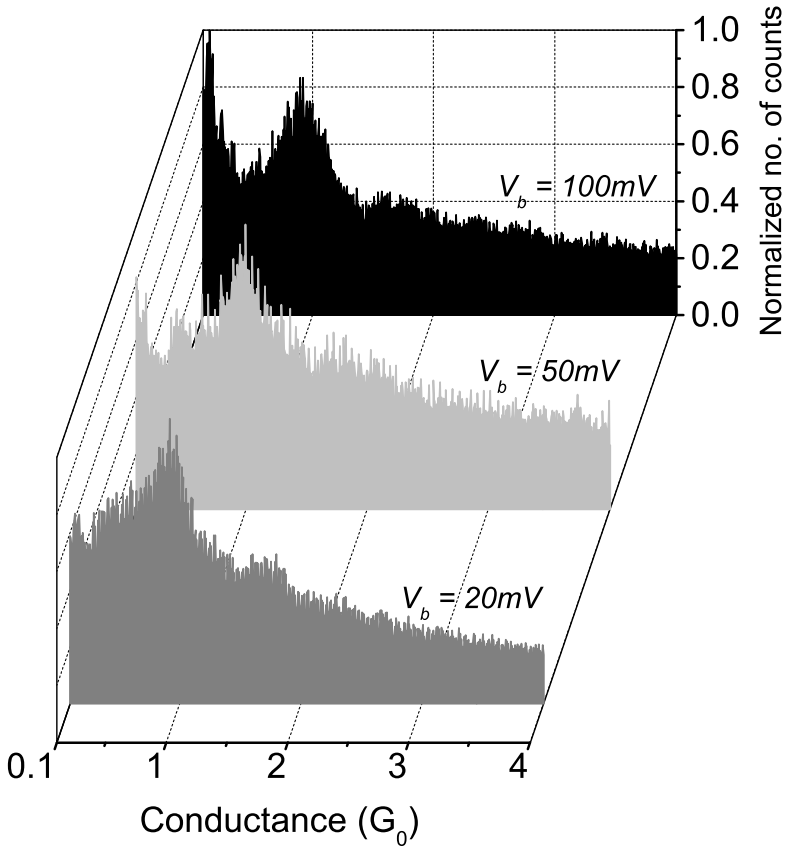

Figure 6.2: *Conductance histogram taken for nickel after oxygen was admitted at T = 5 K for different bias voltages. For all bias voltages a clear peak around 1 G_0 can be resolved. The histograms have been cut off at 0.1 G_0 because of a large tail at low conductance.*

results from a single hydrogen molecule bridging the two electrodes. It is therefore interesting to investigate whether the conductance of 1 G_0 is caused by an oxygen atom or molecule bridging two nickel electrodes.

6.3.2 Atomic chains of nickel and oxygen

Chapter 3 revealed strong evidence that oxygen has a reinforcing effect on the linear bonds in atomic chains of the noble metals, which makes the formation of silver-oxygen and copper-oxygen wires possible. It could be that oxygen has a similar effect when binding to nickel atoms. Therefore the atomic chain formation of nickel with and without oxygen admitted is studied similarly to the noble metals in chapter 3. In figure 6.3 the results are shown. In the upper graph the length histogram of clean nickel (black curve) demonstrates that no

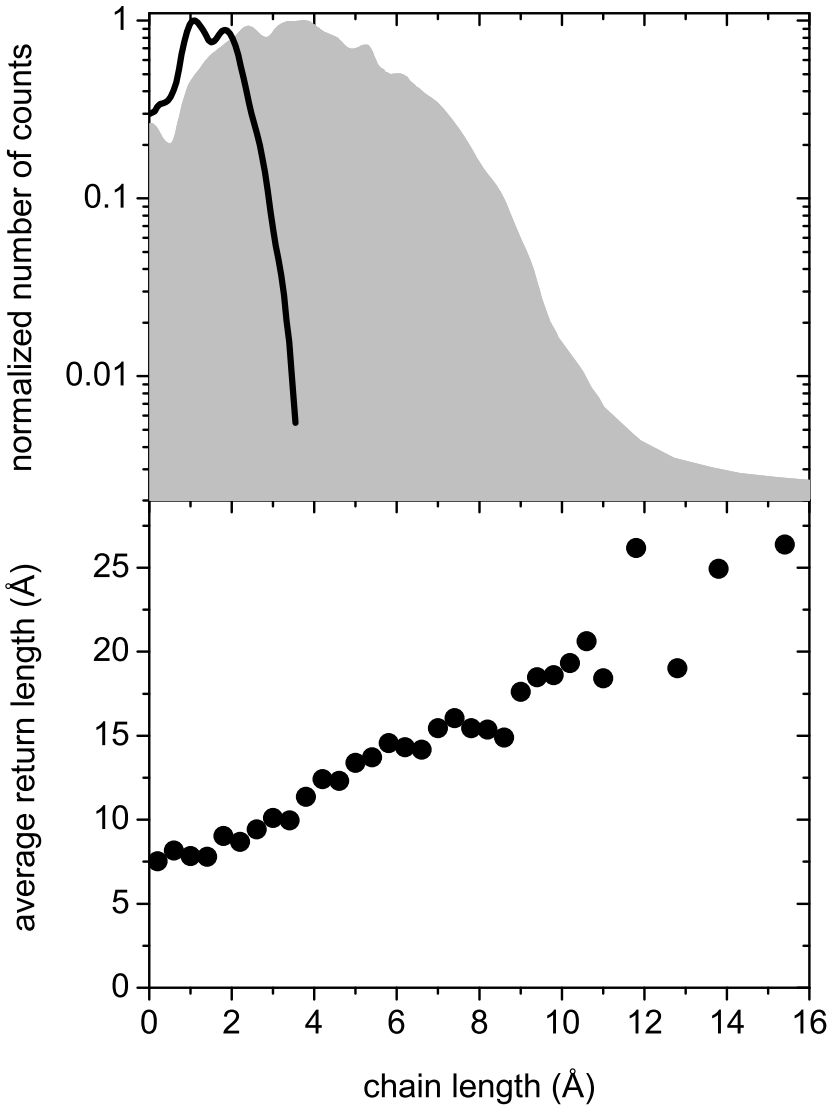

Figure 6.3: *Upper graph: Length histograms for clean nickel (black curve) and nickel with oxygen admitted (grey graph) on a semi-logarithmic scale. The histograms are constructed from electrode displacements in conductance windows 2 $G_0 > G > 1$ G_0 for clean nickel and 1.5 $G_0 > G > 0.5$ G_0 for nickel with oxygen admitted. Lower graph: Average return length of the electrodes after the contact was broken as a function of chain length for nickel with oxygen admitted. All measurements were performed at T = 5 K with 50 mV bias voltage.*

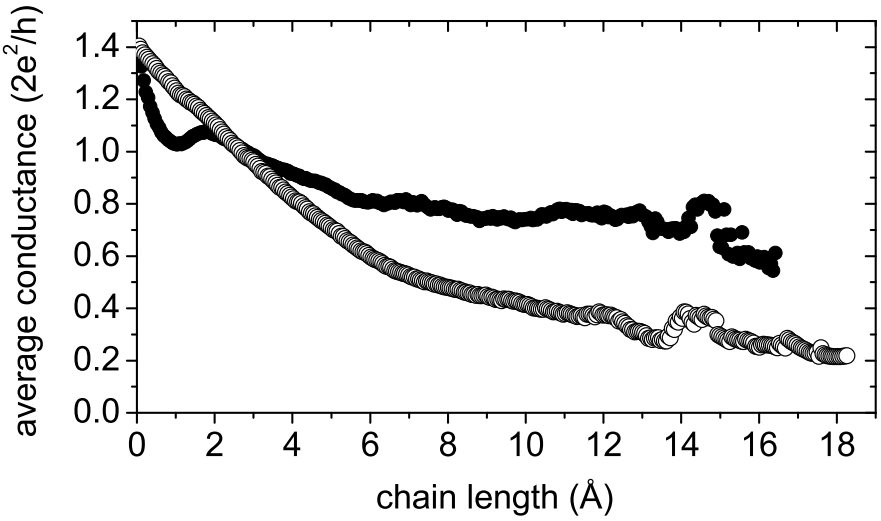

Figure 6.4: *Average conductance for nickel-oxygen atomic chains as a function of chain length. The black dots represent length measurements for 1.5 $G_0 > G > 0.5\ G_0$ and the open circles for 1.5 $G_0 > G > 0.2\ G_0$. All measurements were performed with 50 mV bias voltage.*

atomic chains of bare nickel are formed. The electrode displacement was measured in a conductance window 2 $G_0 > G > 1\ G_0$, which are the boundaries of the broad peak in figure 6.1 that is interpreted as the conductance of a contact of a single Ni atom in diameter. An interesting feature is the double peak, which is probably due to the two different atomic configurations that both result in a conductance between 1 and 2 G_0, as previously discussed.

After oxygen is admitted to the nickel junction the electrode displacement is measured in a conductance window 1.5 $G_0 > G > 0.5\ G_0$, corresponding to the boundaries of the peak in figure 6.2. The resulting histogram is displayed by the grey area in the upper graph of figure 6.3. Clearly the displacements become much longer than without oxygen admission, which would indicate as in the case of the noble metals that oxygen reinforces the linear bonds, making nickel-oxygen chains possible. Several peaks can be resolved in the length histogram that indicate specific configurations that have a higher probability of breaking, a typical feature for atomic chain formation. Support for this interpretation is obtained when the average return length as a function of (supposed) chain length is measured and which is shown in the bottom graph of figure 6.3. Clearly the average return length increases linearly with increasing chain length, which is expected when atomic chain formation is indeed taking place.

In the conductance histograms of figure 6.2 one can see many counts below G = 0.5 G_0, which are due to atomic chains which display a lower conductance due to their composition and/or configuration. This is verified by

analyzing individual breaking traces, which display conductances below G = 0.5 G_0 before rupture of the wires. Figure 6.4 shows the average conductance as a function of chain length for the length histogram of figure 6.3 (black dots), in which the length measurement is stopped when the conductance of the chain becomes smaller than 0.5 G_0. The open circles represent the average conductance of many individual chain-pulling traces when the length measurement is stopped at G = 0.2 G_0. The average conductance becomes smaller for longer chains and that the maximal length of the chains is also somewhat larger.

6.4 Properties of nickel-oxygen atomic chains

6.4.1 Effects due to local vibration modes

Differential conductance measurements can give information on inelastic electron scattering effects due to vibration-modes of the nickel-oxygen wires. Figure 6.5 shows two dI/dV spectra for nickel-oxygen chains that have a conductance lower than 0.5 G_0. Both spectra were obtained for chains with a length of about 10 Å and display clear bias-symmetric peaks in d^2I/dV^2 at about 50 and 60 mV for (a) and (b) respectively. Bias symmetric peaks in d^2I/dV^2 have been observed in the bias voltage range between 45 and 75 mV. Clearly these values are far above the Debye energy of nickel, which indicates that they are likely due to lighter incorporated oxygen. These "regular" vibration-mode spectra were not very often obtained in differential conductance measurements on nickel-oxygen wires. Peak-like features that have been extensively discussed and interpreted as VITLS in chapter 4, have been observed on many occasions for nickel-oxygen chains as well. What distinguishes the majority of the spectra obtained for nickel-oxygen contacts and wires is that the difference between the conductances, σ_0 and σ_1 of the VITLS-model can be very large. In figure 6.6

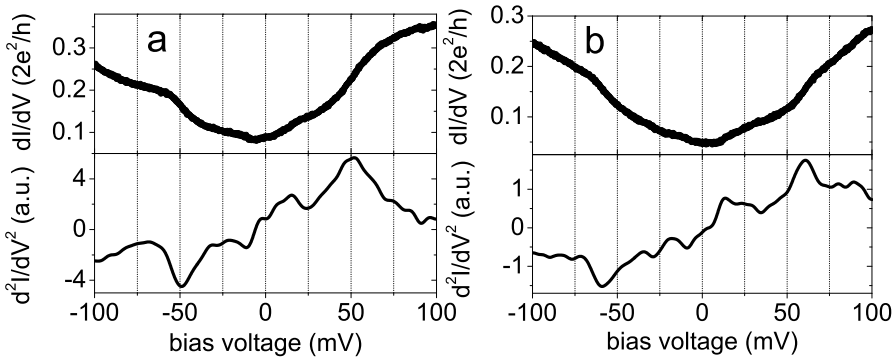

Figure 6.5: *Two differential conductance spectra taken on nickel wires with oxygen admitted at T = 5 K. Clearly bias-symmetric peaks in d^2I/dV^2 are seen. Both spectra (a) and (b) were obtained for chains with a length of about 10 Å.*

two examples are shown and a third is shown in figure 4.12 in chapter 4. In all these cases σ_0 is very small, resulting in a very small conductance of the junction at low bias voltages. At the high bias end however the conductance is high, resulting in a large peak at the energy of a local vibration-mode. Figure 6.6(c) shows a histogram in which the number of times the energies of the peak maxima and minima in dI/dV spectra were observed for three different MBCJ samples. It is clear that there is a large spread in energies at which peaks are observed, but the majority of energies is centered around 32 and 44 meV. Interestingly, the few regular vibration-mode energies are only observed for energies at or above 45 meV. Possibly the VITLS-peaks at lower energies are caused by a different vibration-mode, which has a weak electron-phonon coupling resulting in a smaller inelastic correction to the current. The VITLS peaks at higher energies overlap with the energies at which the regular vibration-

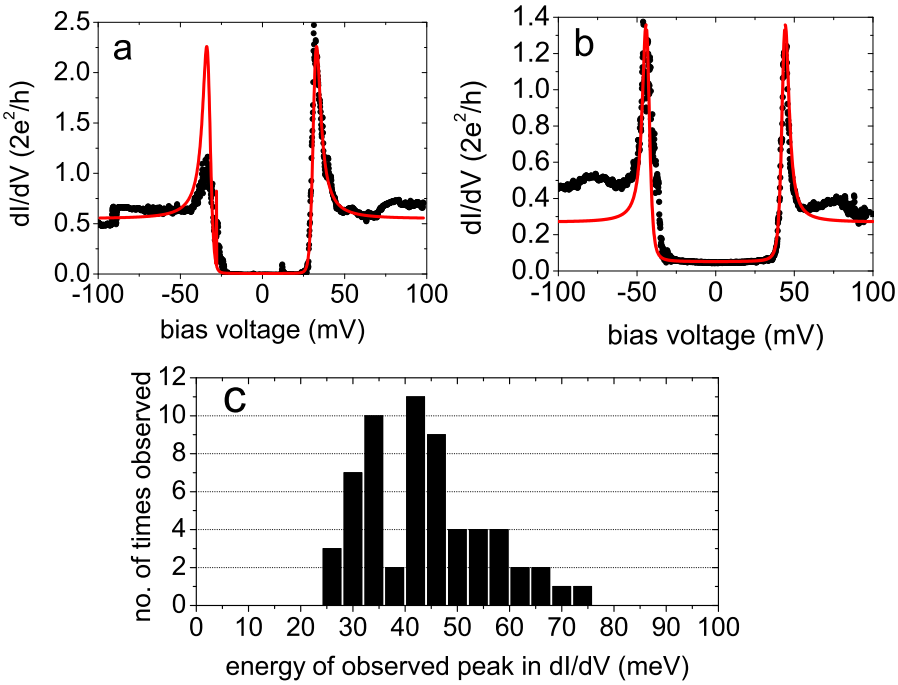

Figure 6.6: *Two examples of VITLS spectra taken for nickel-oxygen atomic chains. The black dots indicate the experimentally obtained dI/dV signal and the curve is a fit obtained with the VITLS model of chapter 4. Fit parameters from the model are* σ_0*=0.005*G_0*,* σ_1*=1.1*G_0*,* $\hbar\omega_v$*=33meV,* Δ_0*=5.0meV, T=8K for figure (a) and* σ_0*=0.04*G_0*,* σ_1*=0.5*G_0*,* $\hbar\omega_v$*=44meV,* Δ_0*=2.5meV, T=8K for figure (b). Note that the fits have been performed on the positive bias side of the spectra. The histogram of figure (c) shows the number of times the energies of the peak maxima and minima in dI/dV spectra have been observed as a function of energy for three different samples.*

mode steps are observed.

6.4.2 Observation of Kondo physics

Apart from the inelastic features in dI/dV spectra related to local vibration-modes of oxygen in the nickel contact, sometimes a large zero-bias peak is observed in these contacts, while for clean nickel it is never observed. In figure 6.7 two dI/dV spectra are shown that display a large zero-bias anomaly. This anomaly resembles a Kondo peak which has been observed in junctions of a single molecule contacted by gold electrodes [126–130]. A major difference is that the Full Width at Half Maximum (FHWM) of the zero-bias Kondo peak in most of those reported cases is only a few mV, while for nickel-oxygen chains the FWHM is much larger, indicating that the Kondo temperature (T_K) is also much larger. The FWHM obtained from a Lorentzian fit on the spectrum of figure 6.7(a) is 18 mV. Since the FWHM is approximately k_BT/e [131], this gives $T_K \approx 100$ K (since $V = 2k_BT/e$). An experiment in which ferromagnetic electrodes were used to contact a single C_{60} molecule, was done by Pasupathy *et al.* [128]. They find very similar zero-bias anomalies, which have similarly large FWHM. By using a lithographically fabricated break junction, they were able to measure dI/dV on a single-molecule junction as a function of temperature and applied magnetic field. In this way they were able to confirm that the zero-bias peak is indeed caused by the Kondo effect. Unfortunately these additional checks to verify whether the observed zero-bias features for nickel-oxygen chains are indeed due to the Kondo effect are not possible with the MCBJ that is used here. Figure 6.7(b) shows additional peaks in the spectrum just above $\pm$50 meV, which could be attributed to an inelastic Kondo effect due to coupling of the Kondo resonance with vibration modes, as has been predicted and observed in single C_{60}-molecule junctions [129,130,132]. The energy of the peak is very close to the energy at which the inelastic features of nickel-oxygen chains were observed (see figures 6.5 and 6.6). Because in a freely suspended atomic wire the coupling to both electrodes is nearly equal, the inelastic Kondo signal would be enhanced according to calculations [132, 133].

It is possible to study the stretching dependence of the zero-bias anomaly with the MCBJ-technique. Recently it was shown by Parks *et al.* [130] that the Kondo temperature can be tuned by varying the spacing between gold electrodes and a C_{60} molecule in the junction. It is demonstrated that by increasing the electrode spacing, and thus decreasing the coupling to the left and right electrode, both the peak height and T_K decrease. The effect of decreasing T_K is larger when the molecule has a more symmetric coupling to the left and right electrodes [130]. The nearly equal coupling to the left and right electrode for a suspended atomic wire would again be an advantage for observing a large Kondo feature, since the maximum of the zero-bias resonance is approximately given by [134, 135]

$$G = \frac{2e^2}{h}\frac{4\Gamma_L\Gamma_R}{(\Gamma_L+\Gamma_R)^2}f(T/T_K) \tag{6.2}$$

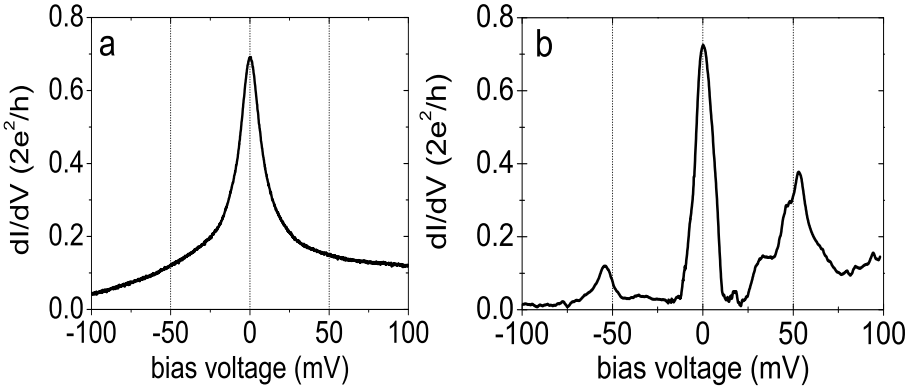

Figure 6.7: *Two examples of Kondo-like zero-bias anomalies obtained for nickel-oxygen atomic chains. Both spectra were obtained at a base temperature of T = 5 K. The full width at half maximum (FWHM) of the zero-bias peaks is 18 meV and 12 meV for spectrum (a) and (b) respectively. This results in an approximate Kondo-temperature of 104 K for (a) and 69 K for (b) (see text).*

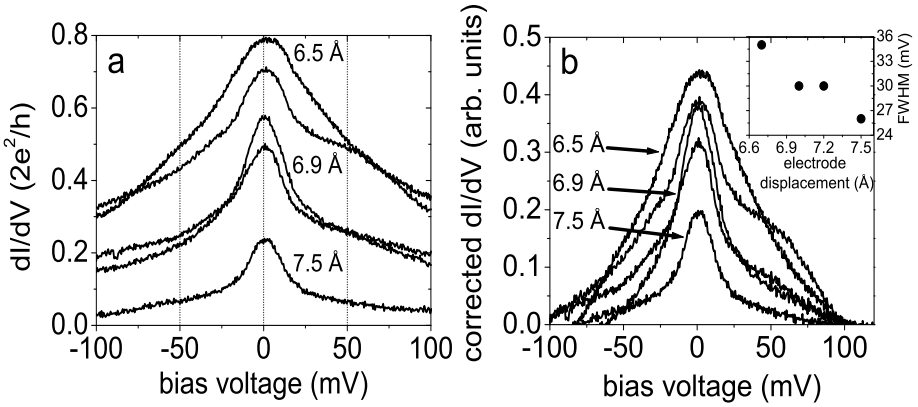

Figure 6.8: *Stretching dependence of a zero-bias Kondo-feature for a nickel-oxygen atomic wire at T = 5 K. Figure (a) shows dI/dV spectra upon stretching the atomic chain for 1 Å. The spectra evolve from a broad feature to a more narrow Lorentzian-shaped peak accompanied by an overall decrease of the conductance. Figure (b) shows the same spectra from (a) but corrected by subtracting the background conductance at 100 mV bias, which reveals a decrease in peak height as well as FWHM of the peak (inset). The inset shows the decrease of the FWHM, and thus T_K, of the peaks obtained by fitting the low bias region between ± 30 mV with a Lorentzian curve.*

in which Γ_L and Γ_R are the coupling-strengths to the left and right electrodes respectively and $f(T/T_K)$ is very close to unity for large T_K given that $T << T_K$. Figure 6.8(a) shows a stretching sequence over a distance of about 1 Å performed on a suspended nickel-oxygen wire. The initial spectrum for a 6.5 Å long wire displays a very broad peak and does not seem to show a clearly defined zero-bias peak. When the wire is stretched the spectrum evolves into a zero-bias peak, while simultaneously the peak conductance decreases. The effect of decreasing conductance can be partially due to weakening bonds in the wire. Therefore in figure 6.8(b) the background conductance (at 100 mV bias) is substracted to demonstrate that the intensity of the zero-bias peak itself also decreases as a function of increased stretching. The dI/dV spectra are not perfect Lorentzian curves, but the low bias part of the spectra have been very well fitted with Lorentzian curves. The FWHMs of these Lorentzian fits are plotted in the inset of figure 6.8(b) and also decrease upon stretching, which implies that the Kondo-temperature decreases as well. This observation supports the claim that the observed zero-bias peaks are due to Kondo physics because T_K is expected to decrease when the coupling of the Kondo system to the leads is reduced as has been observed in previous experiments [129, 130].

Jacob *et al.* [136] have recently investigated the LDOS of a short nickel-oxygen atomic chain consisting of a central nickel atom contacted by oxygen from both sides between nickel electrodes. The $d_{3z^2-r^2}$-orbital of the central nickel atom is weakly coupled to conduction electrons and it is strongly localized because its geometry is not compatible with the electrodes. With an anti-parallel orientation of the magnetization of the electrodes, i.e. the configuration with the lowest energy, the projected LDOS yields a sharp localized peak below and above E_F. The magnetization of the nickel atom is mostly due to the single-spin states of this orbital. By coupling the $d_{3z^2-r^2}$ level to the conduction electrons a linear combination of the spin up and spin down state gives rise to a spin-singlet that could be responsible for the Kondo-effect.

6.4.3 Influence of an external magnetic field

Finally, the influence of an externally applied magnetic field on the conductance of nickel-oxygen atomic chains is studied. From figure 6.2 was seen that the conductance histogram for a bare nickel junction changes when oxygen is admitted. The broad peak centered around 1.5 G_0 disappears and a peak around 1 G_0 appears. By applying an external magnetic field sometimes a peak at a half conductance quantum is observed as shown in figure 6.9. Clearly, when increasing the field the intensity of the half quantum conductance peak grows to a dominant peak by applying a 500 mT field. As was mentioned in the introduction, previous experimental work on clean nickel have reported the observation of half-integer conductance values. The histograms shown in figure 6.2 without an external applied field, do not point to any preferential conductance around 0.5 G_0. Also when an external magnetic field was applied no preferential half-integer conductance values were observed as has also been reported before [118]. But as figure 6.9 shows the combination of admitting

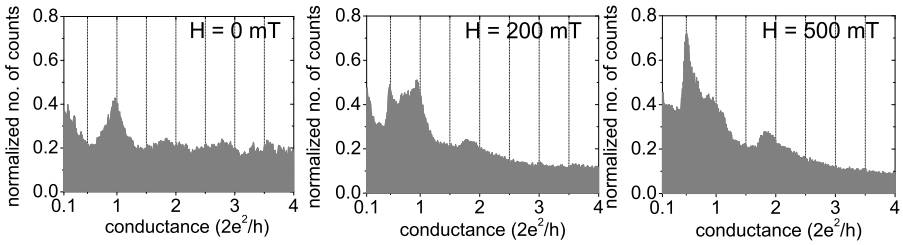

Figure 6.9: *Conductance histograms taken for a nickel junction with oxygen admitted at 50 mV bias, with different applied magnetic fields.*

oxygen to the nickel junction and applying an external magnetic field does sometimes give rise of half-integer quantum conductance. Note conductances around 1 G_0 are also still quite preferential, since the peak does not disappear. The field dependence of the conductance histograms is likely caused by the alignment by the field of the magnetization of the two electrodes.

6.5 Conclusions

This chapter reports on investigations of the effect oxygen has on the physical properties of nickel atomic contacts. As was found for the noble metals in chapter 3, also nickel atomic chains can be formed due to the reinforcing effect of incorporated oxygen on the linear bonds. Atomic wires of several atoms in length can regularly be created and the conductance of these nickel-oxygen wires is typically between 1 and 0.2 G_0. Differential conductance measurements on suspended nickel-oxygen chains have resulted in interesting results. It is possible to identify local vibration-mode energies of the wires due to incorporated oxygen. But perhaps the most interesting feature is the observation of a Kondo-like zero-bias anomaly. The stretching dependence of the zero-bias peak supports the idea that the atomic nickel-oxygen wires can, under favorable circumstances, behave as a Kondo system. Finally, it is also shown that when applying an external magnetic field the nickel-oxygen chains have a higher probability of displaying a preferential conductance close to 0.5 G_0. This sheds a different light on previous experiments that have been performed on nickel atomic contacts in less clean environments, in which a half-quantum conductance has been observed. Those results could be the result of oxygen contamination in the contact.

7

Atom manipulation of self-organized atomic chains

The last chapter of this thesis deals with atom manipulation of self-organized one-dimensional platinum atomic wires on a germanium (001) surface at room temperature. The manipulation of individual dimers is performed with an STM tip. Platinum atomic wires grown on germanium (001) can be hundreds of atoms long and are mostly defect free. It is found that by approaching a designated dimer in an atomic wire very closely it is possible to take the dimer out of the wire and carry it away on the STM tip. By moving the tip back to the same spot and repeating the tip approach the dimer can be placed back without doing any damage to the structure of the wire. This controlled manipulation of the platinum wires presents the first atom manipulation experiments done at room temperature on self-organized atomic structures.[1]

[1]The work described in this chapter has been performed in close collaboration with O. Gurlu, A. van Houselt, B. Poelsema and H.J.W. Zandvliet from the MESA+ Institute for Nanotechnology at the University of Twente and has been published in Nanotechnology **18**, 365305 (2007).

7.1 Introduction to atom manipulation with STM

The experimental results presented in the previous chapters have been obtained by using the mechanically controlled break junction technique. As has become clear this technique is very useful for the creation of adjustable electrodes between which single atoms or molecules can be contacted. The MBCJ technique is also very clean because the junction is opened for the first time when the sample chamber is in a cryogenic vacuum. Thirdly the atomically small junctions created by the MBCJ technique are extremely stable due to the large displacement ratio enabling individual measurements (e.g. differential conductance measurements) on single molecule junctions.

The MCBJ technique is limited in the sense that it is not possible to directly "see" how the single atom or molecule is contacted in the junction. Also the control of the configuration and location of a single atom or molecule in the junctions is very limited. With an STM it is possible to image surfaces on the atomic scale, i.e. one can "see" individual atoms on a conducting surface. Furthermore, single molecules can be imaged on a surface and spectroscopic measurements on the surface-molecule-tip junction can be performed (see e.g. [137, 138]). Binning and Rohrer received the Nobel prize in 1986 for the development of the Scanning Tunneling Microscope (STM) [139, 140]. In 1990 Eigler and Schweizer demonstrated that it is also possible to manipulate the position of ad-atoms, in that case Xe atoms, on a metal surface with the STM tip [2]. The authors performed their experiments at T = 4 K and they dragged the Xe atoms along the surface using the attracting force of the tip apex. This method has been applied successfully to other adsorbate-surface systems [141, 142]. Another method to displace atoms on a surface is to pick them up with the STM tip, carry them to a designated location and place them back to the surface [143]. By positioning atoms to defined places on a surface one can actually construct artificial atomic structures, which display interesting physics [144, 145]. All these atom manipulation experiments have been performed at cryogenic temperatures, which is a necessity because molecules like CO or Xe easily desorb from surfaces at elevated temperatures. Another reason is the high diffusivity of ad-atoms or molecules, which makes positioning on the atomic scale very difficult. In a rare experiment Fishlock *et. al* [146] demonstrated that Br atoms on Cu(001) can be successfully manipulated with atomic precision at room temperature.

Atom manipulation experiments reported in the literature are done by starting off with individual atoms on a surface that are brought together, forming an artificial structure. It will be demonstrated, for the first time, in this chapter that atom manipulation with atomic precision can be performed on self-organized atomic structure at room temperature. The structures under study are Pt atomic chains, which can be hundreds of atoms long, grown on germanium(001). The controlled manipulation of these atomic wires is not evident, since they are self-organized, meaning that the formation of the structures is driven by the minimization of the total energy of the system. A local alteration of these structures could result in the collapse of the structure. It will be

shown that the controlled creation and repair of defects in these wires at room temperature has a very high success rate.

7.2 Preparation and characterization of Pt wires on Ge(001)

Hundreds of atoms long defect free Pt atomic wires were found to be formed on Ge(001) [147]. It has been established that also gold wires can be created on the germanium surface [148]. The Ge(001) samples are cut from a n-type single-side-polished germanium wafer and is placed in a UHV-STM system with a background pressure of less than $5{\cdot}10^{-11}$ mbar. The surface is cleaned by a repeated cycle of 800 eV Ar^+ ion sputtering and subsequent annealing, which results in a clean surface and a 2×1 RHEED pattern. Inside the sample preparation chamber a tungsten heating wire is mounted, which is wrapped with high purity Pt (99.995%) that can be evaporated by heating the wire. After the cleaning cycle the equivalent of 0.25 monolayers Pt is deposited on the Ge(001) surface at room temperature. Subsequently, the sample is annealed at 1050 K for ten minutes and then cooled for at least 40 minutes before placing it in the STM. An etched tungsten tip is used for imaging the germanium surface as well as for the atom manipulation experiments.

The Ge(001) surface displays two distinct types of terraces, namely the so-called α- and β-terraces [147]. The Pt atomic wires grow on the β-terraces between so-called quasi dimer rows, which are newly formed rows due to the replacement of Ge atoms every other dimer. The Pt wires can be as long as the terraces on which they are grown and are always bound by either a step edge or a defect on the surface. In figure 7.1 a 100x100 nm^2 STM image is shown where the Pt wires are nicely seen. Gurlu *et al.* showed by means of differential conductance measurements that the Pt atomic wires are metallic at room temperature [147].

7.3 Room temperature atom manipulation

It is sometimes found that when the STM tip scans the Pt wires with a very low bias voltage, i.e. the tip is very close to the surface, some dimers are removed from the wires. The underlying Ge surface however displays no sign of distortion, indicating that the Pt dimers are loosely bound to the surface. This observation triggered the idea of trying to take away dimers in a controlled way without damaging the surface and thus creating atomic wires of arbitrary length.

The procedure to manipulate the atomic wire is as follows: First a part of the β-terrace with 100% clean Pt wires is chosen and imaged using a 0.4 nA tunneling current and -20 mV bias voltage as is shown in figure 7.2(a). During a second scan of the same area a designated point above one of the atomic wires is chosen where the manipulation will take place (figure 7.2(b)). Once

the tip arrives at that point first the tunneling current is increased to 20 nA and after a short delay of 1 ms the bias voltage is reduced to -2 mV and immediately reset to -20 mV. After a short delay of 1 ms also the tunneling current is recovered to 0.4 nA and the scan is continued. One can see a difference in image resolution in the upper half of the image of (b) after the manipulation event. In the subsequent scan of figure 7.2(c) the effect of the procedure is seen: The absence of a dimer at the exact location where the manipulation event has occurred. In the next scan the manipulation event is repeated with exactly the same parameters and at the same location, being the vacancy in the wire. The result after this event is shown in figure (d) in which the vacancy is filled with a Pt dimer again. This observation indicates that a Pt dimer can be moved from the surface to the tip apex, be carried by the tip and also be placed back onto the surface.

During the manipulation event no physical contact is established between

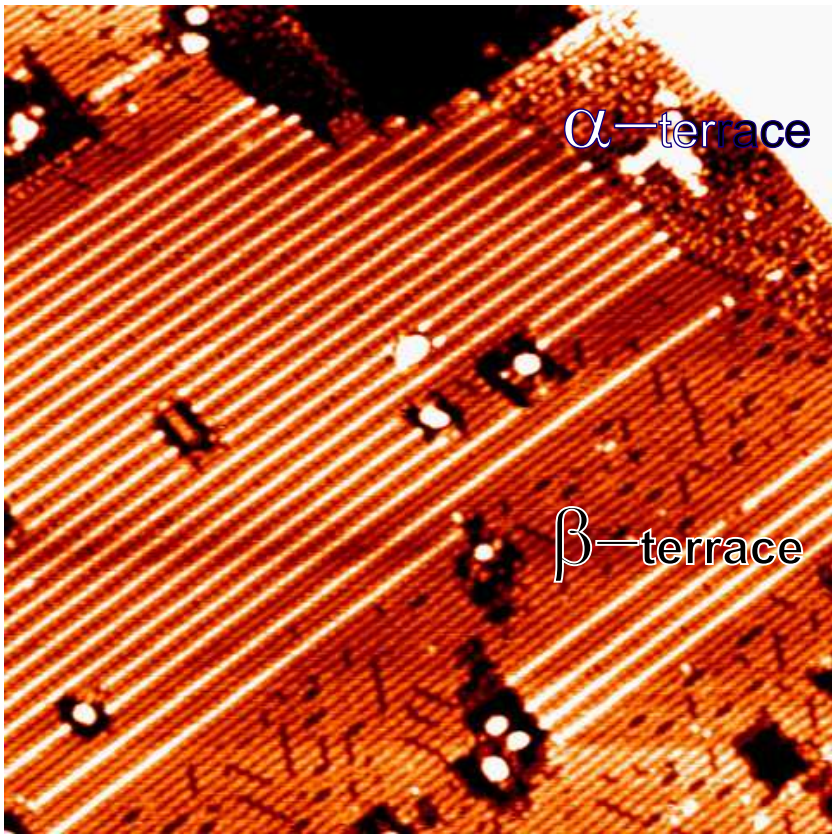

Figure 7.1: *STM image of part of the Ge(001) surface displaying Pt atomic wires (taken with -1.45V sample bias and 0.41nA tunneling current; size 100x100 nm^2). The wires are observed only on β-terraces. In the upper part of the image an α-terrace is visible.*

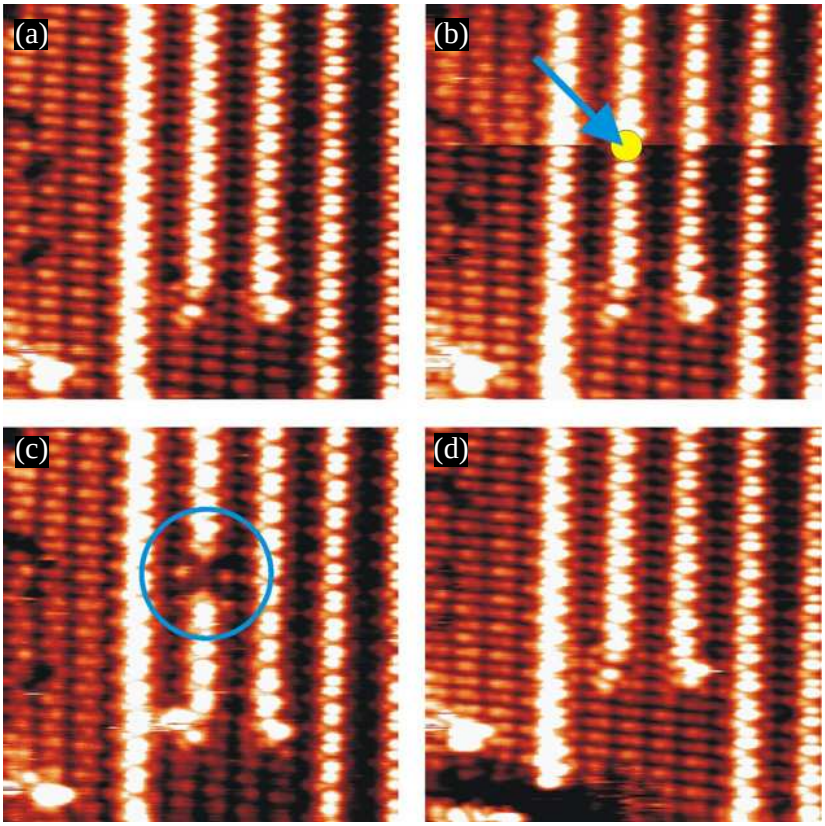

Figure 7.2: *Sequence of removing a Pt dimer from a Pt wire on Ge(001). (a) Pt wires imaged before manipulation (V_b=-20mV, I=0.4nA); (b) While scanning the manipulation event (see text) is applied to a designated point on a Pt wire; (c) Rescan of the area after the manipulation event. The missing dimer is clearly seen; (d) Rescan of the same area after a second manipulation event on the exact location of the vacancy of (c).*

the tip and the Pt wires. During the pickup event the tunnel resistance is reduced to only 100 kΩ, for which it is known that a jump-to-contact can occur between two metal atomic contacts [6, 16, 149]. It is therefore very likely that the dimer jumps to the tip during the pickup event and jumps back to the wire when the tip approaches the vacancy. It is found that it is also possible to repair larger defects in a Pt chain, being several Pt dimers long. Figure 7.3 shows the repair of a four dimer long defect in a Pt atomic wire by transporting individual dimers from other nearby dimers. The removal and subsequent replacement of single Pt dimers located inside atomic wires by means of the above described method has success-rate of more than 90 %. In this way Pt atomic wires of arbitrary length can be created and the electronic properties be measured in a similar manner as has been performed on gold atomic wires, of which the individual gold atoms are collected one by one [150]. Another very interesting

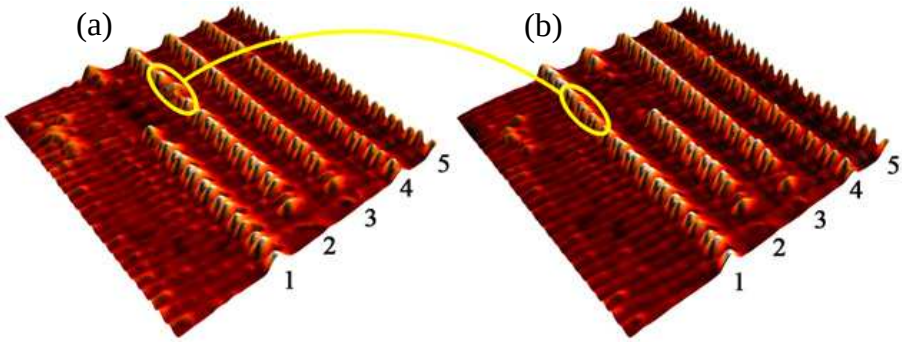

Figure 7.3: *Area of a Ge(001) surface with five Pt atomic wires. In the left image wire 1 has a defect consisting of four missing Pt dimers. In the right image the individual Pt dimers have been carried in a one-by-one fashion from wire 2 to fill the defect in wire 1.*

opportunity would be to try to contact single molecules inside a vacancy of the atomic wire and measure the electronic properties.

7.4 Image resolution and dimer configuration

The probability for a successful pickup of a Pt dimer is very high. Sometimes it has also been observed that when the manipulation position was in between two dimers both dimers were transferred to the tip. It is also possible to pick two dimers sequentially without losing image resolution. A third dimer pickup led to loss of image resolution or the drop of a dimer in practically all cases. Interestingly, it seems that a dimer is bound to the tip apex in two preferential configurations. In one case the image resolution remains atomically sharp upon picking up a dimer, while in the other case the pick-up resulted in a double tip image. This observation is interpreted by assuming that the dimer can be in a vertical or horizontal position at the tip apex resulting in an atomically sharp or double tip resolution, respectively.

7.5 Conclusion

The experiments described in this chapter have demonstrated for the first time that atom manipulation of self-assembled structures at room temperature is possible with a very high success rate. It is possible to create atomic wires of arbitrary length on the Ge surface, which makes it possible to study the physical properties of these wires as a function of length.

Bibliography

[1] G. Binnig and H. Rohrer *Rev. Mod. Phys.*, vol. 3, pp. 615–625, 1987.

[2] D. M. Eigler and E. K. Schweizer *Nature*, vol. 344, pp. 524–526, 1990.

[3] B. J. van Wees, H. van Houten H., C. W. J. Beenakker, J. G. Williamson, L. P. Kouwenhoven, D. van der Marel, and C. T. Foxon *Phys. Rev. Lett.*, vol. 60, pp. 848–850, 1988.

[4] E. Scheer, N. Agraït, J. C. Cuevas, A. Levy Yeyati, B. Ludoph, A. Martín-Rodero, G. Rubio Bollinger, J. M. van Ruitenbeek, and C. Urbina *Nature*, vol. 394, pp. 154–157, 1998.

[5] H. Ohnishi, Y. Kondo, and K. Takayanagi *Nature*, vol. 395, pp. 780–785, 1998.

[6] A. I. Yanson, G. Rubio Bollinger, H. E. van den Brom, N. Agraït, and J. M. van Ruitenbeek *Nature*, vol. 395, pp. 783–785, 1998.

[7] H. Park, J. Park, A. K. L. Kim, and P. L. M. E. H. Anderson A. P. Alivisatos *Nature*, vol. 407, p. 57, 2000.

[8] R. H. M. Smit, Y. Noat, C. Untiedt, N. D. Lang, M. C. van Hemert, and J. M. van Ruitenbeek *Nature*, vol. 419, pp. 906–909, 2002.

[9] C. Kittel, *Introduction to solid state physics*. New York: John Wiley and Sons, 7th ed., 1996.

[10] Y. V. Sharvin *Sov. Phys.-JETP*, vol. 21, pp. 655–656, 1965. [Zh. Eksp. Teor. Fiz. 48, 984-985 (1965)].

[11] R. Landauer *IBM J. Res. Dev.*, vol. 1, pp. 223–231, 1957.

[12] A. Levy Yeyati, A. Martín-Rodero, and F. Flores *Phys. Rev. B*, vol. 56, pp. 10369–10372, 1997.

[13] J. C. Cuevas, A. Levy Yeyati, A. Martín-Rodero, G. Rubio Bollinger, C. Untiedt, and N. Agraït *Phys. Rev. Lett.*, vol. 81, pp. 2990–2993, 1998.

[14] E. Scheer, P. Joyez, D. Esteve, C. Urbina, and M. H. Devoret *Phys. Rev. Lett.*, vol. 78, pp. 3535–3538, 1997.

[15] M. Brandbyge, M. R. Sørensen, and K. W. Jacobsen *Phys. Rev. B*, vol. 56, pp. 14956–14959, 1997.

[16] J. M. Krans, C. J. Muller, I. K. Yanson, T. C. M. Govaert, R. Hesper, and J. M. van Ruitenbeek *Phys. Rev. B*, vol. 48, pp. 14721–14274, 1993.

[17] N. Agraït, J. G. Rodrigo, and S. Vieira *Phys. Rev. B*, vol. 47, pp. 12345–12348, 1993.

[18] L. Olesen, E. Lægsgaard, I. Stensgaard, F. Besenbacher, J. Schiøtz, P. Stoltze, K. W. Jacobsen, and J. K. Nørskov *Phys. Rev. Lett.*, vol. 72, pp. 2251–2254, 1994.

[19] J. M. Krans, J. M. van Ruitenbeek, V. V. Fisun, I. K. Yanson, and L. J. de Jongh *Nature*, vol. 375, pp. 767–769, 1995.

[20] M. Brandbyge, J. Schiøtz, M. R. Sørensen, P. Stoltze, K. W. Jacobsen, J. K. Nørskov, L. Olesen, E. Lægsgaard, I. Stensgaard, and F. Besenbacher *Phys. Rev. B*, vol. 52, pp. 8499–8514, 1995.

[21] M. Paulsson, F. Zahid, and S. Datta, "Resistance of a molecule," in *Nanoscience, Engineering and Technology Handbook* (S. L. W. Goddard, D. Brenner and G. Iafrate, eds.), CRC Press, 2003. Also appeared online: http://arXiv.org/abs/cond-mat/0208183.

[22] D. Djukic, K. S. Thygesen, C. Untiedt, R. H. M. Smit, K. W. Jacobsen, and J. M. van Ruitenbeek *Phys. Rev. B*, vol. 71, p. 161402(R), 2005.

[23] D. Djukic and J. M. van Ruitenbeek *Nano Lett.*, vol. 6, pp. 789–793, 2006.

[24] J. Moreland and J. W. Ekin *J. Appl. Phys.*, vol. 58, pp. 3888–3895, 1985.

[25] C. J. Muller, J. M. van Ruitenbeek, and L. J. de Jongh *Physica C*, vol. 191, pp. 485–504, 1992.

[26] J. M. Krans, *Size effects in atomic-scale point contacts*. PhD thesis, Universiteit Leiden, The Netherlands, 1996.

[27] J. G. Simmons *J. Appl. Phys.*, vol. 34, p. 1793, 1963.

[28] M. Dreher, F. Pauly, J. Heurich, J. C. Cuevas, E. Scheer, and P. Niebala *Phys. Rev. B*, vol. 72, p. 075435, 2005.

[29] A. G. M. Jansen, A. P. van Gelder, and P. Wyder *J. Phys. C: Solid St. Phys.*, vol. 13, pp. 6073–6118, 1980.

[30] I. K. Yanson *Zh. Eksp. Teor. Fiz.*, vol. 66, pp. 1035–1050, 1974. [Sov. Phys.-JETP **39** (1974) 506–513].

[31] I. O. Kulik and A. N. Omelyanchuk *Sov. J. Low Temp. Phys.*, vol. 3, pp. 459–461, 1977.

[32] N. V. Zavaritskiĭ *Sov. Phys. USP.*, vol. 15, pp. 608–625, 1973. [Usp. Fiz. Nauk **108** (1972) 241–272].

[33] A. M. Duif, A. G. M. Jansen, and P. Wyder *J. Phys: Condens. Matter*, vol. 1, pp. 3157–3189, 1986.

[34] A. V. Khotkevich and I. K. Yanson, *Atlas of point contact spectra of electron-phonon interactions in metals*. Dordrecht: Kluwer Academic Publishers, 1995.

[35] J. M. van Ruitenbeek and A. G. M. Jansen, eds., *Proceedings of the second international conference on point contact spectroscopy*, vol. 218 of *Physica B*. Amsterdam: North Holland, 1996.

[36] B. Ludoph, M. H. Devoret, D. Esteve, C. Urbina, and J. M. van Ruitenbeek *Phys. Rev. Lett.*, vol. 82, pp. 1530–1533, 1999.

[37] B. Ludoph, N. van der Post, E. N. Bratus', E. V. Bezuglyi, V. S. Shumeiko, G. Wendin, and J. M. van Ruitenbeek *Phys. Rev. B*, vol. 61, pp. 8561–8569, 2000.

[38] C. Untiedt, G. Rubio Bollinger, S. Vieira, and N. Agraït *Phys. Rev. B*, vol. 62, pp. 9962–9965, 2000.

[39] T. Frederiksen, M. Brandbyge, N. Lorente, and A. P. Jauho *Phys. Rev. Lett.*, vol. 93, p. 256601, 2004.

[40] J. K. Viljas, J. C. Cuevas, F. Pauly, and M. Häfner *Phys. Rev. B*, vol. 72, p. 245415, 2005.

[41] L. de la Vega, N. A. A. Martín-Rodero, and A. L. Yeyati *Phys. Rev. B*, vol. 73, p. 075428, 2006.

[42] M. Galperin, M. A. Ratner, and A. Nitzan *J. Phys. Cond. Matt.*, vol. 19, p. 103201, 2007.

[43] N. Agraït, C. Untiedt, G. Rubio-Bollinger, and S. Vieira *Phys. Rev. Lett.*, vol. 88, p. 216803, 2002.

[44] G. Rubio-Bollinger, S. R. Bahn, N. Agraït, K. W. Jacobsen, and S. Vieira *Phys. Rev. Lett.*, vol. 87, p. 026101, 2001.

[45] G. Rubio-Bollinger, P. Joyez, and N. Agraït *Phys. Rev. Lett.*, vol. 93, p. 116803, 2004.

[46] A. M. C. Valkering, A. I. Mares, C. Untiedt, K. B. Gavan, T. H. Oosterkamp, and J. M. van Ruitenbeek *Rev. Sci. Instr.*, vol. 76, p. 103903, 2005.

[47] R. H. M. Smit, C. Untiedt, A. I. Yanson, and J. M. van Ruitenbeek *Phys. Rev. Lett.*, vol. 87, p. 266102, 2001.

[48] J. A. Torres, E. Tosatti, A. D. Corso, F. Ercolessi, J. J. Kohanoff, F. D. D. Tolla, and J. M. Soler *Surface Science*, vol. 426, pp. L441–L446, 1999.

[49] H. Häkkinen, R. N. Barnett, A. G. Scherbakov, and U. Landman *J. Phys. Chem. B*, vol. 104, pp. 9063–9066, 2000.

[50] L. D. Maria and M. Springborg *Chem. Phys. Lett.*, vol. 323, pp. 293–299, 2000.

[51] S. R. Bahn and K. W. Jacobsen *Phys. Rev. Lett.*, vol. 87, p. 266101, 2001.

[52] A. I. Yanson, *Atomic chains and electronic shells: Quantum mechanisms for the formation of nanowires*. PhD thesis, Universiteit Leiden, The Netherlands, 2001.

[53] F. D. Novaes, A. J. R. da Silva, E. Z. da Silva, and A. Fazzio *Phys. Rev. Lett.*, vol. 90, p. 036101, 2003.

[54] N. V. Skorodumova and S. I. Simak *Phys. Rev. B*, vol. 67, p. 121404, 2003.

[55] S. B. Legoas, V. Rodrigues, D. Ugarte, and D. S. Galvão *Phys. Rev. Lett.*, vol. 93, p. 216103, 2004.

[56] H. Koizumi, Y. Oshima, Y. Kondo, and K. Takayanagi *Ultramicroscopy*, vol. 88, pp. 17–24, 2001.

[57] S. R. Bahn, N. Lopez, J. K. Nørskov, and K. W. Jacobsen *Phys. Rev. B*, vol. 66, p. 081405, 2002.

[58] F. D. Novaes, A. J. R. da Silva, E. Z. da Silva, and A. Fazzio *Phys. Rev. Lett.*, vol. 96, p. 016104, 2006.

[59] N. Agraït, C. Untiedt, G. Rubio-Bollinger, and S. Vieira *Chem. Phys.*, vol. 281, pp. 231–234, 2002.

[60] Z. Gai, Y. He, H. Yu, and W. S. Yang *Phys. Rev. B*, vol. 53, pp. 1042–1045, 1996.

[61] J. L. Costa-Krämer, N. García, P. García-Mochales, P. A. Serena, M. I. Marqués, and A. Correia *Phys. Rev. B*, vol. 55, pp. 5416–5424, 1997.

[62] J. L. Costa-Krämer *Phys. Rev. B*, vol. 55, pp. R4875–R4878, 1997.

[63] D. D. Eley and P. B. Moore *Surf. Sci.*, vol. 76, pp. L599–L602, 1978.

[64] M. Valden, X. Lai, and D. W. Goodman *Science*, vol. 281, pp. 1647–1650, 1998.

[65] H. Häkkinen private communication.

[66] A. J. R. da Silva private communication.

[67] R. H. M. Smit, *From quantum point contacts to monatomic chains: Fabrication and characterisation of the ultimate nanowire*. PhD thesis, Universiteit Leiden, The Netherlands, 2003.

[68] J. M. J. aan de Brugh, "Density functional theory analysis on a nanowire," Master's thesis, Center for Atomic-scale Materials Physics, Technical University of Denmark, Denmark, 2005.

[69] M. Paulsson, T. Frederiksen, and M. Brandbyge *Phys. Rev. B*, vol. 72, p. 201101(R), 2005.

[70] W. H. A. Thijssen, M. Strange, J. M. J. aan de Brugh, and J. M. van Ruitenbeek to be published.

[71] M. Strange, W. H. A. Thijssen, J. M. van Ruitenbeek, and K. S. Thygesen to be published.

[72] M. Taniguchi, K. Tanaka, T. Hashizume, and T. Sakurai *Surf. Sci. Lett.*, vol. 262, p. L123, 1992.

[73] F. Besenbacher and J. K. Nørskov *Progr. Surf. Sci.*, vol. 44, p. 5, 1993.

[74] R. H. M. Smit, C. Untiedt, G. Rubio-Bollinger, R. C. Segers, and J. M. van Ruitenbeek *Phys. Rev. Lett.*, vol. 91, p. 076805, 2003.

[75] L. de la Vega, A. Martín-Rodero, A. L. Yeyati, and A. Saúl *Phys. Rev. B*, vol. 70, p. 113107, 2004.

[76] R. A. Molina, D. Weinmann, and J. L. Pichard *Europhys. Lett*, vol. 67, p. 96, 2004.

[77] W. H. A. Thijssen, D. Marjenburgh, R. H. Bremmer, and J. M. van Ruitenbeek *Phys. Rev. Lett.*, vol. 96, p. 026806, 2006.

[78] S. Csonka, A. Halbritter, and G. Mihály *Phys. Rev. B*, vol. 73, p. 075405, 2006.

[79] J. C. Cuevas, J. Heurich, F. Pauly, W. Wenzel, and G. Schön *Nanotechnology*, vol. 14, pp. R29–R38, 2003.

[80] V. M. Garcia-Suarez, A. R. Rocha, S. W. Bailey, C. J. Lambert, S. Sanvitto, and J. Ferrer *Phys. Rev. B*, vol. 72, p. 045437, 2005.

[81] K. S. Thygesen and K. W. Jacobsen *Phys. Rev. Lett.*, vol. 94, p. 036807, 2005.

[82] D. C. Ralph and R. A. Burhman *Phys. Rev. Lett.*, vol. 69, pp. 2118–2121, 1992.

[83] R. J. P. Keijsers, O. I. Shklyarevskii, and H. van Kempen *Phys. Rev. B*, vol. 51, p. 5628, 1995.

[84] J. Gaudioso, L. J. Lauhon, and W. Ho *Phys. Rev. Lett.*, vol. 85, p. 1918, 2000.

[85] W. Wang, T. Lee, I. Kretzschmar, and M. A. Reed *Nano Lett.*, vol. 4, p. 643, 2004.

[86] J. A. Gupta, C. P. LutzDuprat, A. J. Heinrich, and D. M. Eigler *Phys. Rev. B*, vol. 71, p. 115416, 2005.

[87] D. C. Ralph and R. A. Buhrman *Phys. Rev. B*, vol. 51, p. 3554, 1995.

[88] B. C. Stipe, M. A. Rezaei, and W. Ho *Science*, vol. 279, p. 1907, 1998.

[89] B. C. Stipe, M. A. Rezaei, and W. Ho *Phys. Rev. Lett.*, vol. 81, p. 1263, 1998.

[90] T. Komeda, Y. Kim, M. Kawai, B. N. J. Persson, and H. Ueba *Science*, vol. 295, p. 2055, 2002.

[91] B. N. J. Persson and H. Ueba *Surf. Sci.*, vol. 18, pp. 502–503, 2002.

[92] D. Djukic, *Simple molecules as benchmark systems for molecular electronics*. PhD thesis, Universiteit Leiden, The Netherlands, 2006.

[93] B. Ludoph and J. M. van Ruitenbeek *Phys. Rev. B*, vol. 61, pp. 2273–2285, 2000.

[94] M. Galperin, M. A. Ratner, and A. Nitzan *J. Chem. Phys.*, vol. 121, p. 11965, 2004.

[95] A. Halbritter, P. Makk, S. Csonka, and G. Mihály *Preprint*, pp. http://arXiv.org/abs/cond–mat/0706.2083, 2007.

[96] V. Rodrigues and D. Ugarte *Phys. Rev. B*, vol. 63, p. 073405, 2001.

[97] R. N. Barnett, H. Häkkinen, A. G. Scherbakov, and U. Landman *Nano. Lett.*, vol. 4, p. 1845, 2004.

[98] F. D. Novaes, E. Z. da Silva, A. J. R. da Silva, and A. Fazzio *Surf. Sci.*, vol. 566-568, p. 367, 2004.

[99] P. Jelinek, R. Pérez, J. Ortega, and F. Flores *Phys. Rev. Lett.*, vol. 96, p. 046803, 2006.

[100] T. Frederiksen, M. Paulsson, and M. Brandbyge *Journal of Physics: Conference Series*, vol. 61, p. 312, 2007.

[101] S. Csonka, A. Halbritter, G. Mihály, E. Jurdik, O. I. Shklyarevskii, S. Speller, and H. van Kempen *Phys. Rev. Lett.*, vol. 90, p. 116803, 2003.

[102] R. W. de Blois *J. Appl. Phys.*, vol. 36, p. 1647, 1965.

[103] R. P. Cowburn *J. Phys. D: Appl. Phys.*, vol. 33, pp. R1–R16, 2000.

[104] F. Pauly, M. Dreher, M. H. J. K. Viljas, J. C. Cuevas, and P. Nielaba *Phys. Rev. B*, vol. 74, p. 235106, 2006.

[105] T. Ono, Y. Ooka, H. Miyajima, and Y. Otani *Appl. Phys. Lett.*, vol. 75, pp. 1622–1624, 1999.

[106] H. Oshima and K. Miyano *Appl. Phys. Lett.*, vol. 73, pp. 2203–2205, 1998.

[107] F. Komori and K. Nakatsuji *J. Phys. Soc. Jap.*, vol. 68, pp. 3786–3789, 1999.

[108] F. Elhoussine, S. Mátéfi-Tempfli, A. Encinas, and L. Piraux *Appl. Phys. Lett.*, vol. 81, pp. 1681–1683, 2002.

[109] M. Shimizu, E. Saitoh, H. Miyajima, and Y. Otani *J. Magn. Magn. Mat.*, vol. 239, pp. 243–245, 2002.

[110] V. Rodrigues, J. Bettini, P. C. Silva, and D. Ugarte *Phys. Rev. Lett.*, vol. 91, p. 096801, 2003.

[111] N. Agraït, A. Levy Yeyati, and J. M. van Ruitenbeek *Phys. Rep.*, vol. 377, pp. 81–279, 2003.

[112] N. Garcia, M. Muñoz, and Y.-W. Zhao *Phys. Rev. Lett.*, vol. 82, pp. 2923–2926, 1999.

[113] S. H. Chung, M. Muñoz, N. García, W. F. Egelhoff, and R. D. Gomez *Phys. Rev. Lett.*, vol. 89, p. 287203, 2002.

[114] H. D. Chopra and S. Z. Hua *Phys. Rev. B*, vol. 66, p. 020403, 2002.

[115] S. Z. Hua and H. D. Chopra *Phys. Rev. B*, vol. 67, p. 060401, 2003.

[116] M. R. Sullivan, D. A. Boehm, D. A. Ateya, S. Z. Hua, and H. D. Chopra *Phys. Rev. B*, vol. 71, p. 024412, 2005.

[117] M. Viret, M. Gabureac, F. Ott, C. Barreteau, G. Autes, and R. Guirado-Lopez *Eur. Phys. J. B*, vol. 51, pp. 1–4, 2006.

[118] C. Untiedt, D. M. T. Dekker, D. Djukic, and J. M. van Ruitenbeek *Phys. Rev. B*, vol. 69, p. 081401(R), 2004.

[119] C. Sirvent, J. G. Rodrigo, N. Agraït, and S. Vieira *Physica B*, vol. 218, pp. 238–241, 1996.

[120] D. Jacob, J. Fernández-Rossier, and J. J. Palacios *Phys. Rev. B*, vol. 71, p. 220403(R), 2005.

[121] A. Smogunov, A. D. Corso, and E. Tosatti *Surf. Sci.*, vol. 507-510, pp. 609–614, 2002.

[122] A. Smogunov, A. D. Corso, and E. Tosatti *Surf. Sci.*, vol. 532-535, pp. 549–555, 2003.

[123] A. Bagrets, N. Papanikolaou, and I. Mertig *Phys. Rev. B*, vol. 70, p. 064410, 2004.

[124] N. Papanikolaou *J. Phys. Cond. Matt.*, vol. 15, p. 5049, 2003.

[125] D. Jacob, J. Fernández-Rossier, and J. J. Palacios *Phys. Rev. B*, vol. 74, p. 081402(R), 2006.

[126] J. Park, A. N. Pasupathy, J. I. Goldsmith, C. Chang, Y. Yaish, J. R. Petta, M. Rinkoski, J. P. Sethna, H. D. Abruña, P. L. McEuen, and D. C. Ralph *Nature*, vol. 417, pp. 722–725, 2002.

[127] W. Liang, M. P. Shores, M. Bockrath, J. R. Long, and H. Park *Nature*, vol. 417, pp. 725–729, 2002.

[128] A. N. Pasupathy, R. C. Bialczak, J. Martinek, J. E. Grose, L. A. K. Donev, P. L. McEuen, and D. C. Ralph *Science*, vol. 306, p. 86, 2004.

[129] L. H. Yu and D. Natelson *Nano Lett.*, vol. 4, p. 79, 2004.

[130] J. J. Parks, A. R. Champagne, G. R. Hutchinson, S. Flores-Torres, H. D. Abruña, and D. C. Ralph *prl*, vol. 99, p. 026601, 2007.

[131] J. Nygøard, D. H. Cobden, and P. E. Lindelof *Nature*, vol. 408, p. 342, 2000.

[132] J. Paaske and K. Flensberg *Phys. Rev. Lett.*, vol. 94, p. 176801, 2005.

[133] J. König, H. Schoeller, and G. Schön *Phys. Rev. Lett.*, vol. 76, p. 1715, 1996.

[134] L. I. Glazman and A. V. Khaetskii *JETP Lett.*, vol. 48, pp. 591–595, 1988.

[135] T. K. Ng and P. A. Lee *Phys. Rev. Lett.*, vol. 61, p. 1768, 1988.

[136] D. Jacob and J. J. Palacios private communication.

[137] B. C. Stipe, M. A. Rezaei, and W. Ho *Science*, vol. 280, p. 1732, 1998.

[138] W. Ho *J. Chem. Phys.*, vol. 117, p. 11033, 2002.

[139] G. Binning, H. Rohrer, C. Gerber, and E. Weibel *Appl. Phys. Lett.*, vol. 40, p. 178, 1981.

[140] G. Binning, H. Rohrer, C. Gerber, and E. Weibel *Phys. Rev. Lett.*, vol. 49, p. 57, 1982.

[141] P. Zeppenfeld, C. P. Lutz, and D. M. Eigler *Ultramicroscopy*, vol. 42, p. 128, 1992.

[142] M. F. Crommie, C. P. Lutz, and D. M. Eigler *Science*, vol. 262, pp. 218–220, 1993.

[143] D. M. Eigler, C. P. Lutz, and W. E. Rudge *Nature*, vol. 352, p. 600, 1991.

[144] H. C. Manoharan, C. P. Lutz, and D. W. Eigler *Nature*, vol. 403, pp. 512–515, 2000.

[145] A. J. Heinrich, C. P. Lutz, J. A. Gupta, and D. M. Eigler *Science*, vol. 298, pp. 1381–1387, 2002.

[146] T. W. Fishlock, A. Oral, R. G. Egdell, and J. B. Pethica *Nature*, vol. 404, p. 743, 2000.

[147] O. Gurlu, O. A. O. Adam, H. J. W. Zandvliet, and B. Poelsema *Appl. Phys. Lett.*, vol. 83, p. 4610, 2003.

[148] J. Wang, M. Li, and E. I. Altman *Phys. Rev. B*, vol. 70, p. 233312, 2004.

[149] U. Dürig, O. Züger, and D. W. Pohl *Phys. Rev. Lett.*, vol. 65, pp. 349–352, 1990.

[150] T. M. Wallis, N. Nilius, and W. Ho *Phys. Rev. Lett.*, vol. 89, p. 236802, 2002.

Samenvatting

De interesse van mensen in de fundamentele wetenschap is meestal het grootst wanneer het onderwerp over het hele groote zoals de plek van de aarde in het heelal, of het hele kleine zoals individuele atomen gaat. Dit is waarschijnlijk zo omdat mensen zich moeilijk een beeld kunnen vormen van zowel het hele groote als het hele kleine, waardoor het een zekere mystiek oproept en hen fascineert. Welnu, dit proefschrift beschrijft een studie naar de eigenschappen van individuele atomen en moleculen die het kleinst mogelijke contact vormen tussen twee electroden. Ik hoop dan ook dat het met interesse gelezen wordt.

Atomen en moleculen zijn de bouwstenen van de fysieke wereld zoals wij die elke dag waarnemen. De afmetingen van individuele atomen en moleculen zijn een factor 10^9 tot 10^{10} kleiner dan de afmetingen in meters waarmee mensen het meest vertrouwd zijn. Het kleinste atoom is het waterstof atom en heeft een diameter van ongeveer één tien miljardste meter, 10^{-10} m, ook wel een Ångstøm (Å) genoemd. Alle atomen en de kleinere moleculen hebben afmetingen van een paar Å.

We kunnen atomen niet zien met onze ogen en ook met de beste optische microscoop lukt dat niet. Dit komt omdat de golflengtes in het elektromagnetische spectrum die onze ogen kunnen waarnemen vele malen groter zijn dan de afmeting van een individueel atoom. Maar sinds begin jaren 1980 is het mogelijk om individuele atomen te visualiseren met behulp van een Scanning Tunneling Microscoop. Een heel scherpe metalen naald beweegt op een afstand van slechts enkele atoomlengtes over een geleidend oppervlak. De afstand tussen het oppervlak en het uiteinde van de naald wordt constant gehouden. Wanneer de naald over een atoom heen beweegt zal de naald iets omhoog bewegen om de afstand constant te houden en op deze manier worden de atomen in beeld gebracht. Tevens is het met deze naald mogelijk om contact te maken met een atoom op het oppervlak en individuele atomen te verplaatsen.

Dit proefschrift behandelt de elektrische en mechanische eigenschappen van contacten van slechts één atoom of molecuul. In hoofdstuk 2 wordt de theorie samengevat van de elektrische geleiding van zeer nauwe constricties en contacten van slechts een enkel atoom in diameter. Elektrisch transport door een enkel atoom of molecuul kan plaats vinden wanneer één of meerdere elektronische orbitalen van het gecontacteerde atoom of molecuul energetisch

opgelijnd zijn met de zogenaamde Fermi energie van het metaal dat het molecuul contacteert. De maximale geleiding van een enkele orbitaal is het fundamentele geleidingskwantum $2e^2/h$ wat overeenkomst met een weerstand van ongeveer 13.000 Ω. Ook geeft hoofdstuk 2 een inleiding in de experimentele opstelling die gebruikt is voor het meten van de eigenschappen van enkel-molecuul contacten. Contacten van één atoom in diameter kunnen worden gemaakt met de mechanisch controleerbare breekjunctie techniek. Met deze techniek wordt een macroscopische metaaldraad op een buigbaar substraat in een driepuntsconfiguratie met behulp van een piezoëlektrisch element gebroken. Dit breken kan zo nauwkeurig dat er uiteindelijk een contact van slechts één atoom overblijft en stabiel gehouden kan worden.

Vervolgens worden in hoofdstuk 3 de allerdunste draden van slechts één atoom dik geïntroduceerd. Het bestaan van deze draden is enige jaren geleden o.a. in Leiden ontdekt en ze zijn vervolgens intensief bestudeerd. Deze draden zijn tot nu toe alleen van goud, platina of iridium waargenomen en er bestaat een model dat verklaart dat alleen van deze hele zware atomen atomaire draden gevormd kunnen worden. In dit werk zijn de interacties van deze draden met zuurstof bestudeerd en het blijkt dat zuurstof zich kan nestelen in de keten en daardoor de lineaire bindingen in de draad verstevigt. Dit effect is zo sterk dat andere metalen zoals zilver en koper met zuurstof nieuwe draden vormen terwijl ze dat in pure vorm niet doen. Met behulp van gevoelige metingen van de zogenaamde differentiële geleiding als functie van de aangelegde spanning is de aanwezigheid van één of meerdere zuurstofatomen in een metaal draad aangetoond. Dit gebeurt door de energie van de vibratietoestanden van het aanwezige molecuul te meten. Wanneer elektronen door het molecuul stromen kunnen ze, als ze voldoende energie hebben, botsen met het molecuul en een vibratie aanslaan. Hierbij draagt het elektron energie over aan de vibratietoestand om vervolgens terug te reizen tegen de elektronstroom in. Daardoor zal dit elekton niet meetellen in de effectieve elektronstroom door het molecuul en wordt dus bij de energie van een vibratietoestand een kleine correctie op de stroom door het molecuul gemeten.

Deze differentiële geleidingsmetingen zijn uitgevoerd op veel verschillende enkel-molecuul contacten van verschillende moleculen en contactmetalen. Behalve de hierboven beschreven correctie in de spectra worden ook vaak scherpe pieken gemeten. Hoofdstuk 4 presenteert een theoretisch model dat kan verklaren wat de oorzaak van deze pieken is. Stel je voor dat een molecuul op twee verschillende manieren in een contact gebonden kan zijn, met slechts een klein verschil in bindingssterkte en elektrische geleiding tussen die twee. Door de extreem lage temperatuur zal het molecuul zich bevinden in die gebonden toestand met de hoogste bindingsterkte en dus de laagste energie. Wanneer nu een interne vibratietoestand van het molecuul wordt aangeslagen, komt het molecuul in een hogere energetische toestand waardoor het kan overspringen naar de andere gebonden toestand, die een iets andere contactgeleiding veroorzaakt. Daarna kan het weer opnieuw aangeslagen worden en overspringen. Op deze manier ontstaat een zogenaamd twee-toestanden systeem dat door een vibratietoestand geïnduceerd wordt. De pieken in differentiële

geleiding kunnen met dit model gebruikt worden om vibratietoestanden van enkele-molecuul contacten te identificeren.

Enkele jaren geleden is aangetoond dat het meest eenvoudige molecuul, het waterstof molecuul, door platina elektrodes gecontacteerd kan worden. De reactie van waterstof met atomaire goud draden is door andere groepen al bestudeerd. Het is nog niet helemaal eenduidig of waterstof zich in atomaire of moleculaire vorm nestelt in de draad. Hoofdstuk 5 beschrijft een studie naar de structurele en geleidings eigenschappen van goud-waterstof draden. De energie afhankelijkheid van een vibratietoestand is tegelijk met de geleiding van de draad als functie de uitrekking van de draad gemeten. Samen met enkele theoretische modelen is vervolgens aannemelijk gemaakt dat dit gedrag alleen te verklaren is door de aanwezigheid van één of meerdere waterstof moleculen in de atomaire draad.

Nikkel is een metaal dat ferromagnetisch is bij kamertemperatuur en lagere temperaturen. Magnetisme wordt op atomair niveau veroorzaakt door de spin van elektronen, die een klein magnetisch moment met zich meedragen. De electron-spin kan zich in de zogenaamde up of down toestand bevinden. Als in een materiaal de meeste aanwezige spins een bepaalde kant op gericht staan, is het materiaal gemagnetiseerd. Wanneer nu de orbitaal die voor de geleiding van elektronen door het enkele atoom of molecuul zorgt, selectief is met betrekking tot de toestand van de spin van de elektronen zou zogenaamd spin-afhankelijk transport kunnen plaatsvinden. Dit zou tot uiting kunnen komen door de waarneming van geleidingswaardes van halve geleidingskwanta. Verschillende experimenten zijn in het recente verleden geïnterpreteerd als zou dit bij atomaire contacten van zuiver nikkel zijn waargenomen, terwijl berekeningen erop duiden dat het niet zou kunnen. In hoofdstuk 6 worden nikkel contacten bestudeerd onder invloed van opnieuw zuurstof. Zuurstof blijkt opnieuw atomaire draden mogelijk te maken en de nikkel-zuurstof draden gedragen zich soms als een zogenaamd Kondo-systeem. Een Kondo-systeem kan ontstaan door de interactie van geleidingselectronen met een gelocaliseerde zwak gekoppelde spin-toestand, zoals een orbital van een zuurstof atoom in de draad. Geleidingswaarden van een half geleidingsquantum zijn ook waargenomen, maar alleen wanneer zuurstof aanwezig was in het nikkel contact.

Het proefschrift wordt afgesloten met hoofdstuk 7, dat ook atomaire draden betreft, maar van een andere aard en met een andere techniek bestudeerd. De experimenten zijn aan de Universiteit Twente in nauwe samenwerking met Twentse wetenschappers gedaan, omdat daar specifieke experimentele condities voor handen waren. In Twente heeft men onlangs atomaire platina draden op een germanium oppervlak kunnen creëren. Met behulp van een Scanning Tunneling Microscoop is het mogelijk om met een zeer hoge succeskans willekeurig individuele dimeren (twee aan elkaar gebonden atomen) uit de draden op te pakken en elders neer te leggen zonder dat de draad wordt beschadigd. Deze techniek is in het verleden toegepast op individuele atomen. Wat de experimenten van hoofdstuk 7 bijzonder maakt is dat het de eerste atoommanipulatie experimenten aan zelf-georganiseerde nanostructuren bij kamertemperatuur zijn.

List of publications

- F. Pulizzi, W.H.A. Thijssen, P.C.M. Christianen, J.C. Maan, D.R. Ossau, T. Wojtowicz, G. Karczewski and J. Kossut, *Motion of neutral and negatively charged excitons in high magnetic fields*, Physica B, vol. 298, pp. 397-401, 2001.

- F. Pulizzi, W.H.A. Thijssen, P.C.M. Christianen, J.C. Maan, *Diffusion of two dimensional magnetoexcitons* , Physica B, vol. 298, pp. 441-445, 2001.

- Z.V. Popović, A. Cantarero, W.H.A. Thijssen, N. Paunović, Z. Dohcević-Mitrović and F. Sapiña, *Short range charge/orbital ordering in* $La_{1-x}Sr_xMn_{1-z}B_zO_3$ *(B = Cu, Zn) manganites*, Journal of Physics: Condensed Matter, vol. 17, pp. 351-360, 2005.

- Z.V. Popović, A. Cantarero, W.H.A. Thijssen, N. Paunović, Z. Dohcević-Mitrović and F. Sapiña, *Novel phase transitions in B-site doped manganites*, Physica B, vol. 359-361, pp. 1276-1278,2005.

- W.H.A. Thijssen, D. Marjenburgh, R.H. Bremmer and J.M. van Ruitenbeek, *Oxygen-Enhanced Atomic Chain Formation*, Physical Review Letters, vol. 96, p. 026806, 2006.

- W.H.A. Thijssen, D. Djukic, A.F. Otte, R.H. Bremmer and J.M. van Ruitenbeek, *Vibrationally Induced Two-Level Systems in Single-Molecule Junctions*, Physical Review Letters, vol. 97, p. 226806, 2006.

- O. Gurlu, A. van Houselt, W.H.A. Thijssen, J.M. van Ruitenbeek, B. Poelsema and H.J.W. Zandvliet *Controlled damaging and repair of self-organized nanostructures by atom manipulation at room temperature*, Nanotechnology, vol. 18, p. 365305, 2007.

- W.H.A. Thijssen, M. Strange, J.M.J. aan de Brugh and J.M. van Ruitenbeek, *Formation and properties of metal-oxygen atomic chains*, submitted to New Journal of Physics.

Nawoord

Experimenteel natuurkundig onderzoek is teamwork. De afgelopen vijf jaar heb ik met veel prezier samengewerkt met talloze fantastische mensen in het Kamerlingh Onnes Laboratorium. Van de vele discussies in de koffiekamer tot het gezelschap tijdens het meten laat in de avond. Sander, Darko, Ancuta, Christian, Roel, Carlos, Alex, Oren, Annemarie, Reyes, Monica, Manabu, Tadashi, bedankt voor alle inzichten en hulp die ik van jullie heb gekregen. Rolf, Femke en Daniël, jullie waren fantastische studenten en zonder jullie was dit proefschrift nooit zo mooi geworden.

Buiten de AMC vakgroep wil ik Marcel Rost, Koen Schoots, Federica Galli, Marcel Hesselberth en Gertjan van Baarle bedanken voor hun adviezen.

Zoals gezegd is experimenteel onderzoek teamwork en zonder de ondersteuning van Ruud van Egmond, Christiaan Pen en Ewi de Kuijper van de fijn mechanische dienst was er geen werkende opstelling geweest. Marcel Pohlkamp en Bert Crama van de electronische dienst zorgden voor de juiste electronica en een lage ruis op de metingen. Hans van Kuijk en Wilfred van der Geest zorgden ervoor dat er vloeibaar helium voorradig was om de opstellingen af te koelen. Ruud Zweistra en Fred Kranenburg van het systeembeheer waren meestal snel ter plaatse om computerproblemen te verhelpen.

Ik had het geluk te mogen samenwerken in Twente met Arie van Houselt, Oguzhan Gurlu en Harold Zandvliet, die me een andere techniek hebben bijgebracht om atomen te kunnen manipuleren.

Finally I want to thank all those people who have contributed by discussing especially the theory behind my measurements. Mikkel Strange, Kristian Thygesen, David Jacob, Juan José Palacios, Joaquín Fernandez Rossier, Antonio da Silva, Pavel Jelinek and many more...

Curriculum Vitae

I was born in Groesbeek on August 25, 1977. After receiving my VWO diploma from High School "Nijmeegse Scholengemeenschap Groenewoud"in Nijmegen I started my physics study at the University of Nijmegen in late summer 1995. During my study I chose to focus on experimental physics and did my Master's research at the High Field Magnet Laboratory under the supervision of Prof. dr. ir. J.C. Maan and dr. P.C.M. Christianen. There I studied the diffusion properties of electron-hole pairs in semiconductor quantum wells under the influence of an external magnetic field and received my Master's degree in August 2000.

After my graduation I traveled independently around the world for one year before joining the University of Valencia in Spain as junior researcher in the group of dr. A. Cantarero working on the magnetotransport properties of CMR materials. I returned to The Netherlands prematurely and started my PhD research at Leiden University in the group of Prof. dr. J.M. van Ruitenbeek in November 2002. My project was financially supported by the "Stichting voor Fundamenteel Onderzoek der Materie"and the work carried out is described in this thesis. During this time I had the opportunity to perform experiments at the University of Twente in the group of Prof. dr. ir. H.J.M. Zandvliet. Apart from my scientific work I have been a member of the University Council during my time in Leiden as well as chairman of the Leiden PhD Students Association.

Since May 2007 I work as a Policy Advisor for the Ministry of Economic Affairs in The Hague.